Aus dem Biomedizinischen Centrum
Einrichtung der Ludwig-Maximilians-Universität München
Lehrstuhl für Molekularbiologie

Functional Analysis of the cardiogenic Transcription Factor *mespa* in Mesoderm Differentiation in *Xenopus laevis*

Dissertation zum Erwerb des Doktorgrades der Medizin
an der Medizinischen Fakultät der
Ludwig-Maximilians-Universität zu München

vorgelegt von
Christian Roeßler
aus Bergen auf Rügen

2021

Mit Genehmigung der Medizinischen Fakultät

der Universität München

Berichterstatter:	Prof. Dr. Ralph A. W. Rupp
Mitberichterstatter:	Prof. Dr. Dr. Lesca Holdt PD Dr. Mathias Orban
Dekan:	Prof. Dr. med. dent. Reinhard Hickel
Tag der mündlichen Prüfung:	18.02.2021

Eidesstattliche Versicherung

Roeßler, Christian

Name, Vorname

Ich erkläre hiermit an Eides statt,
dass ich die vorliegende Dissertation mit dem Thema

Functional Analysis of the cardiogenic Transcription Factor *mespa* in Mesoderm Differentiation in *Xenopus laevis*

selbstständig verfasst, mich außer der angegebenen keiner weiteren Hilfsmittel bedient und alle Erkenntnisse, die aus dem Schrifttum ganz oder annähernd übernommen sind, als solche kenntlich gemacht und nach ihrer Herkunft unter Bezeichnung der Fundstelle einzeln nachgewiesen habe.

Ich erkläre des Weiteren, dass die hier vorgelegte Dissertation nicht in gleicher oder ähnlicher Form bei einer anderen Stelle zur Erlangung eines akademischen Grades eingereicht wurde.

München, 06.03.2021 — Ort, Datum

Christian Roeßler — Unterschrift Doktorand

Table of Contents

Zusammenfassung

Aus dem mesodermalen Keimblatt entspringen Vorläuferzellen für Herz, Blutgefäße, Muskel, Binde- und Stützgewebe, Gonaden sowie Nieren und ableitende Harnwege. Die Kenntnis über die während der Induktion und Differenzierung ablaufenden, hochkomplexen Prozesse und beteiligten Faktoren ist von großem wissenschaftlichem und insbesondere medizinischem Interesse. Mithilfe dieses Wissens können einerseits molekulargenetische Grundlagen angeborener Fehlbildungen verstanden und andererseits neue Therapiemethoden personalisierter Medizin entwickelt werden.

Als essentieller Masterregulator der Kardiogenese ist der bHLH-Transkriptionsfaktor *mesp1* in den Mittelpunkt der Forschung gerückt. Dabei konnte gezeigt werden, dass *mesp1* bereits früh während der Gastrulation exprimiert wird und weitere wichtige Regulatoren der kardiovaskulären Differenzierungsprogramme aktiviert. Der Knockout des *mesp1* Gens in Mäusen führt zu einer sogenannten Cardia bifida, einer fehlerhaften Fusion früher Herzanteile, wohingegen die gleichzeitige Deaktivierung von *mesp1* und dem verwandten *mesp2* in einem vollständigen Fehlen der Herzanlage resultiert.

Aufgrund der frühen Aktivierung von *mesp1* und seinem Homolog *mespa* im afrikanischen Krallenfrosch wurden darüber hinausragende Funktionen bei der Differenzierung weiterer mesodermaler Gewebe vermutet. *Xenopus laevis* eignet sich insbesondere aufgrund der einfachen Manipulierbarkeit und Zugänglichkeit aller Entwicklungsstadien als hervorragender Modellorganismus.

In dieser Studie konnten mittels Genexpressionsanalysen nach Knockout sowie Überexpression Zusammenhänge zwischen *mespa* und Vorläuferzellen mesodermaler Gewebe in verschiedenen Entwicklungsstadien untersucht werden. Dabei konnte gezeigt werden, dass *mespa* die Expression der frühen mesodermalen Marker *eomes* und *xbra* während der Gastrulation und Neurulation beeinflusst. Darüber hinaus spielt *mespa* eine Rolle in der Entwicklung von Skelettmuskeln und fazialen Strukturen, jedoch reicht *mespa* allein nicht aus um Marker der Myogenese zu aktivieren. Weiterhin wurde demonstriert, dass *mespa* in der Vaskulogenese und der embryonalen Hämatopoese involviert ist. Vorbeschriebene Effekte auf Markergene der epithelialen-mesenchymalen Transition (EMT) konnten nicht bestätigt werden. Ebenso zeigte sich kein direkter Zusammenhang zur Nephrogenese.

Zusammenfassend wurde demonstriert, dass *mespa* weitreichende Funktionen in der Entwicklung mesodermaler Gewebe ausübt.

Summary

Progenitors of the heart, the vasculature, musculature, connective and supporting tissue, the gonads, the kidneys and lower urinary tract derive from the mesodermal germ layer. The knowledge about the highly complex processes and involved factors during induction and differentiation of progenitor cells are of great scientific and medical interest. It helps understand the underlying molecular genetical basics of congenital malformations on one hand and develop new therapeutic options for personalised medicine on the other hand.
The bHLH transcription factor *mesp1* became the focus of research as master regulator of cardiogenesis. It was shown that *mesp1* is already expressed early during gastrulation and that *mesp1* activates additional important regulators of cardiovascular differentiation. The knockout of the *mesp1* gene in mice leads to a so-called cardia bifida, a failed fusion of the heart tube, whereas the simultaneous deactivation of *mesp1* and the related *mesp2* result in a complete loss of the heart anlagen.

Since *mesp1* and its homologue *mespa* of the African claw frog *Xenopus laevis* are activated early, further exceeding functions concerning the differentiation of further mesodermal tissues are supposed. *Xenopus laevis* is a particularly proper model organism due to its easy manipulability and approachability of all developmental stages.
In this study, relations between *mespa* and mesodermal precursor cells have been examined in different developmental stages based on gene expression analysis after knockout or overexpression of *mespa*. It was shown, that *mespa* is required for the expression of early mesodermal markers *eomes* and *xbra* during gastrulation and neurulation. Moreover, *mespa* plays a role in skeletomyogenesis and in the development of facial structures, but is not sufficient to activate myogenic markers on its own. Furthermore, it was demonstrated that *mespa* is involved in the development of precursors of vasculogenesis and embryonic haematopoiesis. Formerly described effects on the epithelial-to-mesenchymal transition could not be confirmed. Likewise, no direct relation towards nephrogenesis was shown.
In conclusion, it was demonstrated that *mespa* exerts extensive functions during the development of mesodermal tissues.

1. Introduction

1.1 Clinical background

Congenital anomalies are a major burden of worldwide children's health. With a wide variety of causitive factors of genetic, infectious and nutritional or environmental origin, congenital anomalies constitute a total of 303.000 neonatal deaths worldwide in 2015 (WHO, 2018). Congenital heart defects (CHD) belong to the most common and most severe anomalies affecting around 8 of 1000 new-borns worldwide with a wide ethnical variance (van der Linde et al., 2011). Complex heart defects require immediate diagnostic and therapeutic intervention during the first months of life. Although interventional and surgical methods for correction of anatomical anomalies exist, heart diseases continue to be one of the leading causes of infant death (Gilboa, Salemi, Nembhard, Fixler, & Correa, 2010). Since the number of transplantable organs remains insufficient, big effort has been made to advance in new therapeutic options. In this regard, cell therapy using reprogrammed stem cells emerged as an option to reconstruct malformed structures or necrotic tissue (Tsilimigras et al., 2017). Therefore, unravelling the mechanisms and regulatory networks involved in the process of differentiation and specification of progenitor cells is crucial to generate the desired cells. Knowing the genetic correlate causing congenital heart defects opens the door towards gene therapy: Recently, new techniques of gene editing were discovered which precisely facilitate insertion, deletion or modification of genes, which might help to treat genetic defects causing congenital diseases (Ho, Loh, Chan, & Soh, 2018). To accomplish these challenges, a deep and entire understanding of the underlying molecular orchestra during developmental processes like cardiogenesis that leads to congenital anomalies is crucial to localise potential therapeutic targets.

Moreover, congenital heart defects show a high association with complex genetic syndromes, for which no causal treatment exists. New emerging techniques to specifically modify damaged genes constitute promising approaches to address genetic defects. To evaluate risks and potentials for future treatment, upstream and downstream players of key regulators in the programme of developmental processes have to be uncovered. Talking about genetic syndromes, monogenetic diseases can be distinguished from defects with partial or entire chromosome loss or numeric aberration. Congenital heart defects are commonly associated with aneuploidies like trisomy 15, 18 or 21 of which

only the latter possesses a normal life expectancy. Thus, the location of the genetic defect within the genome and the role of the respective coding genes decide about the viability of the embryo or the newborn.

Interestingly, a large spectrum of syndromes including congenital heart diseases are accompanied by craniofacial defects. The complex of DiGeorge Syndrome, caused by a microdeletion on chromosome 22q11, includes cardiac abnormalities, abnormal facies, thymic aplasia, cleft palate and hypocalcaemia/hypoparathyroidism. Cardiac defects range from ventricular septum defect to tetralogy of Fallot. Similarly, the microdeletion on chromosome 8q12 in the gene of CHD7 results in the CHARGE syndrome, an acronym replacing coloboma, heart defect, atresia of choanae, retarded length growth and developmental retardation, genital anomalies and ear malformations (Kliegman, Stanton, Geme, & Schor, 2016). These genetic syndromes are representative for a big variety of syndromes with simultaneous malformations of heart and head, suggesting a common developmental path.

1.2 *Mesp* genes in mesoderm differentiation and cardiovascular development

A wide spectrum of perturbed mechanisms during cardiovascular development underlies congenital heart defects. They range from physiologic variants or small anomalies that are not relevant for the circulation to complex structural malformations that are life threatening for newborn or unborn children.

The heart, the first functional organ of mammals, develops from two fields deriving from mesodermal cells. They fuse in order to form the cardiac tube. The heart tube is subsequently looped in order to generate its physiological shape consisting of chambers, atria and in- and outflow tract. In the process of murine cardiovascular development, the bHLH transcription factor *mesp1* was found to be an essential player since its homozygous knockdown led to major defects in the heart formation and mice exhibited two separated heart tubes, also called cardia bifida (Saga, 1998). Moreover the embryos showed growth retardation, aberrant head and somite formation and died early during development. Interestingly, *mesp1* was detected in all nascent mesodermal cells that depart from the primitive streak (Saga et al., 1996), suggesting that *mesp1* plays an important role at the initiation of mesoderm formation. The basic helix-loop-helix (bHLH) transcription factor *Mesp1*, referring to ‘mesoderm posterior 1’, is meant to be one of the earliest transcription

factors exclusively expressed in mesoderm in a crescent like pattern and thus thought to have regulatory function. Basic HLH proteins bind to a designated palindromic sequence CANNTG called E-Box (Murre et al., 1989), which facilitates homo- and heterodimerization for more efficient binding to interaction partners like other bHLH transcription factors or E-proteins and thereby activation of target genes. *Mesp1* was first discovered by Saga et al. (1996) during investigations on the formation and specification of primordial germ cells (PGC) in the posterior mesoderm. The first cells that ingress from the primitive streak form the extraembryonic, cranial and heart mesoderm. Since *mesp1* depleted mesodermal precursors do not manage to depart appropriately from the primitive streak and *mesp1* deficient mice exhibited defects in heart tube formation, knockout experiments suggested a striking involvement of *mesp1* in differentiation and migration of cardiovascular precursor cells (Saga et al., 1999). Further investigations led to the finding that *mesp1* expression marks the beginning of cardiovascular development, since cells deriving from *mesp1*$^{+}$ cells form not only the heart but also major vessels like intersomitic and cranial vessels and the dorsal aorta (Saga, Kitajima, & Miyagawa-Tomita, 2000).

Mesp-related genes were also cloned in *Xenopus*, first designated *Thylacine*, thereafter *mespa* (Sparrow et al., 1998), and in zebrafish, called *mesp-a* (Sawada et al., 2000). *Mesp1/mespa* became the centre of cardiovascular research due to its promising potential as master regulator, which provided deeper insight into the mechanisms underlying cardiovascular development. *Mesp1*$^{+}$ multipotent cardiovascular progenitors (MCP) are the source for the establishment of the unipotent first heart field (FHF) and the bipotent second heart field (SHF). While the FHF forms the left ventricle and both atria, the SHF gives rise to the right ventricle, atrial cells and cells of the vascular outflow tract. By contrast, two further populations of *mesp1* negative cells contributed to the heart, one of neural crest origin and another one that formed the cardiac conduction system of the developing heart (Kitajima, Miyagawa-Tomita, Inoue, Kanno, & Saga, 2006). Overexpression experiments uncovered that *mesp1* is sufficient to activate the programme for cardiovascular differentiation since several studies proved ectopic or precocious differentiation of cardiomyocytes (Bondue et al., 2008; David et al., 2008; Lindsley et al., 2008). In this context, *Wnt* signalling promotes the initial steps of heart development, while it inhibits the cardiac differentiation and specification in the progress of cardiogenesis (David et al., 2008; Ueno et al., 2007). By activating the Wnt-inhibitor

Dkk1, *mesp1* paves the way for cardiovascular progenitors to undergo further specification. Recent studies demonstrated that the *Xenopus* homologue *mespa* possesses comparable potential to confer cardiovascular fate on mesodermal progenitor cells (Kriegmair et al., 2013).

A second bHLH transcription factor, called *mesp2*, was found to share almost the same amino acid sequence within its bHLH motif (Saga, Hata, Koseki, & Taketo, 1997). Both genes are located in close spatial relation on chromosome 7 (Saga et al., 1996; Saga et al., 1997). *Mesp1* and *mesp2* have two phases of expression, first being expressed in the early mesoderm and second in the presomitic mesoderm. However, *mesp2* is expressed later and initially at lower levels. In *mesp1/2* double knockout embryos no embryonic mesoderm was formed including heart, gut and somites (Kitajima, Takagi, Inoue, & Saga, 2000). These findings implicate, that *mesp1* and *mesp2* also participate in somitogenesis. *Mesp2* was found to be essential for the establishment and maintenance of the sclerotomal polarity, meaning the rostrocaudal segment polarity of the sclerotome at the initiation of segmentation (Saga, 1998; Takahashi et al., 2000). Interestingly, *mesp1* and *mesp2* show a functional redundancy since they can compensate for each other. *Mesp1* overexpression rescues the disrupted somite morphogenesis in *mesp2* knockout embryos (Saga, 1998), while gastrulation defects of *mesp1* deficient embryos can be rescued by *mesp2* overexpression (Kitajima et al., 2000). However, *mesp1* is the more momentous player due to its early expression during mesoderm formation and cardiovascular development. Functional differences between *mesp1* and *mesp2* were proven to be conserved between various vertebrate species (Hitachi et al., 2009).

A third member of the *mesp* family, *mesogenin* or *mespo* respectively (Joseph & Cassetta, 1999) contributes to the segmentation of the presomitic mesoderm in the process of somitogenesis since somites and expression of genes of the PSM are disrupted in *mespo* morphants (Wang, Li, Chen, & Ding, 2007). In mice, the deletion of the *mespo* homologue *pMesogenin* leads to a complete failure of somite formation and segmentation of the trunk and tail (Yoon & Wold, 2000).

The establishment of mesoderm marks a pivotal step in the development of the embryo body plan, which shifted it into the focus of research for decades. In this study, I focussed on functional classification and characterisation of *mespa*, the homologue of *mesp1* in the African claw frog *Xenopus laevis*, due to its promising potential as a player in cardiac development and mesodermal specification. Although the function of *mespa* in cardiac

development has been well described up to now, its function in patterning of other mesodermal lineages remains elusive. Being expressed in all cells of the nascent mesoderm of the primitive streak in mice, *mesp* genes act at the transition from mesoderm induction to mesoderm differentiation. In the following, I will give a brief overview of the process of mesoderm induction.

1.3 Mesoderm induction in *Xenopus laevis*

Mesodermal tissues originate from the marginal zone at the equator of the topographically organised embryo. The anterior-posterior body axis and the laterality of the embryo are determined by the first cleavage of the fertilised egg (Nieuwkoop & Faber, 1994). At this time, the embryo consists of a pigmented animal pole and an unpigmented vegetal pole. The formation of the marginal zone, the prospective mesoderm and its derivatives depend on inductive signals from the vegetal pole, i.e. the prospective endoderm. Kiecker, Bates, and Bell (2016) reviewed the current understanding of germ layer formation. Induction describes a bilateral process in which one cell, the inducer, commits or directs another one, the responder, with extracellular signals to a different fate (Harland, 1988). During development groups of cells, rather than single cells, are involved in this process. As pioneering tissue explant assays by Nieuwkoop revealed, vegetal cells possess the power to commit ectodermal cells to mesodermal fate. In this process, direct proximity of vegetal cells to animal pole cells is mandatory to fulfil induction (Sargent, Jamrich, & Dawid, 1986). Spemann postulated that an organiser region located in the dorsal marginal zone of the early gastrula, the so-called "Spemann's organiser", regulates further mesoderm formation (Spemann H., 1924). Big effort has been made to identify the signalling factors, which led to the finding of members of the FGF (Fibroblast Growth Factors) and Nodal protein families as mesoderm inducing factors (Kimelman & Kirschner, 1987; Smith, 1987).

During evolution organisms gained functional and morphological complexity, which is reflected by the fact of extensive and closer networks of regulatory factors. Thus, the families of signalling factors consist of numerous members. The process of induction itself can be subdivided into three parts: initiation, maintenance and patterning. According to our current understanding, four families of signalling factors are involved in mesoderm induction. Nodal factors play important roles during the initiation of mesoderm induction, while FGFs and Wnts (from 'Wingless-related integration site') guide the maintenance of

the mesodermal fate. BMPs (Bone morphogenetic proteins) are known to be crucial for the mesodermal patterning especially of the dorsoanterior to ventroposterior axis. However, no strict epistasis is established and they incorporate overlapping functions during development (Kimelman, 2006).

The first steps of mesoderm induction, which result in the formation of the three germ layers, are characterised by the temporal and spatial adjustment of concentrations of inducing factors and inhibitors (Kiecker et al., 2016; Kimelman, 2006). Although all of the above-mentioned families of inducing factors are involved in the early mesoderm formation, important differences of the precise course of activation can be delineated between different species. In *Xenopus*, VegT, a T-Box transcription factor which is initially localised in and fixed to the vegetal pole, starts to activate signalling factors of the Nodal family, also called Nodal-related genes (in *Xenopus Xnr*) at the midblastula stage (MBT). This is the time point during development when zygotic transcription is initiated. It was shown, that high concentrations of VegT induce endoderm, while low concentrations induce mesoderm (Kavka & Green, 2000).

Vg1, a member of the Transforming Growth Factors ß (TGFß) family, is initially expressed in a similar manner as *VegT* with a high concentration at the vegetal pole of *Xenopus* embryos. By contrast, several reports describe an expression in the animal hemisphere of zebrafish embryos (Marlow & Mullins, 2008) and ubiquitous appearance during early developmental stages (Helde & Grunwald, 1993). Thus, *Vg1* might exert an important function in the formation of head and axial mesoderm by activating Wnt and BMP antagonists (Birsoy, Kofron, Schaible, Wylie, & Heasman, 2006; Dohrmann, Kessler, & Melton, 1996) and left-right patterning (Peterson, Wang, & Yost, 2013).

Most recent reports concerning the controversially discussed pioneer mesodermal inducer demonstrated that heterodimers of Nodal and Vg1 are responsible for mesendoderm induction in zebrafish (Montague & Schier, 2017).

One of the first dorsalising signals emerges from genes of the Nodal family in a dorsal to ventral gradient, with high levels on the dorsal side of the embryo (Kiecker et al., 2016). The dorsoanterior to ventroposterior gradient of Nodal signals incorporates one of the important promotors for the establishment of the body axis. One designated member of the Nodal family, *Activin* is capable of inducing mesodermal fates by stimulating the Nodal pathway. In tissue explant assays, Okabayashi and Asashima (2003) revealed that depending on the injected concentration of *Activin* and the use of cofactors, distinct

mesodermal lineages could be generated. Since evidence increases that the progenitors of these lineages are spatially organised in the future marginal zone and also involute sequentially during gastrulation, this supports the hypothesis of a gradient of induction signals. While high concentrations of *Activin* induce more dorsoanterior tissues like cranial structures and cardiogenic mesoderm, low concentrations form ventroposterior tissues like haematopoietic cells. Animal caps treated with intermediate doses differentiate into cells of the notochord, cartilage and muscles. Highest concentrations (>100ng/ml) of *Activin* have been found to induce endodermal tissue such as liver, pancreas and intestine (Okabayashi & Asashima, 2003).

Due to a microtubule-driven rotation of the cell cortex against the inner cytoplasmic core of the egg that is directed by the sperm entry point, *ß-CATENIN* gets enriched at high levels on the prospective dorsoanterior side of the embryo. This produces high maternal *ß-CATENIN* protein levels on the prospective dorsal side of the embryo, which are crucial for the development of the head and other dorsoanterior structures (De Robertis, Larrain, Oelgeschlager, & Wessely, 2000). Among others, the Nodal genes *Xnr5* and *Xnr6* are targets of a *ß-CATENIN/Tcf* complex activation in the cascade of the initiation of mesoderm induction (Yang, Tan, Darken, Wilson, & Klein, 2002), establishing a link between the two signalling pathways of Nodal/Activin and Wnt/ß-CATENIN. Thus, both pathways contribute to specify the dorsoanterior to ventroposterior and the animal vegetal body axes (Kiecker et al., 2016).

At the dorsal side of the embryo, the organiser region, also called Spemann's organiser, is established. In a former understanding, the organiser region emits signals in order to pattern and subdivide the adjacent dorsolateral mesoderm. Further fate mapping studies specified the body axis to be rather in a dorsoanterior to ventroposterior direction. This permitted a better determination of the organisation of the marginal zone and even the location of the mesodermal progenitors within this field (Lane & Sheets, 2006).

In the course of maintenance and patterning, distinct regulatory programmes for the head, trunk and tail mesoderm induction can be distinguished. While in the head Nodal, FGF and Wnt pathways are inhibited by secreted molecules, they guide the mesoderm formation in the trunk together with transcription factors like *Xbrachyury*, *Tbx6* or *VegT* (Goering et al., 2003). They establish positive feedback loops activating FGFs to maintain their own transcription (Isaacs, Pownall, & Slack, 1994). In contrast, the tail mesoderm

develops under the influence of BMP and Notch signalling, which control the outgrowth of tail structures from the tail bud (Beck, Whitman, & Slack, 2001).
As Kiecker et al. (2016) reviewed, FGFs are only weak mesoderm inducers and they are more likely competence factors, which are needed to respond to the induction signal by TGFß family members like *Activin* and Nodals.
In summary it can be said, that a large gene regulatory network underlies mesoderm induction, which needs to be fully elucidated.

1.4 Advantages of *Xenopus laevis* as model organism

The African claw frog *Xenopus laevis* is an approachable and versatile model organism to study processes of germ layer formation, differentiation and patterning of mesodermal derivatives and cell migration, as Krneta-Stankic, DeLay, and Miller (2017) referred it to organogenesis. Female animals can be primed by injecting ß-human chorionic gonadotropin (ß-hCG). Laying vast amounts of fertile eggs (100-600), they provide a high throughput of individuals to analyse. Since embryos are large and develop extracorporally, they can be manipulated by microinjection of antisense-oligonucleotides, i.e. morpholinos, for knockdown or mRNA for overexpression and induction. Furthermore, every developmental stage can be observed under the microscope, which facilitates the best accessibility for the study of cell differentiation and migration and the development of various organ systems. Due to the fact, that already the first cleavage of the fertilised eggs decides about the position of the body axis and the laterality of the embryo, one side can be modified without impairment of the contralateral side, offering an internal control. Gastrulation and neurulation occur only a few hours after fertilisation and even functional organs like the kidney or the heart develop within 2 to 3 days.
The prior work in *Xenopus* provided profound knowledge of embryogenesis whereupon our current understanding of mammalian embryogenesis is built. This demonstrated that regulatory networks and pathways in the course of development of vertebrates are evolutionarily conserved and knowledge can be transferred to higher vertebrates and human biology.

1.5 Objectives

The functional homology of the mammalian *mesp1* and the *Xenopus mespa* in mind, this work aims at demonstrating the broad function of *mespa* during embryogenesis by revealing interaction of *mespa* and possible downstream target genes.

Loss-of-function and gain-of-function experiments were performed by microinjection of either translation-blocking antisense oligonucleotides (morpholinos) or mRNA into two- to four-cell-stage embryos or animal cap explants. By taking advantage of mRNA *in situ* hybridisation, the mRNA of specific target genes, the distribution within the embryo and thus a possible interaction with *mespa* could be visualised on a morphological level in the whole-mount embryos or in pluripotent cell explants.

As Chan et al. (2013) and Lindsley et al. (2008) demonstrated, *mesp1* exerts functions that exceed the regulation of cardiovascular differentiation (Saga et al., 2000). The function of the *Xenopus* homologue *mespa* has not been examined entirely (Kriegmair et al., 2013).

First, I focused on the T-Box transcription factors *eomes* and *xbra,* which are expressed early during development and overlap spatially and temporally with *mespa*. Since *eomes* and *xbra* are crucial for the development of the axial mesoderm, *mespa* could play a role in the network of early anterior versus posterior patterning.

Chan et al. (2013) revealed that *mesp1* could drive murine precursor cells to skeletomuscular identity. To analyse the effects of *mespa* on skeletomyogenesis throughout *Xenopus* development, *myoD* and *myf5* were chosen as possible target genes.

Since the development of the heart and the vascular system are closely linked, Saga et al. (2000) demonstrated that *mesp1* is a key regulator during the formation of major vessels. Therefore, the influence of *mespa* on the *apelin receptor (aplnr)* as a representative of the vascular precursors was examined in *Xenopus* in a third step.

According to Chan et al. (2013), *mesp1* promotes haematopoietic development under certain conditions. To examine the influence of *mespa* in *Xenopus* haematopoiesis, we chose *α-globin (hba1)* as a definitive marker for erythropoiesis.

Fifth, I investigated, whether *mespa* also drives the development of the kidney, as another organ arising from mesodermal progenitors. The target gene *pax2* plays an important role during kidney development and differentiation, as it contributes to the formation of pronephric tubule and duct epithelia (Carroll, Wallingford, & Vize, 1999). The interaction of *mespa* and *pax2* has not been examined so far in *Xenopus* embryos.

Finally, *mesp1* was reported to influence cell migration of cardiovascular precursors during the formation of the heart tube (Saga et al., 1999). Lindsley et al. (2008) showed that *mesp1* is capable of activating *snai1* and *twist1*, two transcription factors that control EMT, e.g. in differentiating ES cells during gastrulation. With this study, we expand our understanding of the function of *mespa* during EMT and migration in *Xenopus laevis.*

2. Material and Methods

2.1 Gadgets and equipment

Gadget	Name	Manufacturer
Camera	Leica DFC 310FX	Leica
Centrifuges	5417C Micro 22R Sigma 3-18 PicoFuge	Eppendorf Hettich Zentrifugen Sigma Laborzentrifugen Stratagene
Flourescence Microscope	M205 FA	Leica
Incubators	Heraeus; Standard-430	GS
Injection needles	Glass Thin Wall Capilllary, 4", w/Fil, 1.,0 mm	World precision Instruments
Injector	Pli-100	Digitimer Ltd. Medical Systems Corp. Greenvale NY 11548 (Welwyn Garden City, England)
Injector Lightsource	KL 1500 electronic/ KL 1600 LED	Schott Pulch + Lorenz
Software	Illustrator CS5 Photoshop CS5 Office 2013 Endnote X8 Leica Appl. Suite V3 3.0	Adobe Adobe Microsoft Thomson Leica
Spectrophotometer	Nano Drop ND-1000	PeqLab
Microneedle puller	P-87	Shutter Instrument (Novato, CA, USA)
Stereomicroscope	Stemi SV-6	Zeiss
Water Bath	Minitherm 2	Dinkelberg

2.2 Reagents

2.2.1 Chemicals

Agarose	Bio&SELL Feucht /Nürnberg
Chicken Serum	Gibco/BRL
Gentamycin	Sigma
ß-hCG OVOGEST 1000 I.E./ml	MSD Animal Health Intervet Deutschland GmbH Unterschleißheim, Germany
L-Cysteine	AppliChem Darmstadt, Germany
Tricaine methanesulfonate	Sigma
Alexa Fluor 488	Invitrogen

2.2.2 Kits

QIAprep Spin Miniprep Kit	Qiagen
RNeasy Mini Kit	Qiagen

2.2.3 Enzymes

Alkaline Phosphatase	Roche
Proteinkinase K	Sigma Aldrich
rAPid Alkaline Phosphatase	Roche
Restriction Endonucleases	Roche, NEB
RNasin	Promega
RNA Polymerase (SP6, T3, T7)	Promega

2.3 Plasmids

2.3.1 Plasmids for in-vitro-transcription

Plasmid name	**Cloning Sites**	**Restiction Enzyme**	**Polymerase**
pSP6 – Globin – **XL*Mespa* -** IRES-EGFP	Sac1/Sal1	Afl2	SP6

(pSP6 – Globin – XlMesp1like – IRES-EGFP – intronfree)			
pSP6-Globin-Δ5'UTR- **x*Mespa***-IRES-EGFP	Sac1/Sal1	Afl2	SP6
pCS2-***MyoD***	EcoRI/XbaI	xbaI	SP6
pCS2-n-ßGal		Not1	SP6

2.3.2 Plasmids for *in situ* hybridisation probes

Plasmid Name	Cloning Sites	Restriction Enzym	Polymerase
pSP73-**myf 5**	EcoRI	BamH1	SP6
*pSP72***xBra**		Hind III	T7
pSP72-**snail 1**		Bgl2	SP6
pSPT18-**α-globin**	PstI/BamHI	Pst I	T7
pT7T5-**pax 2**		EcoR1	T3
*pCS2+**X***myoD**b**		EcoR1	T7
pBS-SK-**eomes**	EcoRI/NotI	EcoR1	T3
pKS-**twist1**		EcoR1	T7
pIBI 31wt-**aplnr** (Msr)		Bgl2	T7

2.4 Morpholino oligonucleotides

Morpholinos are single-stranded antisense oligonucleotides with an ideal length of about 25 bases. Introduced by microinjection, morpholinos block the translation of specific mRNAs by undergoing Watson-Crick basepairing. In these nucleic acid analogs, nucleic acid bases are attached to morpholine rings, which are interconnected by non-ionic phosphorodiamidate linkage. Therefore, they are resistant to restriction endonucleases. The neutrally charged backbone reduces unspecific interaction and toxicity.

All morpholinos were synthetised by the company GENE TOOLS LLC (http://gene-tools.com/vivomorpholinos). For best knockdown results, a mismatch of four or fewer basepairs is recommended and they should not show any secondary structure. The morpholino should be designed to target the sequence between the 5' cap and not more than 25 bases 3' of the translation start AUG. The 'GC' content should be about 50 %. Morpholinos are stored at -20°C and heated to 65°C before using in order to achieve a good water solubility. The standard Control MO is targeted against the human ß globin pre-mRNA (Eisen & Smith, 2008).

Morpholino	**Oligo-Sequence**
xmespa MO	5'-AACTAGGAATAAACAAGACATGGAT-3'
xmespo MO	5'-TACTACTGATGGAGACTCTGCACCA-3'
Control MO	5'-CCTCTTACCTCAGTTACAATTTATA-3'

2.5 Antibodies

Alkaline phosphatase staining was carried out to visualise mRNA expression patterns by whole mount RNA *in situ* hybridisation. For this purpose, we used the following antibody, provided by Roche.

Anti-dig-antibody: Sheep anti-Digoxigenin Fab fragment, linked to alkaline phosphatase (1:2000)

2.6 Molecular biological methods

2.6.1 Solutions

Alkaline Phosphate (AP-) Buffer	
100 mM	Trichlorethan Tris/HCL 9.5
100 mM	NaCl
50 mM	$MgCl_2$
Antibody solution	**stored at -20°C**
2%	Boehringer-Mannheim-Block in 1x MAB pH 7.2

Bleaching solution		**freshly prepared**
1%	H_2O_2	
5%	Formamide	
0,5x	SSC	
DEPC-H_20		**stirred at RT overnight and autoclaved afterwards**
0.1%	Diethylpyrocarbonate (DEPC)	
	MilliQ water	
Hybridisation solution		**stored at -20°C**
5x	SSC	
50 %	Formamide	
1 %	Boehringer-Mannheim Block	
0.1 %	Torula yeast RNA	
0.01 %	Heparin	
0.1 %	Tween-20	
0.1 %	CHAPS	
5mM	EDTA	
5 x Loading dye		
50 %	Glycerine	
10mM	EDTA	
0.05 %	Orange G	
Maleic Acid Buffer (MAB)		**pH 7,6 at 23°C**
500mM	Maleic acid	
750mM	NaCl	
MEMFA		**freshly prepared**
100mM	3-(N-Morpholino)-propanesulfonic acid	
2mM	EGTA	
1mM	$MgSO_4$	
3,7%	Formaldehyd	pH 7,4

10x MOPS Buffer		**pH to 7.0 with NaOH**
200mM	MOPS	
50mM	Natriumacetat	
10mM	EDTA	
Paraformaldehyde		**stored at -20°C**
4%	Paraformaldehyde in PBSw	
Phosphate Buffered Saline (PBS)		
137mM	NaCl	
2,7mM	KCl	
8mM	Na_2HPO_4	
1,7mM	KH_2PO_4	pH 7.2
PBSw		
1x	PBS	
0.1 %	Tween-20	
Proteinkinase K		**Stored at -20°C**
10µg/ml	Proteinkinase K in H_2O	
20x SSC		**pH 7.0 at 23°C**
3M	NaCl	
300mM	Sodium Citrate	
Staining Solution		**Freshly prepared**
1ml	AP buffer	
3,5µl	5-Cromo 4-Chloro-Indolylphosphate	50mg/ml
	in 100% Dimethylformamide	stored at -20° C, Biomol
4,5µl	Nitroblue Trazoliumchloride	75mg/ml
	in 70 % DImethylformamide	stored at -20°C; Biomol
TE Buffer		**pH 8.0 at 23°C**
1mM	EDTA	
10mM	TRIS Base Tris/HCl 9.5	
TBE Buffer		**pH 8.6 at 23 °C**
83 mM	Borate	

0.1mM	EDTA
100mM	TRIS Base Tris/HCl 9.5
10mM digoxin labelled NPT mixture	**stored at -20°C**
10mM	ATP, CTP, GTP
6.5mM	UTP
3.5mM	Dig-11-UTP

2.6.2 Agarose gel electrophoresis

The electrophoresis of the DNA or RNA fragments was performed on horizontal 1% TBE agarose gels (Biozym) depending on the fragment size. The Ethidium bromide concentration in the gel was 0.25µg/µl. A 1x loading dye was added to the samples. As standard size of DNA ladders 1kbp or 100bp were used. The fragments were visualised by UV light.

2.6.3 Concentration measurement and purity control

The concentration of newly synthesised RNA was measured with the spectrophotometer Nano-Drop ND-1000. The ratio of the absorption at 260nm and 280nm (A_{260} / A_{280}) provided information about the purity of a sample. It was considered as pure if the ratio was about 1.8.

2.6.4 Plasmid digestion for IVTR

Before *In-vitro*-transcription can be progressed, the DNA plasmids have to undergo restriction digestion. The following mix has to be incubated for 1 hour at 37 °C. (Depending on the used enzyme).

10µg	Plasmid
4µl	10x Digestion buffer
3µl	Restriction enzyme
a.d. 40µl	DEPC treated H_20

The end concentration should be measured (0,250µg/µl). The linearised plasmids are stored at -20°C.

2.6.5 *In-vitro*-transcription (IVTR) of messenger RNA

To save mRNA from intracellular degradation or immediate translation, mRNA has to be capped prior to microinjection. The following mix has to be incubated for 4- 5 hours at 37°C.

2 µg (8µl)	Template
10µl	5x Transcription buffer
2,5mM	G (5')pppGcap analog BioLab #1407
1mM	NTP-Mix
10 mM	DTT
20u	RNasin (0.5µl of 40u/µl)
2µl	RNA-Polymerase
Add to 50µl	DEPC treated H_2O

All components were incubated at 37°C for two hours. Subsequently 1µl of RNA-Polymerase was added and the setup was incubated for another two hours or overnight at 37°C. A DNA-digestion was performed "on-column" using 1µl DNAse (10u/µl). A RNA-Cleanup with the Qiagen Rneasy Mini Kit helped purifying the RNA following the manufacturer's protocol. After measuring the concentration in the spectrophotometer 5µl aliquots were stored at -80°C.

2.6.6 *In-vitro*-transcription of digoxygenin-labeled RNA probes

Digoxygenin-labeled RNA probes were synthesised for *in situ* hybridisation. Plasmids were linearised as mentioned above. The following setup was incubated for 2 hours at 37°C.

2µg	Linearised plasmid
1x	Transcription buffer

0,1mM	Dig-NTP Mix (Roche)
40U	RNAsin
20U	DNA dependent RNA polymerase (SP6, T3, T7)
add to 50µl	DEPC-treated H_2O

Subsequently 1µl of RNA-Polymerase was added and the setup was incubated for another two hours or overnight at 37°C. DNA-digestion was performed "on-column" using 1µl DNAse (10u/µl). RNA-Cleanup with the Qiagen Rneasy Mini Kit helped purifying the RNA following the manufacturer's protocol. 1µg of the transcribed RNA was used for quality control by gel electrophoresis. A 1:1 mix of synthesised RNA product and formamide was stored in aliquots at -20°C.

2.6.7 RNA *in situ* hybridisation

For the RNA *in situ* hybridisation embryos need to be fixed in MEMFA solution for 1,5 – 2h, followed by three washings in 1x PBS solution for 5 minutes each. Then, embryos have to be dehydrated in 100% ethanol 5x 12min. Afterwards they have to be stored at least over night at -20°C to dissolve cellular lipid membranes.

The rehydration was performed in a series of decreasing ethanol concentration (75%, 50% and 25%) in PBSw, each step for 5 mins, at room temperature. Hereafter the embryos have to be washed three times in PBSw. *Xenopus laevis* embryos were digested with Proteinase K for 20 min and animal explants for five mins at max. 22°C in order not to over-digest them. A short rinse and two more washing steps are needed before refixation with a solution of PBSw and 4% of paraformaldehyde for 20 mins at room temperature (0,5ml per vial). It is also important not to over-fix the embryos.

After a short PBSw rinse and five subsequent washings with PBSw, 5 mins each step, the embryos were prepared for hybridisation by changing from PBSw to hybridisation solution in two steps. First in a 50% PBSw: 50% hybridisation solution followed by 100% hybridisation solution for about 3min each step without agitation at room temperature. (Use 1ml hybrid solution per step). Afterwards the solution was discarded and 0.5 ml of fresh hybridisation solution was added to each vial. Subsequent incubation at 65°C for 1

hour inactivated endogenous phosphatases. The embryos were prehybridised at 60°C for 2 to 6 hours.

100µl of hybridisation solution and 3µl of a dig-labeled RNA probe per vial were heated to 95°C for 2 -5 min. The probe/hybridisation solution mix was added to the embryos. Alternatively, the hybridisation solution can be completely replaced by 0.5ml of a recycled probe. The samples were hybridised at 60°C overnight.

The following washing steps serve to eliminate non-hybridised RNA, which can cause background staining. The embryos were washed ten minutes in hybridisation solution at 60°C, followed by a short rinse with 2x SSC, three washings with 2x SSC for 20min each, a short rinse with 0.2x SSC and another two washings with 0.2xSSC for 30mins all steps at 60°C.

The samples were changed to MAB Buffer with two washes for 15min at room temperature in motion. In the following, they are incubated in 1ml antibody buffer per vial 2% BMB in MAB for 1 hour at RT with rocking to block unspecific antibody binding sides.

After removing, the antibody buffer 0.5ml of anti-dig antibody 1:2000 in antibody buffer was added and incubated for 4 hours at room temperature with rocking. In this period, the antibody binds to the hybridised probe. Afterwards, the samples are shortly rinsed with and kept in MAB overnight at 4°C.

Three to four washes in MAB for 60 mins each at room temperature clear the samples from not bound antibody. In case, the antibody incubation was performed overnight, embryos have to be washed six times for 60 minutes each.

After a short rinse with AP buffer embryos were equilibrated in AP buffer for 15 min. Replacing the AP buffer by 0,5ml of NBT/BCIP staining solution subsequently started the colour reaction. The reaction was proceeded at room temperature in the dark and if necessary kept at 4°C overnight. As soon as the first staining was visible, the colour reaction was stopped by washing twice in PBS for 10 min.

After fixing the embryos a last time for at least 90 minutes (there is no maximum in this step), one has to dehydrate them twice for 30 minutes each step in a 75% ethanol in PBS solution. For better visualisation of the staining, the natural pigment of the embryos was reduced by bleaching in a solution of 1% H_2O_2; 5% Formamide and 0.5% SSC for 1 – 2 hours on a light box at room temperature.

2.7 Histological techniques

2.7.1 Solutions

MEMFA		**Freshly prepared**
100mM	3-(N-Morpholino)-propanesulfonic acid	
2mM	EGTA	
1mM	$MgSO_4$	
3,7%	Formaldehyd	pH 7.4
PBS (Phosphate buffered saline)		
137mM	NaCl	
2,7mM	KCl	
8mM	Na_2HPO_4	
1,7mM	KH_2PO_4	pH 7.2
X-Gal staining solution		
5mM	$K_3Fe(CN)_6$	
5mM	$K_4Fe(CN)_6$	
2mM	$MgCl_2$	
0,25mM	X-Gal	
add PBS		

2.7.2 LacZ staining

LacZ staining is a histochemical method to visualise the progeny of lacZ mRNA injected cells. LacZ mRNA codes for the enzyme ß-Galactosidase. LacZ staining is performed after stopping the embryo's development by fixing them in MEMFA solution for 30 min and subsequently washing them twice for 10 min each with 1x PBS. The staining reaction takes place in the dark at room temperature by incubating the embryos in X-Gal solution for 1h. Cells with ß-Galactosidase activity are able to split off the galactose linked to a substituted indole of the X-Gal solution. The free indoles can dimerise and create a blueish dye. Depending on the desired intensity, the incubation can be prolonged for another 30 min. After washing the samples twice for 10 min in 1x PBS to stop the staining reaction, embryos were refixed for 30 min in MEMFA. Two washes for 10 min in 1x PBS were performed before storing them in 100% ethanol overnight at -20°C.

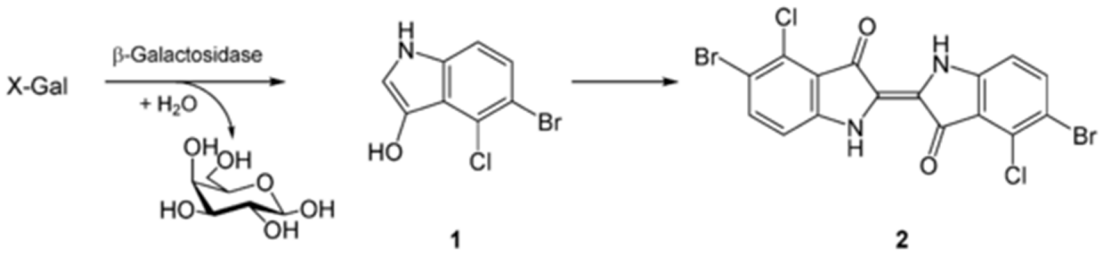

https://en.wikipedia.org/wiki/File:X-Gal_reaction.png

2.7.3 Fluorescent labelling of embryos

Embryos which should be analysed after neurulation and the beginning of elongation were coinjected with Alexa 488, a green fluorescent dye. At the tailbud or tadpole stage, they were sorted under the Fluorescence Microscope (Leica M205 FA) into left and right side-injected embryos before RNA *in situ* hybridisation, because the fluorophore does not resist/is destroyed by the dehydration step.

2.8 Embryological methods

2.8.1 Solutions

Human Chorionic Gonadotropin (ß-hCG) **MSD**		
1000 IU/ml in ddH_2O		
MBS		**pH 7,6 at 23 °C**
88mM	NaCl	
1mM	KCl	
5mM	HEPES	
1mM	$MgSO_4$	
2,5mM	$NaHCO_3$	
0,7mM	$CaCl_2$	added shortly before use
MBS (high salt)		
1x	MBS	
50nM	NaCl	

Cystein solution		**pH 7.7 – 7.8 at 23° C adjusted with 10M NaOH**
0.1x	MBS	
2%	L- Cystein	AppliChem
MBS / Gentamycin		
0.1x	MBS	
10µg/ml	Gentamycin	

2.8.2 Laboratory animals

Keeping and handling of laboratory animals was performed according to Deutsches Tierschutzgesetz. The use of *Xenopus laevis* embryos for experimental purpose has been licensed by Regierung von Oberbayern. Adult animals were provided by Nasco and Xenopus Express. Animals are housed in groups in water bassins with a temperature of 17 to 19 °C. Regular feeding and exchange of water is carried out by personnel of the Central Animal Model Facility, BMC Munich.

2.8.3 ß-hCG-Priming

ß-hCG-Priming was performed as a standard technique as recommended by xenbase.org. Ovogest hCG by MSD Animal Health is purchased from Henry Schein Vet GmbH with 10000 Units per vial and has to be dissolved in 10 ml of sterile water. As the hormone is protein-based, one should avoid generation of bubbles by great agitation of the vial of forcing the dissolution in order to not denature the proteins and reduce the efficacy.
The females were always injected at the same time and kept in the dark at 18°C overnight. According to the size of the females the ß-hCG dosage varied between 500 and 700u (1u/µl). The frog is held firmly with one hand, the frog's head facing to the injector's wrist. The hormone is injected posteriorly into the dorsal lymph sac. Each individual is kept in a separated container during ovulation.
After using the females are stored one more night at 18°C not to contaminate the basins with eggs. The frogs are not reused for at least 3 months to offer an appropriate period for oocyte production.

2.8.4 Extraction of testis

For anaesthesia, male *Xenopus laevis* frogs were kept in a 0.5% Tricaine methanesulfonate solution for 30 to 45 minutes. They were subsequently killed by neck dissection using strong short-branched scissors. The abdomen was opened by a ventral incision and the two testes were liberated from the adjacent intestinal fat. The testes were stored in MBS/CS at 4°C and could be used for a maximum of 5 days.

2.8.5 *In-vitro*-fertilisation

About 16 hours after ß-hCG priming *Xenopus* females start with egg deposition. Eggs were collected in petri dishes by gently squeezing (massaging) the abdomen, while the hindlegs are immobilised by the experimentor's index fingers.
A piece of testis was macerated in 1x MBS solution and mixed with the clutch. After 5 minutes, the petri dish was filled with 0.1x MBS and incubated at 18 -23°C. Fertilised eggs can be distinguished by the upward rotation of the pigmented animal pole, which follows the earth's gravitational field.

2.8.6 Microinjection and cultivation of *Xenopus laevis* embryos

For manipulations like microinjections, it is necessary to remove the jelly coat that surrounds *Xenopus laevis* eggs. Freshly prepared 2% cysteine solution with a pH of 7.7 – 7.8 dissolves the jelly within 5 to ten minutes under gentle shaking. When eggs roll freely, they should be washed twice in 0.1x MBS to stop the reaction.
1.0 mm glass capillaries (World Precision Instruments, Inc) were first prepared by using the Microneedle puller (setting: heat 800, mode: pull, time: 139, velocity: 140) and placed in the holding system of the injector. By breaking the tip with Dumont tweezers, they were calibrated to eject drops of 5nl at a pressure of 30psi in 40ms.
Injections were carried out with embryos placed in 1% Agarose grid plates with predefined holes of 1mm diameter. For the duration of injection, the cultivation buffer was aspirated to keep the embryos from moving.
Embryos were cultivated in 1% Agarose plates with 0.1x MBS and Gentamicin 1:1000 to prevent infections and reduce mortality of the clutches. The cultivation solution was changed at least every 24h.

2.8.7 Animal cap explants

Animal cap explants are a long used standard technique to examine development in isolated ectoderm, consisting of pluripotent embryonic cells at the time of dissection. The vitelline membrane of mid-blastula staged embryos (NF 8) was removed with two Dumont tweezers by stitching and grasping it on the vegetal side and tearing it apart. In 0.5 x MBS, animal cap explants were prepared by 3-4 cuts with the tweezers and transferred to grid plates in order to separate them during cultivation. The developmental stage was controlled with siblings from the same clutch.

2.9 Statistical analysis

Significance analysis of morphological phenotypes was performed by using two-tailed Fisher's exact test.

3. Results

3.1 Spatial and temporal coexpression of *mesp* genes and mesodermal transcription factors suggests broader regulatory interactions

Mesp genes start to exhibit their activity during the early processes of mesoderm formation and differentiation. They coincide with the first half of gastrulation (i.e. Nieuwkoop & Faber (NF) stage 10 to 11), when the three germ layers endo-, meso- and ectoderm are formed and the anteroposterior axis is specified. At the initiation of gastrulation the embryo is topographically organised (Gerhart, 2002; Kumano & Smith, 2002; Lane & Sheets, 2002). While the pigmented animal pole, the prospective ectoderm, forms skin and neural tissue later during development, the yolk rich vegetal pole gives rise to entodermal tissue like the gut. The two hemispheres are separated by the marginal zone, from which mesodermal and endodermal tissues arise. The marginal zone can be subdivided into an involuting marginal zone (IMZ) located towards the vegetal pole and the more animal half of the non-involuting marginal zone (NIMZ). At 50° from the animal pole on the prospective dorsal side of the embryo involution occurs. Therefore, the apices of so-called bottle cells are constricted and bottle cells elongate towards the interior, being pulled by the migrating anterior mesodermal cells to which they remain attached. During this process the apical surface of the bottle cells shrinks, which concentrates the pigment in the cortical cytoplasm. Thus, the blastoporal groove, a thin line of concentrated pigment, appears on the embryo's surface, and subsequently extends into a circular blastopore. Cells from the IMZ then start to shift position within the embryo revolving around the blastoporal groove.

According to the revised fate map, the marginal zone is devided into bands. The animal band forms dorsal mesoderm, the vegetal band forms ventral mesoderm. The side on which the organiser is established will become anterior or rostral, the signalling center on the opposite side of the organiser corresponds to posterior or caudal (Gerhart, 2002; Kumano & Smith, 2002; Lane & Sheets, 2002).

As described in previous studies by our research group (Kriegmair et al., 2013), *xmespa* and *xmespo* genes exhibit a horseshoe-like expression pattern around the blastopore during gastrulation (Fig. 1 A, B), while they are not expressed in the dorsoanterior part, the so-called Spemann's organiser. As depicted in Figure 1 G and H, the expression

domains of specific transcription factors of dorsal mesoderm, chordin (*chd*) and goosecoid (*gsc*), delineate this regulatory field (Cho, Blumberg, Steinbeisser, & De Robertis, 1991).

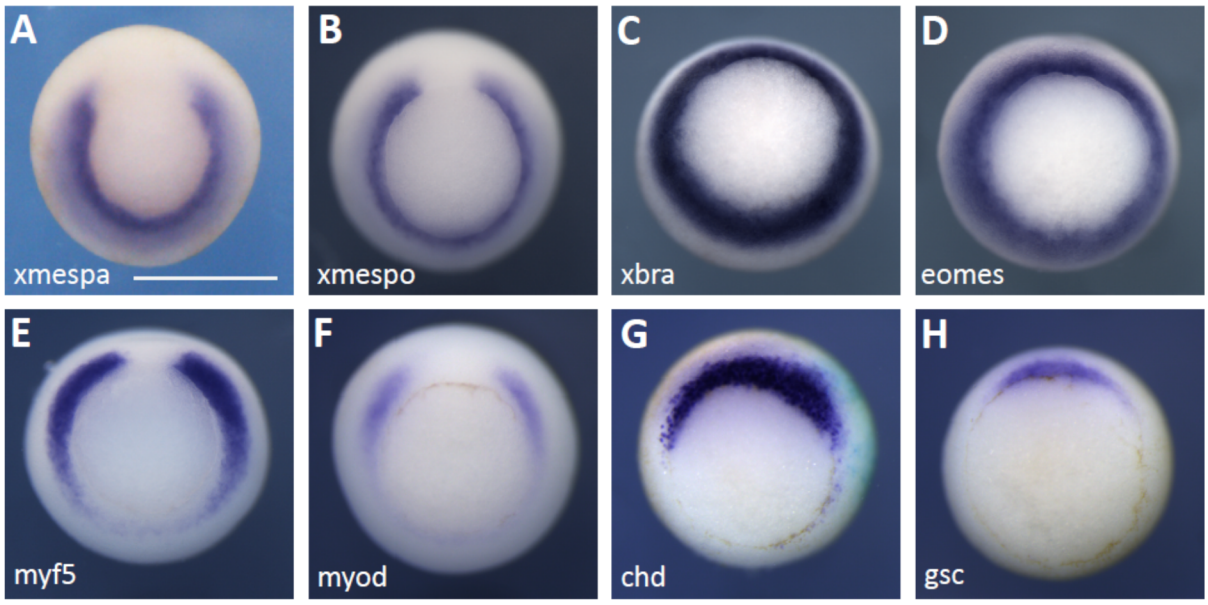

Figure 1: Comparative expression patterns of mesodermal subdomains during gastrulation in *Xenopus laevis* embryos
Xmespa **(A)**, *xmespo* **(B)**, panmesodermal markers and myogenic markers show spatial and temporal overlap in their expression. The displayed *mesp* genes and myogenic transcription factors are not expressed in the so-called Spemann's organiser, i.e. in the dorsal mesoderm. The images depict whole mount mRNA *in situ* hybridisations of *xmespa* **(A)** and *xmespo* **(B)**, panmesodermal T-Box transcription factors *xbra* **(C)** and *eomes* **(D),** myogenic transcription factors *myf5* **(E)** and *myoD* **(F)** and transcription factors of the dorsal mesoderm *chd* **(G)** and *gsc* **(H)** at the gastrula stage (NF 11). View onto the blastopore, dorsal uppermost, ventral on the bottom. Scale bar indicates 1mm.

Initial investigations of *mesp1*, the *mespa* homologue in mice, revealed a striking role in determination of cardiovascular cell fate and migratory processes (Saga et al., 1999). Since cardiovascular progenitors arise from two small portions of mesoderm adjacent to each side of the organiser region during gastrulation, the *mespa* gene expression domain exceeds the territory of the prospective heart anlagen as defined by fate mapping analysis (Gerhart, 2002; Moody, 1987). As the marginal zone develops the capacity to form the head organiser, it still needs to be elucidated whether *mespa* either has to be expressed broadly throughout the marginal zone in order to adjoin to the forming organiser, or whether *mespa* plays a role in the areas located more posteroventrally.

Fate mapping showed a variable contribution of 32-cell stage blastomeres to specific tissues. As illustrated in Figure 1, *mespa* and *msgn,* of which the synonym *mespo* is used in this work, overlap spatially and temporally with the expression domains of key mesodermal regulatory genes. Hence, we expected coexpression in at least some of the cells between *mesp* genes and the T-Box transcription factors *xbrachyury* (*tbxt;* also known as *xbra*, which is used in this work; Fig. 1 C) and *eomesodermin* (*eomes;* Fig. 1 D),

as well as the myogenic transcription factors *myoD* (Fig. 1 E) and *myf5* (Fig. 1 F). Furthermore, the apelin receptor (*aplnr)*, involved in vasculogenesis, *α-globin* (*hba1*), an indicator of haematopoiesis, *pax2*, involved in pronephrogenesis, and *twist1* and *snai1*, markers for epithelial-to-mesenchymal transition (EMT), ingression and the formation of the mesodermal mantle, were additionally included in the investigations of later developmental stages (chapters 3.4 to 3.7). In contrast to *mespa* and *mespo*, expression of the third member of the *mesp* gene family *mespb* starts later during development and thus does not form a horseshoe-like pattern during gastrulation (Hitachi et al., 2009; Sawada et al., 2000). Although, *mespa* and *mespb* have a functional overlap and they are able to compensate for each other in single, homozygous gene mutants, essential differences concerning their role in development have been described (Saga, 1998). However, *mespa* and *mespo* are activated and expressed early during gastrulation. This makes them potential key players in mesodermal differentiation and specification, with *mespo* acting downstream of *mespa* (Kriegmair et al., 2013). In this study, I analysed the regulatory interaction between candidate target genes and *mespa* and *mespo*, respectively, in different developmental stages *in vivo*.

3.2 Mesoderm patterning

The T-Box transcription factors *eomesodermin* (*eomes*) and *xbrachyury* (*xbra*) belong to a family of the earliest expressed factors contributing to mesodermal patterning as they determine mesodermal progenitors in the primitive streak of mice (Showell, Binder, & Conlon, 2004). Sharing a specific sequence in the DNA-binding domain, the so-called T-domain, they can activate target genes for mesoderm induction and differentiation. Both can be directly induced by *activin*, while a combination of *eFGF* and *xWnt8* induce *xbra,* but not *eomes,* transcription (Ryan, Garrett, Mitchell, & Gurdon, 1996).

As expression pattern analysis during early gastrulation in *Xenopus* embryos has shown, T-Box transcription factors *eomes* and *xbra* overlap spatially and temporally with *mespa*, which is considered a regulator in patterning of anterior mesodermal structures. As both *eomes*, expressed in a dorsal to ventral gradient (Ryan et al., 1996) and *xbra*, expressed in periblastoporal, posterior mesoderm, are crucial for the development of the axial mesoderm, *mespa* could play a role in the network of early anterior versus posterior patterning. Both panmesodermal markers are expressed by a thick ring of cells around the blastopore in the preinvoluted mesoderm with a notably wider area than *mespa*. In

this context, “panmesodermal” refers to the marker’s expression in the entire early pre-involuted mesoderm. *Eomes* is also required for the induction of endodermal progenitors, which is why the *eomes* expression domain exceeds the one of *xbra* (Ryan et al., 1996). It was reported that *eomes* and *xbra* are able to promote cardiogenesis by inducing *mespa* expression and cardiogenesis from ES cells (Lescroart et al., 2010). Because stable gene regulatory networks rely on feedback loops and crossregulatory interactions, we wondered whether *mespa* might play a role in regulating the T-Box transcription factors *eomes* and *xbra* in the overlapping subpopulation of preinvoluted or involuting mesoderm.

3.2.1 Knockdown of *mesp* genes impairs expression of *xbra* in gastrula and neurula

To address this question I first performed a *mespa* knockdown experiment by using translation-blocking morpholinos (MO) for two early expressed *mesp* family members, i.e. *mespa* and *mespo*. The specificity and efficacy of these tools has been validated in previous studies from our lab (Kriegmair et al. (2013); Frenz (2017)). I injected 20ng of MO solution, specific for either *mespa*, *mespo*, or Control MO, together with *lacZ* mRNA into one cell of two-cell stage embryos. At this dose, the *mespa* MO is known to achieve maximal penetrance and strength of the knockdown phenotype.

Since the embryo’s laterality is determined by the position of the first cleavage furrow at the two-cell-stage, which gives rise to the left and right halves of the body, this type of injection manipulates one side of the embryo, while the other side serves as an internal control.

In this first experiment, I took a closer look at the effects of *mesp* protein knockdown on the panmesodermal markers *xbra* and *eomes* during gastrulation and neurulation. Notably, these genes are induced in the entire preinvoluted mesoderm, including organiser and non-organiser regions. While organiser-derived cells form head mesoderm and notochord, the non-organiser mesoderm is the origin of lateral and ventral mesoderm derivatives including heart, somites, muscles, kidneys and blood. Contrary to the model of Dale and Slack (1987), which suggested that the organiser patterns the ventrolateral non-organiser mesoderm, Kumano and Smith (2002) identified organiser-independent patterning of the marginal zone.

The *Xenopus tbxt* gene, of which the encoded protein is called BRA/brachyury, is one of the crucial mesoderm key regulators. It is induced at the beginning of gastrulation in a

ring-like, suprablastoporal domain. After closure of the blastopore, *xbra* mRNA is visible in the surrounding deeper cell layers, known as posterior mesoderm, and in a dorsal midline stripe, representing the notochord. At the neurula stage, *xbra* is only expressed by involuted cells in the posterior mesoderm and the notochord (i.e. axial mesoderm). MO-based knockdown experiments with *mespa* and *mespo* during gastrulation showed important alterations in *xbra* gene expression. In *mespa*-deficient embryos, *xbra* levels were strongly reduced (Fig. 2C) in nearly all injected embryos (n=61/63). Consistent with the finding that *xbra* is required for mesoderm involution and the subsequent formation of posterior mesoderm (Conlon, Sedgwick, Weston, & Smith, 1996), the blastopore failed to close in *mespa*-depleted embryos. In contrast, *mespo* depletion has no effect on the *xbra* domain and gastrulation (53/55 embryos), since no obvious blastopore closing defects were visible (Fig. 2 D). This shows that the effect of *mespa* knockdown on *xbra* expression differs from that of *mespo* knockdown.

To observe the dynamics of gastrulation after loss-of-function and a possible short-term compensation, my second end-point was set at early neurula stage (NF 14). Almost all *mespa*-deficient embryos exhibited blastopore closing defects and slightly reduced but broader stains. X*bra* expression was not ablated entirely, but was residual on the injected side. This might be due to its ability to maintain mesodermal stem cells and its own expression by an autoregulatory loop via fibroblast growth factor signalling (FGF) (Schulte-Merker & Smith, 1995). The broadening could be due to either insufficient dorsal convergence or anterior migration of the cells. Cells from the morphant side could not contribute to the formation of the notochord, leading to an asymmetrical morphology (see Fig. 2 F; 33/35 embryos). As Figure 2 G illustrates, *mespo*-deficient embryos (39/45 embryos) showed only slightly broader expression domains compared to controls (compare Fig. 2 E) and closed the blastopore at the same time as uninjected control embryos. In contrast to *mespa* morphants, *mespo*-deficient embryos only presented a subtle migratory defect.

These data allow us to distinguish between an early and a late effect of *mespa*. Since *xbra* expression was almost completely abolished in midgastrula (stage NF11), these data suggest an inductive potential of *mespa* in coexpressing cells. However, slightly later in time, *mespa* knockdown prevents *xbra*-expressing cells from involution and migration. This might be a consequence of a perturbed EMT during gastrulation itself and during neurulation, when convergent extension becomes important (see chapters 3.7 and 4.6).

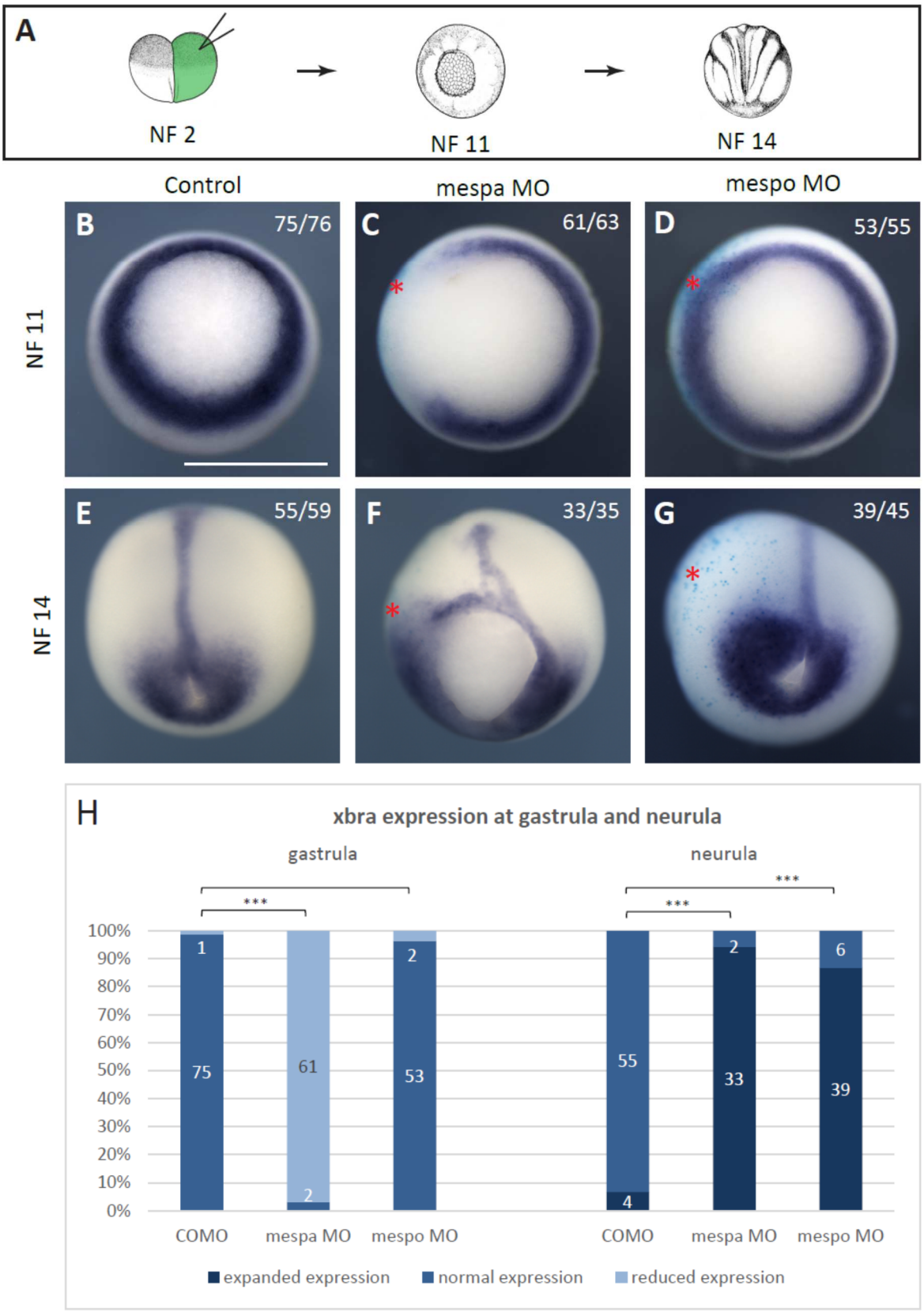

Figure 2: The regulatory interaction of *mesp* genes and *xbrachyury* during early development
20ng of morpholino were injected into one blastomere at the two-cell stage **(A).** mRNA is detected by whole mount *in situ* hybridisation. *Xbra* expression is strongly reduced in *mespa* morphants during gastrulation. *Mespa* and *mespo* morphants exhibit an expanded domain at the neurula stage. **(B) + (E)** *Xbra* expression in uninjected control, **(C) + (F)** *mespa* MO injected embryos, **(D) + (G)** *mespo* MO injected embryos. **(B - D)** Embryos during gastrulation with vegetal

view onto the blastopore. **(E - G)** Embryos during neurulation with view from dorsoposterior. **(H)** Phenotypic penetrance of *xbra* expression in gastrula and neurula stage embryos; ***, $p<0.0001$; n ≥ 5 biological replicates; red star indicates injected side; scale bar: 1 mm

Although the activating input from *mespa* is lost, *xbra* still possesses its own autocatalytic loop via fibroblast growth factor (FGF) signalling (Schulte-Merker & Smith, 1995). The RNA *in situ* hybridisation suggests that this feedback loop is not sufficient to provide normal mRNA levels in the absence of *mespa* during the initial activation of the gene, but it may compensate until NF 14. Over the course of gastrulation, *xbra*$^+$ cells need *mespa* to involute, as demonstrated by the fact that *xbra* cells piled up in NIMZ when *mespa* has been knocked down.

3.2.2 *Eomes* expression is regulated by *mespa* during gastrulation and neurulation

Eomes, another T-Box transcription factor, plays an important role during early mesoderm formation and specification. In contrast to *xbra*, *eomes* reaches its peak expression much earlier than all other panmesodermal transcription factors. As a bridge in mesendodermal fate selection, *eomes* can be induced by vegetal cells and mesodermal inducing factors. Both *xbra* and *eomes* are sufficient to initiate mesoderm formation and axial development. Expressed in the entire, preinvoluted mesoderm during gastrulation, *eomes*$^+$ cells contribute to the dorsal mesoderm and migrate anteriorly along with leading edge mesoderm during neurulation. Later during development, *eomes*$^+$ cells are exclusively found in the forebrain of *Xenopus* embryos due to an activation in neural cell lineages, independent from mesendodermal tissue (Mione, Shanmugalingam, Kimelman, & Griffin, 2001; Ryan, Butler, Bellefroid, & Gurdon, 1998).

The influence of the two *mesp*-genes on *eomes* did not show up as early as the effects of *xbra* do. Due to normal individual variability of the developmental age during gastrulation one could observe slight differences in expression. Most *mespa* morphants presented a mild increase in *eomes* expression (46/73 embryos; Fig. 3 B). Similar to the response of *xbra*, the *eomes* expression domain is broadened in *mespo* morphants (50/58; Fig. 3 C).

The neurula stage provided much more information concerning the developmental progression in the manipulated organisms. Most *mespa*-deficient embryos did not manage to close the blastopore. They failed to involute *eomes*-expressing cells, which piled up in a zone of preinvoluted deep layer cells that extended towards the animal pole (see Fig. 3 E). On the control side of the embryo, *eomes* mRNA was maintained in the leading edge mesoderm, while disappearing from the posterior involuted mesoderm. This

indicates that *mespa* expression is crucial for involution and that either an accumulation or a further stimulation of non-involuting *eomes*$^{+}$ cells occur.

The *mespo*-deficient embryos were characterised by a slight delay of mesodermal cell migration (33/42 embryos), although notably, they did arrive at their normal destination (compare Fig. 3 D, F). No blastopore closing defects could be observed and *eomes* expression was extinguished in the posterior mesoderm. Thus, *mespo* morphants seemed to go through gastrulation more easily than *mespa*-deficient embryos, which could imply a more important role for *mespa* during involution. The apparent expansion of expression domains in *mespo*, an effect which was even more pronounced in *mespa* morphants, allowed us to conclude that, due to a failure to close the blastopore, *eomes*-expressing cells of the IMZ could not involute properly. These results most likely suggest a migratory deficiency of *eomes*-expressing cells, as opposed to a direct interaction of *mesp* genes with *eomes*.

3.2.3 Interaction of *mespa* and T-box transcription factors does not persist until the tadpole stage

To extend the investigation of the effects of *mesp*-genes on panmesodermal markers during development, unilateral morphants were cultivated until the early tadpole stage (appr. stage NF 32). For a better assessment of gene expression patterns, Alexa 488 dextrane was used as lineage tracer for these experiments. Since Alexa fluorescence is extinguished during the RNA *in situ* hybridisation procedure, the embryo cohorts were sorted into left- and right-side-injected embryos prior to fixation (not shown) and processed separately. Hence, no additional colour (e.g. blue *lac*Z staining) interfered with the evaluation of expression patterns.

After gastrulation, *Xenopus bra*, although omnipresent in preinvoluted mesoderm, is maintained exclusively in the forming notochord. After neurulation is completed, *xbra* is expressed in the chordoneural hinge and posterior wall of the forming tail, i.e. posterior-most mesoderm, also known as tail bud blastema, which is an unpaired entity (Beck & Slack, 1998). At the endpoint, embryos differed slightly concerning their developmental stage, which is normal. Yet all control embryos and 51 out of 53 *mespa* morphants showed a normal *xbra* expression (compare Fig. 4 A – D), which, as far as we can tell from these analyses, points to a compensation over time of the early temporary *mespa* effects. *Mespo*

morphants were not analysed for this condition, because the effect of the knockdown was already marginal at the neurula stage.

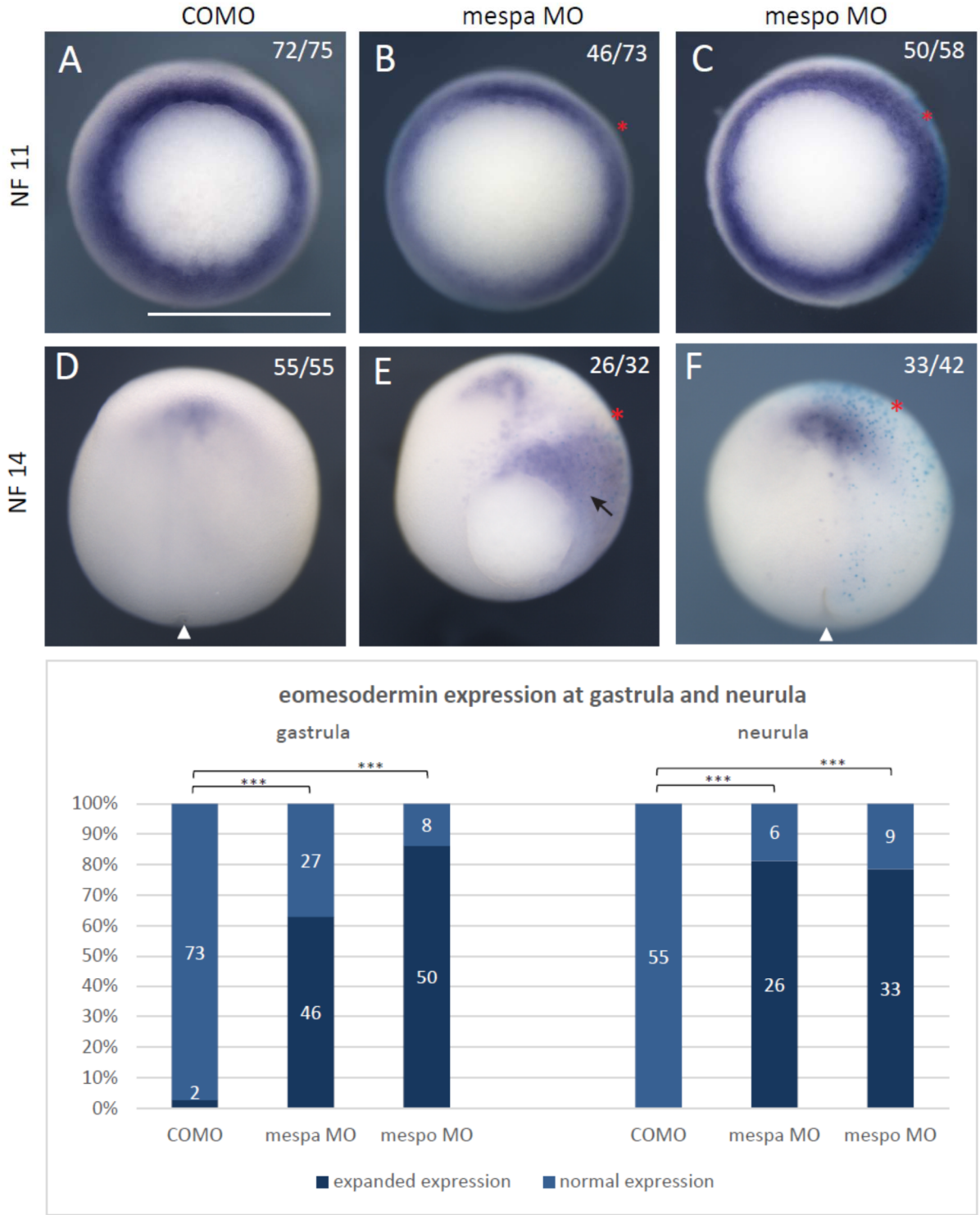

Figure 3: *Eomesodermin* expression is regulated by *mesp* genes during gastrulation and neurulation
20ng of morpholino were injected into one blastomere at the two-cell stage. Embryos were collected at the gastrula stage (NF 11) respectively neurula stage (NF 14). *Eomes* expression was analysed by subsequent whole mount *in situ* hybridisation. **(A - C)** Gastrula stage, view from posterior, dorsal is on top; **(D - F)** Neurula stage, view from dorsoposterior. **(A) + (D)** Uninjected control embryos. **(B) + (E)** *mespa* MO injected embryos. **(C) + (F)** *mespo* MO injected embryos. **(D)** *mespo* MO injected embryo rotated dorsal view. White arrowhead indicates closed blastopore. Black arrow points out uppiling *eomes*$^{+}$ cells, which do not manage to involute. **(G)** Distribution of *eomes* phenotypes of control, *mespa* and *mespo* morphants at the gastrula and neurula stage; n≥4 biological replicates; ***, $p<0.0001$; red star indicates injected side; scale bar: 1 mm.

Taking part in mesoderm induction during early mesoderm formation, *eomes*-expressing cells migrate anteriorly at the mesodermal leading edge after involution in order to contribute to axial development. After down-regulation in mesodermal cells at the late neurula stage, *eomes* expression is activated de novo in neuronal tissue of the telencephalon at the early tail bud stage (Ryan et al., 1998). In tadpole-stage embryos, the two separated hemispheres are the only areas in which *eomes*-expressing cells can be found.

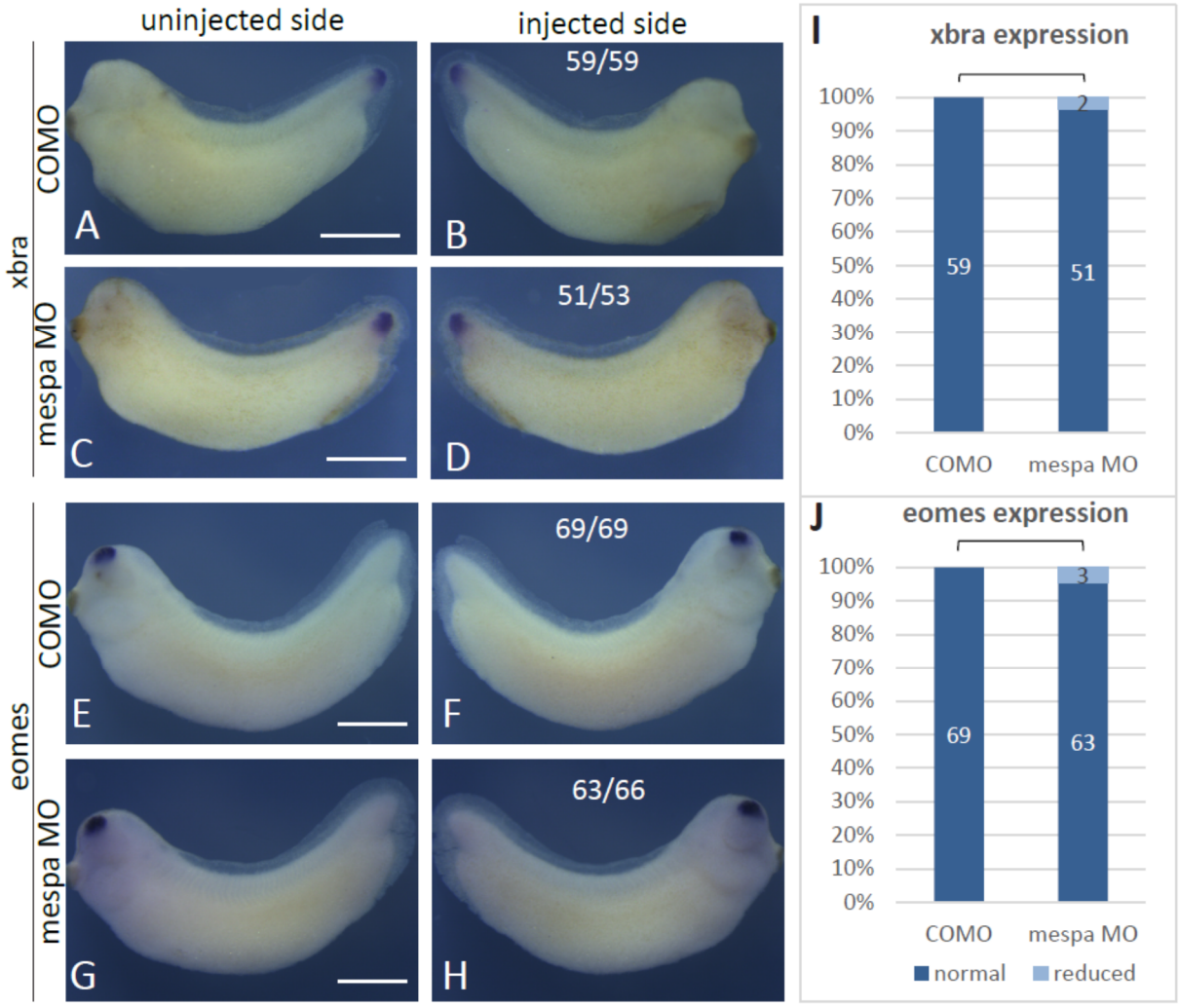

Figure 4: *Mesp* interaction with panmesodermal genes is not persistent until the tadpole stage
All embryos have been injected into one side at the two-cell stage with 20 ng of morpholino and Alexa 488 and sorted into left and right side injected before proceeding. The expression pattern was analysed by whole mount RNA *in situ* hybridisation at the tadpole stage (NF 32). At NF 32, *xbra* is only expressed in the posterior-most mesoderm of the tailbud **(A - D)**. Mesodermal *eomes* expression has ceased and is activated in the telencephalon from tailbud stage on **(E - H)**. No significant alterations of the expression patterns could be observed after *mespa* knockdown. Phenotypic penetrance of *xbra* **(I)** and *eomes* expression **(J);** $p > 0.05$; n = 3 biological replicates; scale bar represents 1mm.

In my knockdown experiments, *mespa*-depleted embryos at the tadpole stage showed normal *eomes* patterns in contrast to earlier stages of development. All controls and 63 out of 66 *mespa* morphants presented a normal expression pattern (Fig. 4 E – H). Hence,

morphant and control expression did not differ significantly. As expected due to the lack of any lineage relation, *mespa* did not influence *eomes* expression cells in the telencephalon.

In summary, the loss-of-function experiments of *mesp*-related genes at the gastrula, neurula and tadpole stages revealed an important loss of *xbra* expression in the preinvoluted mesoderm during the early development of *mespa*-deficient embryos. This loss persisted until neurulation, but recovered until the tadpole stage. Moreover, it has to be considered that within the tail bud blastema, as an unpaired entity, it is very difficult to distinguish from which side cells originate in order to contribute to the formation of the blastema. However, *mespo*-depleted embryos showed a slight expansion of the *xbra* domain during gastrulation and neurulation.

Concerning *eomes* expression, knockdown of *mesp*-related genes led to an expansion of expression most pronounced for *mespa* during neurulation due to blastopore closing defects and prevention of involution. Further assessment of the dynamics of *eomes* expression until tail bud stage, when *eomes* expression is downregulated in mesoderm, would be necessary to define the exact way and timepoint of a possible compensation over time after mespa knockdown. Anteroposterior patterning of the CNS involves signals from the underlying axial mesoderm. The observed normal *eomes* expression in the telencephalon indicates indirectly that the *mespa* knockdown has no lasting consequences on this process.

All modifications appear to be transient, as modified embryos showed rather normalised expression patterns in later developmental stages. However, the most striking impact after *mespa* knockdown occurred in dorsolateral mesoderm in which *xbra* expression was lost during gastrulation and *xbra*$^{+}$ cells of the injected side failed to contribute to notochord formation. Paraxial (presomitic) mesoderm flanks axial (dorsal) mesoderm and is subdivided into somites, giving rise to muscles and connective tissues. The following investigations focus on these mesodermal derivatives.

3.3 Skeletomyogenesis / Differentiation of mesodermal derivatives

Since *mesp*-related genes play important roles during somitogenesis (Durbin et al., 2000; Sawada et al., 2000), a contribution to skeletomyogenesis can be expected. Recent publications reveal that trunk and head muscle development are subject to different regulatory mechanisms (Harel et al., 2009). It was unveiled by clonal analysis that head muscles and cells from the second heart field derive from common progenitors (Lescroart et al., 2010). Depending on the time point and context of *mesp1* activation, cell lineages can be driven to cardiovascular, haematopoietic or skeletomuscular identity (Chan et al., 2013). Chan et al. (2013) state three conditions under which *mesp1* is able to favour haematopoietic development: *mesp1* activation in an early responsive window (first wave), the absence of Wnt-signaling and the presence of enhancer-binding-factor E12 as a binding partner. In a second wave, *mesp1* can promote cardiovascular lineage, and, in the absence of serum-derived factors, even skeletomuscular development, primarily of head muscles. As Figure 1 depicts, *mespa* and *mespo* expression patterns clearly overlap with myogenic transcription factors *myoD* and *myf5* in the preinvoluted mesoderm during gastrulation. Moreover, fate mapping demonstrated a relation of *mesp*-genes and muscle progenitors in dorsolateral mesoderm. In light of these findings, and to further verify the relevance of *mespa*, I investigated the expression of key myogenic regulatory factors in *mesp*-morphant embryos.

3.3.1 *Mesp*-genes influence expression of myogenic bHLH transcription factors

The myogenic regulatory factors (MRF) are a family of bHLH transcription factors that comprises *myoD*, *myf5*, *myogenin* and *MRF4*. Forming heterodimers with E-Proteins like E12 or E47, MRFs bind to the promotors of muscle target genes, thereby committing myogenic precursor cells to become skeletal muscle (Olson, 1990; Weintraub et al., 1991). The *myoD* gene is equipped with an autocatalytic feedback loop to promote and maintain its own expression, in addition to the ability to cross-activate other MRFs (Braun et al., 1989; Steinbach, Ulshofer, Authaler, & Rupp, 1998).

In the first wave of myogenesis, *myoD* is expressed in the entire marginal zone except for the prospective axial mesoderm i.e. the notochord (Della Gaspera et al., 2012), while *myf5* expression is restricted to the dorsolateral mesoderm (Sabillo, Ramirez, & Domingo, 2016). At the neurula stage, *myoD* and *myf5* remain in the unsegmented PSM, from which

somites arise. At the tadpole stages, which cover the second myogenic wave, *myf5* is chiefly expressed in differentiating cells of the epaxial and hypaxial myotome. *MyoD* can be found in the segmented myotome of developing somites. There, *myoD* mRNA is arranged around the nuclei of vertically stacked myoblasts. Moreover, Maguire, Isaacs, and Pownall (2012) demonstrated a reverse relationship of activation: While *myoD* fosters *myf5* expression in early mesoderm, the opposite can be said of *myoD's* effect on *myf5* in somites.

In my study, I first obtained information about interactions between *mesp*-genes and the myogenic markers through loss-of-function experiments based on a unilateral injection of 20ng of MO into two-cell-stage embryos (Fig. 5). In each case, the injected side was traced by the activity of ß-galactosidase after *lacZ* mRNA coinjection. The majority of *mespa*-deficient embryos showed no expression of *myoD* at the gastrula stage (Fig. 5B; 35/38 embryos), while *mespo* ablation rendered a strongly reduced phenotype (Fig. 5C; 27/33 reduced, six normal). As development progressed, striking effects on myogenic precursors were observed.

At the neurula stage, *mespa* morphants closed their blastopores belatedly and asymmetrically, which deforms the regular shape of the presomitic myogenic mesoderm into *myoD*-positive wing-like structures (Fig. 5 E). Anterior migration of the leading edge mesoderm and the consequent pulling of the mesodermal mantle appeared to proceed more slowly and less efficiently on the manipulated side. Additionally, the majority (36/47 embryos) still showed a significantly reduced *myoD* expression. *Mespo* morphants did already show largely normal expression patterns by the neurula stage, with symmetrically and equally stained domains, as displayed in Fig. 5 F.

Myf5 expression is similarly affected in *mespa* and *mespo* morphants, as one can see in Figure 6 B and C. 62 out of 64 *mespa* morphants showed a sharply reduced or completely absent expression, while expression in *mespo* morphants was strongly downregulated, but not lost (53/63 embryos). Fig. 6 E illustrates that, at the neurula stage, the alterations of *myf5* expression in mespa morphants were consistent with those found for *myoD*: they presented an asymmetrical and twisted pattern due to cell movement and elongation being perturbed on one hand, and the reduction of intensity and size of the expression domain (22/24 embryos) on the other hand. This demonstrates a persisting, but partly compensated effect on *myf5* transcription. *Mespo* morphants restore *myf5* expression up to the neurula stage and achieve a slightly expanded expression domain (Fig. 6 F; 24/42

embryos expanded, 18 normal), which could be explained by a migratory deficit. Yet sections revealed that the number of *myf5*$^{+}$ cell layers remained more or less constant. Up to and during the neurula stage, embryos developed symmetrically, achieving blastopore closure just before neurulation.

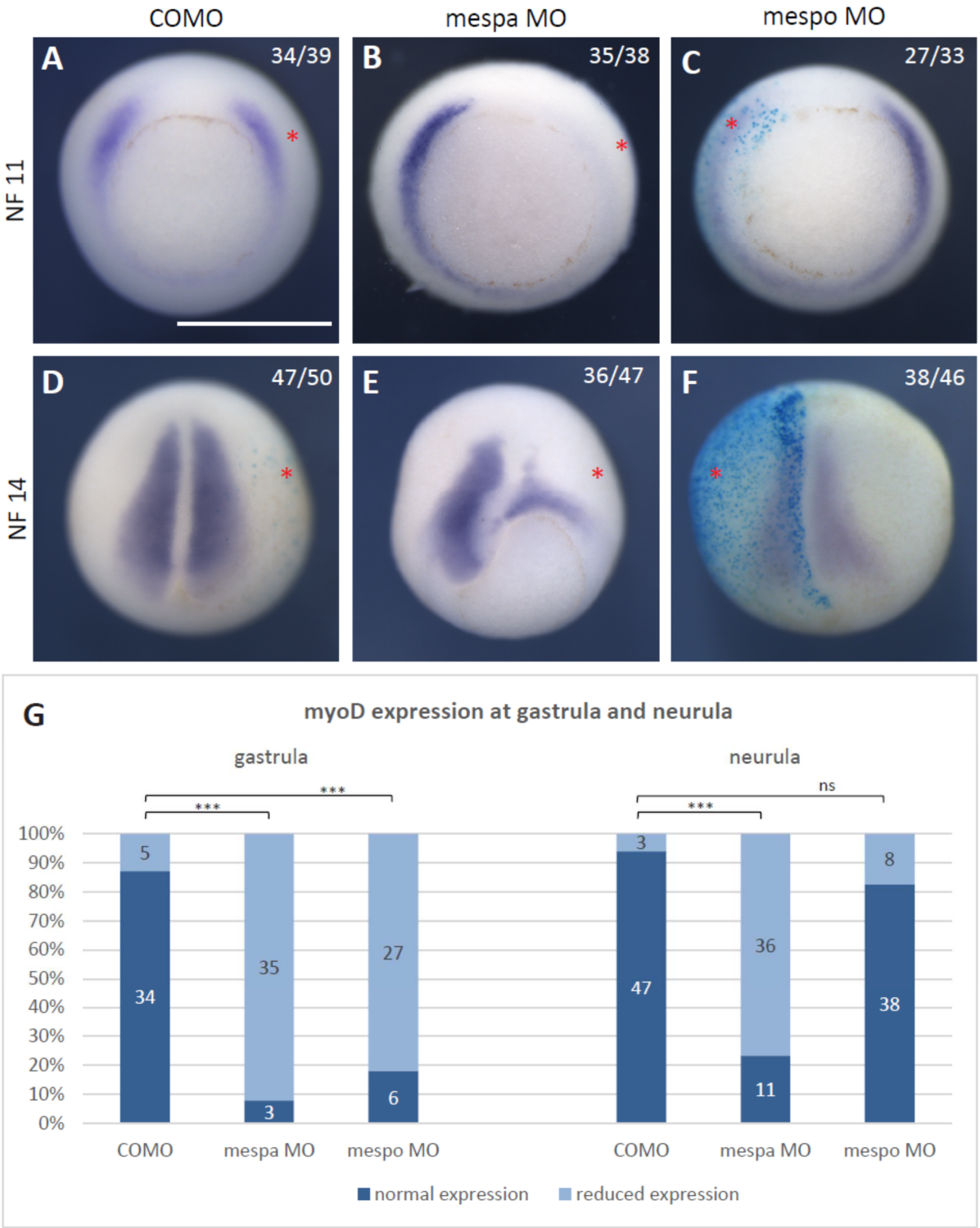

Figure 5: *Mesp* genes show striking impact on myogenic progenitors expressing *myoD* during early development
Two-cell-stage embryos were injected unilaterally with 20ng of morpholino. Embryos were observed at the gastrula respectively neurula stage by whole mount RNA *in situ* hybridisation. A noticable abolishment of the *myoD* stain at the

gastrula stage and reduction at the neurula stage can be observed. Reduction of *myoD* expression in *mespo* morphants seems to be transient and is normalised until the neurula stage. **(A - C)** NF 11, view from posterior onto blastopore; **(D - F)** NF 14, dorsoposterior view; **(G)** Analysis of phenotypic distribution of *myoD* expression at the gastrula and neurula stage; ***, $p<0.0001$; **ns**, not significant; n≥3 biological replicates; red star shows injected side; scale bar: 1mm.

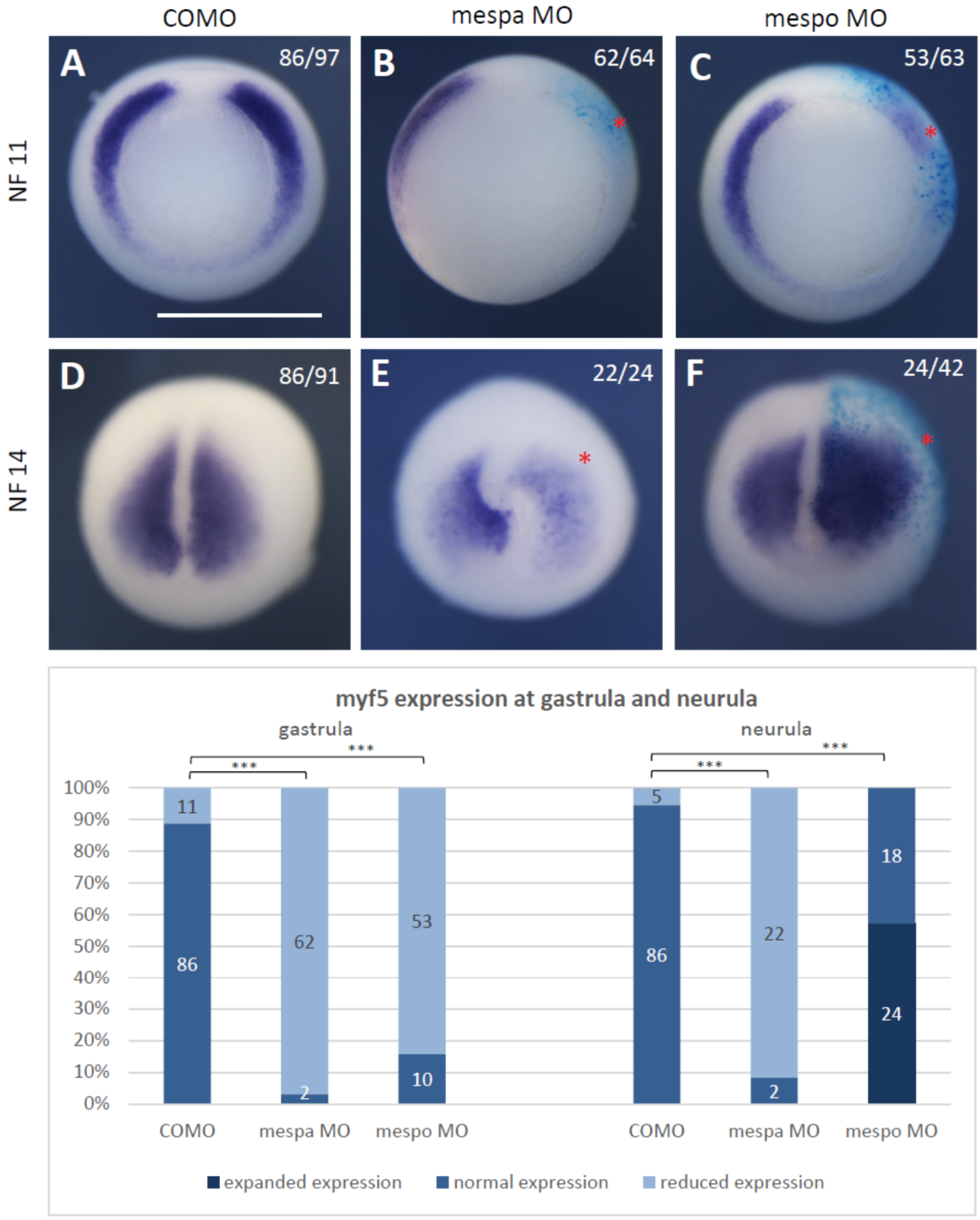

Figure 6: *Mesp* genes influence myogenic determination during early development
20 ng of morpholino have been injected into one blastomere at the two-cell-stage. Embryos were analysed at NF 11 and NF 14 by whole mount RNA *in situ* hybridisation. *Mespa* depleted embryos show abolished expression at the gastrula stage and a reduced stain at the neurula stage. A reduction at the gastrula, but an expansion and enhancement of the expression is visible in *mespo* MO injected embryos. Red star shows injected side; **(A - C)** NF 11, view from posterior onto the blastopore, **(D - F)** NF 14; dorsoposterior view; **(G)** Phenotypic distribution of *myf5* expression pattern during gastrulation and neurulation; ***, $p<0.0001$; n≥3 biological replicates; scale bar: 1mm.

Summarising the results from loss-of-function experiments of *mespa* and *mespo*, one can observe an early gastrula stage abolishment of the myogenic markers *myf5* and *myoD*, which can be partly restored during neurulation in *mespa* morphants. *Mespo* depletion only leads to a short and temporary down-regulation of myogenic markers. This suggests a transient effect and a compensatory mechanism.

3.3.2 Reduction of myogenic markers in *mespa*-depleted embryos persists until the tadpole stage

In light of this development, I wanted to know whether this early reduction or absence of myogenic expression due to *mespa* depletion persists until the tadpole stage, when organogenesis is completed. Hence, I injected Alexa 488 and 20ng of either *mespa* MO or COMO, and cultivated the embryos up until the tadpole stage, while replacing the cultivation buffer and grids on a daily basis. At the tadpole stage (NF 32), embryos were sorted into left- and right-side injected groups based on their fluorescence.

As Figures 7 C and D illustrate, early *mespa* depletion even led to a strong reduction of *myoD* expression at the tadpole stage and a lack of body axis elongation. More than 80% of morphants presented with such a growth deficit, which appeared to be caused by perturbed somitogenesis.

Upon comparing *mespa* morphants with controls, statistical analysis revealed a reduction of the mean somite count on the injected sides by 14 somites (six somites on the injected side of *mespa* morphants vs. 20 in control embryos) (Fig. 14). Even the uninjected sides were indirectly affected due to the unilateral growth retardation of the *mespa*-morphant embryos. The normal process of somite formation from anterior to posterior could not occur properly in *mespa* morphants. *MyoD* expression of most embryos was restricted to the unsegmented PSM and did not extend to the segmented myotome. This led us to conclude that either anterior cells did not express *myoD*, or *mespa*-deficient mesodermal cells were unable to allow the mesodermal mantle to migrate anteriorly. This process takes place long before actual segmentation, which marks the second wave of myogenesis. Hence, the effect of *mespa* on mesodermal cells from the first wave is prolonged, and remains visible through to later stages.

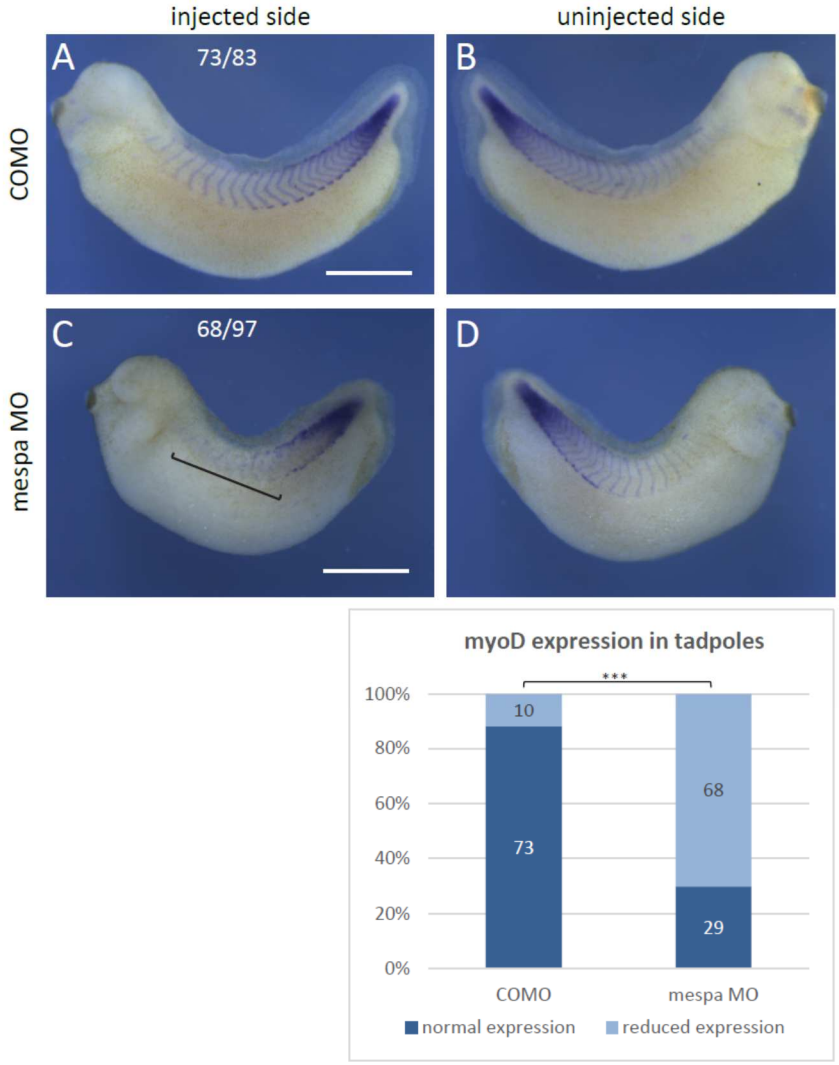

Figure 7: Myogenic progenitors require early *mespa* activation for expression at the tadpole stage
Embryos were injected with 20ng of morpholino into one blastomere at the two-cell-stage. *MyoD* expression patterns were analysed by whole mount RNA *in situ* hybridisation. **(A) + (B)** COMO. **(C) + (D)** *mespa* morphants show lacking anterior somites (bracket), a shortage of axis and a reduced number of somites. **(E)** Phenotypic distribution of *myoD* expression in tadpoles; n ≥ 3 biological replicates; ***, $p<0.0001$; scale bar: 1mm.

With the same experimental approach, we investigated the influence of *mespa* knockdown on *myf5* expression at the tadpole stage (NF 32). Since *myf5*'s expression pattern is more complex, I distinguished four expression domains: the trunk with the hyp- and epaxial cell lineages, the branchial arches, the jaw and, lastly, the extraocular eye muscles (Figure 8).

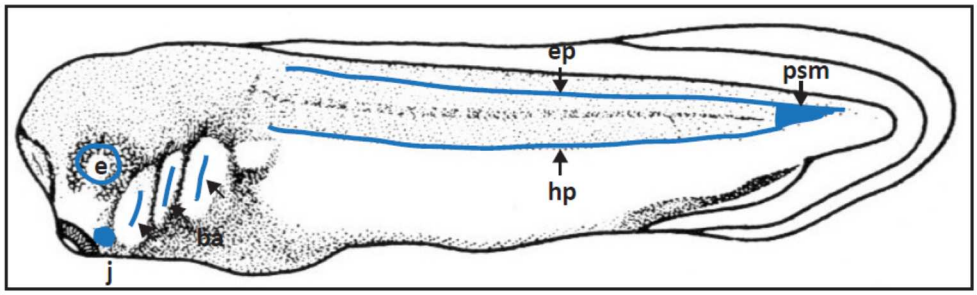

Figure 8: *Myf5* expression pattern in tadpole embryos (NF 32)
From rostral to caudal: **e**: eye muscles, **j**: jaw, **ba:** branchial arches, **ep:** epaxial myotome, **hp**: hypaxial myotome, **psm**: presomitic mesoderm

Expression in the myoblasts in these areas can be uncovered by *in situ* hybridisation at different developmental stages. From posterior to anterior, *myf5* expression first becomes visible in the PSM, then in the trunk and the jaw, followed by the branchial arches and, finally, by the periocular muscles. Interestingly, early effects of *mespa* knockdown endured over the entire course of development.

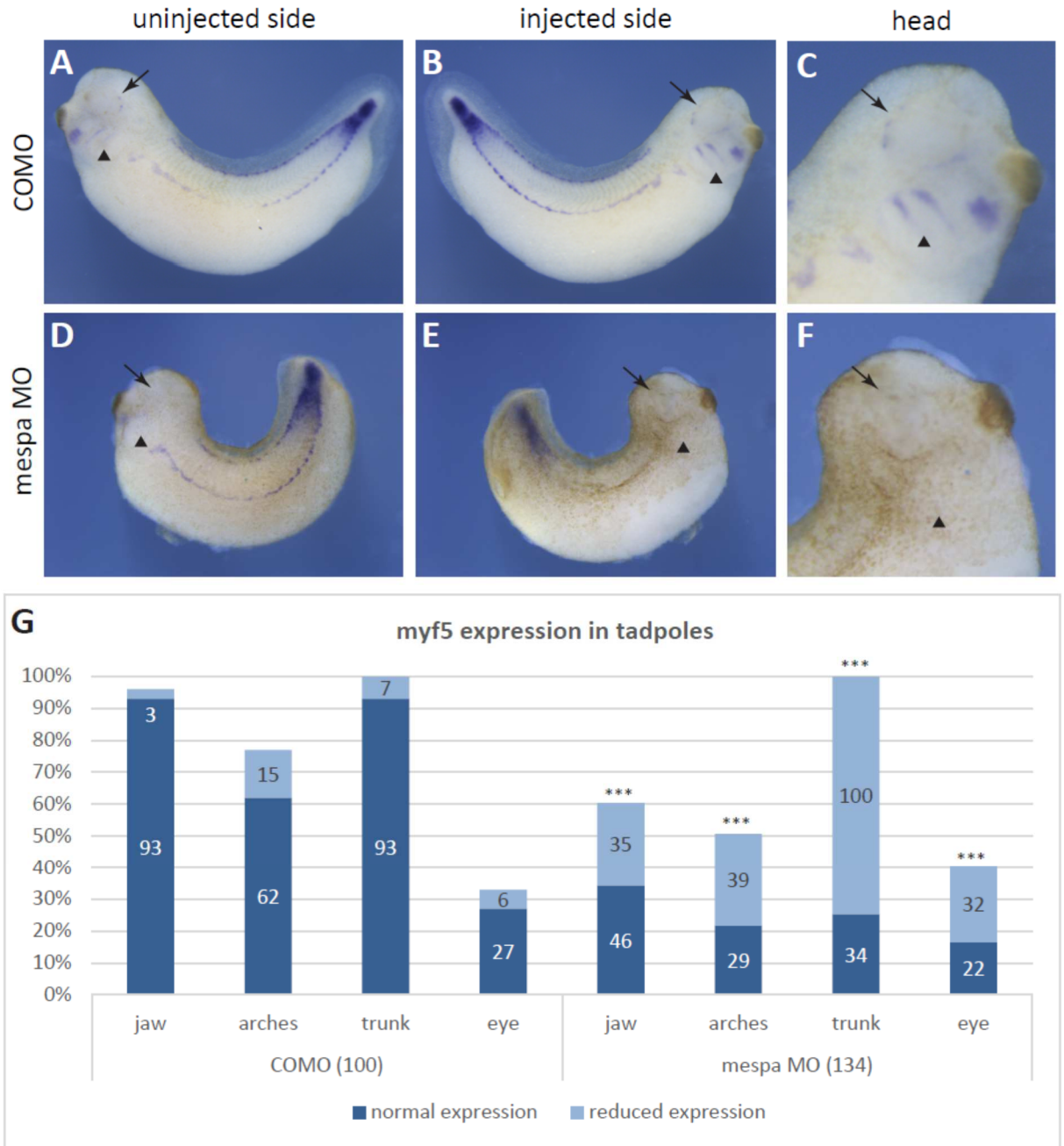

Figure 9: *Mespa* depletion leads to massive loss of *myf5* expression in tadpole embryos
20ng of morpholino (COMO and mespa MO respectively) were injected into one blastomere of two-cell stage embryos. Embryos were cultivated and sorted at NF 32 and subsequently whole mount RNA *in situ* hybridisation was performed for *myf5*. Compared to controls, *mespa* deficient embryos lack *myf5* expression especially in the jaw, eye muscles, branchial arches and trunk area. Images show lateral view onto the injected **(B + E)** and uninjected side **(A + D)** of COMO or *mespa* MO injected embryos. **(C) + (F)** Magnifications of the head region. **(G)** Differential *myf5* expression analysis of modified embryos in distinct *myf5* expressing areas. Total number of analysed embryos in brackets. Arrow heads point at branchial arches. Arrows indicate eye region. ***, $p<0.0001$; n≥3 biological replicates; scale bar indicates 1mm.

As shown in Figure 9, *myf5* expression was mainly reduced in *mespa* morphants, and exclusive to the presomitic mesoderm. Due to the delay in development in the *mespa*-depleted embryos and the lack of elongation, the majority of the "retarded" embryos only exhibited trunk staining in the PSM. Moreover, *mespa*-deficient embryos did not manage to elongate properly and exhibited a shortened axis. This retardation in development resulted in an absence of *myf5* expression in the extraocular muscles, the branchial arches and the jaw at my study's predefined end point (Fig. 9 E, F). The control side was only marginally influenced.

In these experiments, *mespa* knockdown at early time points led to a significant reduction of myogenic expression of both *myf5* and *myoD*, which could not be compensated during later development.

3.3.3 Myogenic gene expression can be rescued by coinjection of *xmespa* mRNA

Up to this point, knockdown experiments had given a first impression of interaction and regulatory cascades, but had not provided any proof of specificity of *mespa*'s effects on either panmesodermal or myogenic markers. Specificity of phenotypes can be proven by rescue experiments and subsequent overexpression experiments to test direct inducibility. Since my research focused on the persistence of – and compensation for – early effects through to late developmental stages, overexpression and rescue experiments concerning those early stages were not performed.

Subsequently, we investigated the specificity of the effect of *mespa* knockdown on the phenotype of myogenic transcription factors *myoD* and *myf5*. To see a possible dose-dependent effect, I coinjected 20ng of *mespa* MO with either 500pg or 750pg, of morpholino-insensitive *xmespa* mRNA into one blastomere of two-cell-stage embryos. The injected sides were identified by Alexa 488 lineage tracing. In the trial with 500pg, embryos were more likely to be retarded in their development and show a morphologically reduced *myoD* expression pattern, effects comparable to those of single *mespa* knockdown (Fig. 10 A, B). As for the somite count, the injected and uninjected sides still differed significantly, by five somites. However, compared to *mespa* MO the mean number of somites were higher on both sides (Fig. 14). Moreover, injection of 750pg of *xmespa* mRNA demonstrated the capacity to restore *myoD* expression in tadpoles.

Embryos tended to be shaped as would be expected of wild-type embryos and more than half of the embryos showed a normal expression pattern in their somites (Fig. 10 C, D).

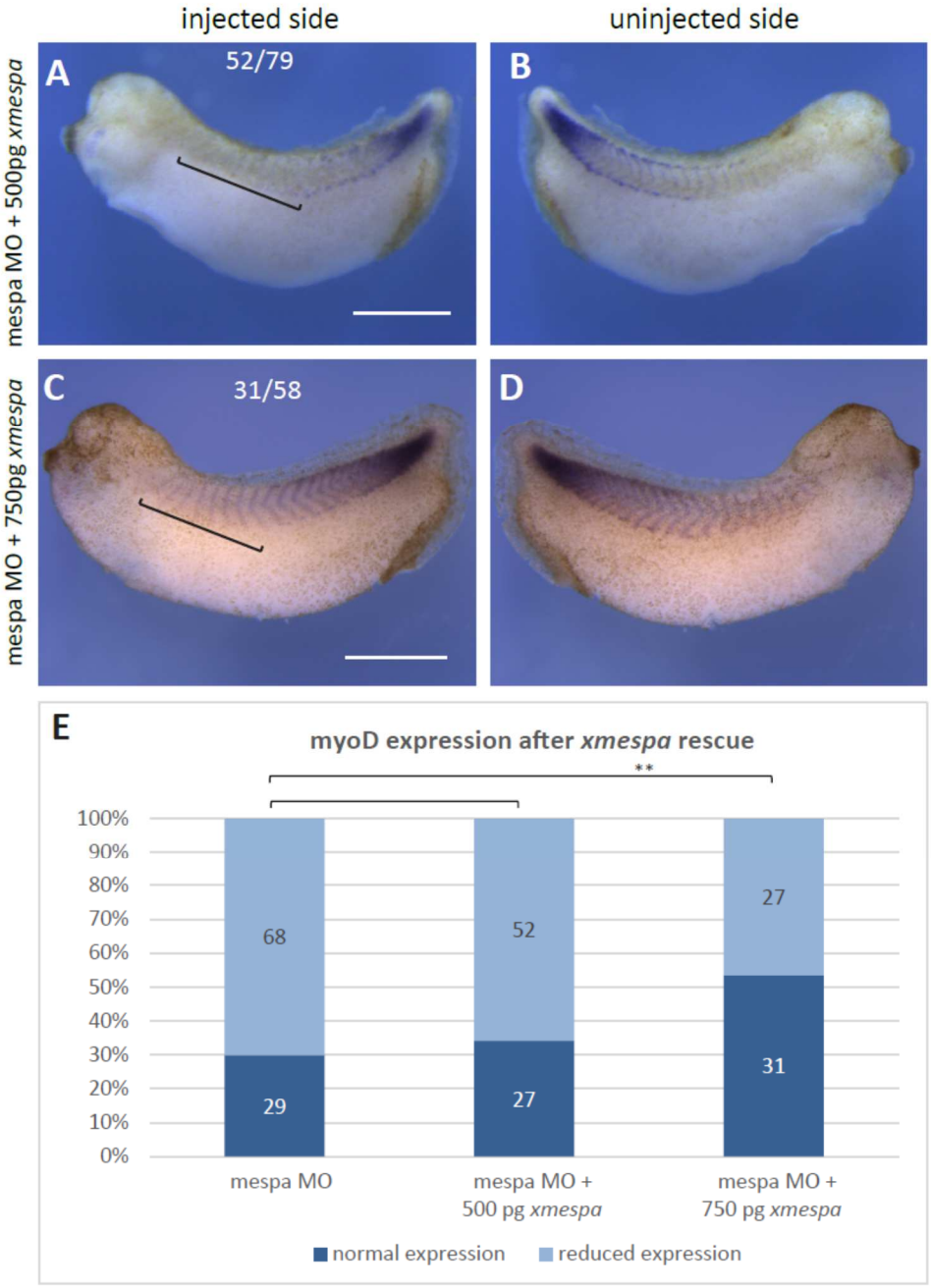

Figure 10: *MyoD* expression in tadpoles can be rescued by coinjection of *xmespa* mRNA dose-dependently
Injections of 20ng of morpholino plus 500pg and 750pg *xmespa* mRNA respectively were performed unilaterally at the two-cell stage. At the tadpole stage (NF 32) whole mount RNA *in situ* hybridisation was performed: **(A) + (B)** *mespa* MO + 500pg *xmespa* mRNA. The embryos' development is less retarded, but the expression is still reduced in the majority of the cases. **(C) + (D)** *mespa* MO + 750pg *xmespa* mRNA. A higher dose of *xmespa* mRNA is able to rescue the phenotype as regards the length of the axis and the *myoD* expression pattern. Brackets indicate anterior somites that could be reestablished with a higher dose of *xmespa* mRNA. **(E)** Phenotypic penetrance of *myoD* expression in tadpoles under rescue conditions in three independent biological repeats, n ≥ 3 biological repeats; **, $p<0.01$; Scale bar represents 1mm.

A similar dose-dependent rescue was observed for *myf5* expression. As Figure 11 depicts, coinjection of *mespa* MO and 500pg *xmespa* mRNA did not lead to a rescue of the phenotype. Embryos stayed shortened and, in most of them, *myf5* expression remained

restricted to the PSM (Fig. 11 A, B, C). However, at a dose of 750pg per embryo, coinjected *mespa* mRNA restored the penetrance of *myf5* expression in *mespa* morphants. The majority of these embryos appeared wild-type-like, displayed normal *myf5* expression in the jaw, the trunk and the branchial arches (Fig. 11 D, E, F). However, *myf5* mRNA was still reduced in extraocular muscles. The proportion of embryos with normal to reduced expression did not change, but the embryos expressing *myf5* in jaw and eye muscle progenitors as well as branchial arches made up a larger fraction of the total population. *Myf5* expression in epaxial and hypaxial myoblasts was rescued significantly (Fig. 11 G).

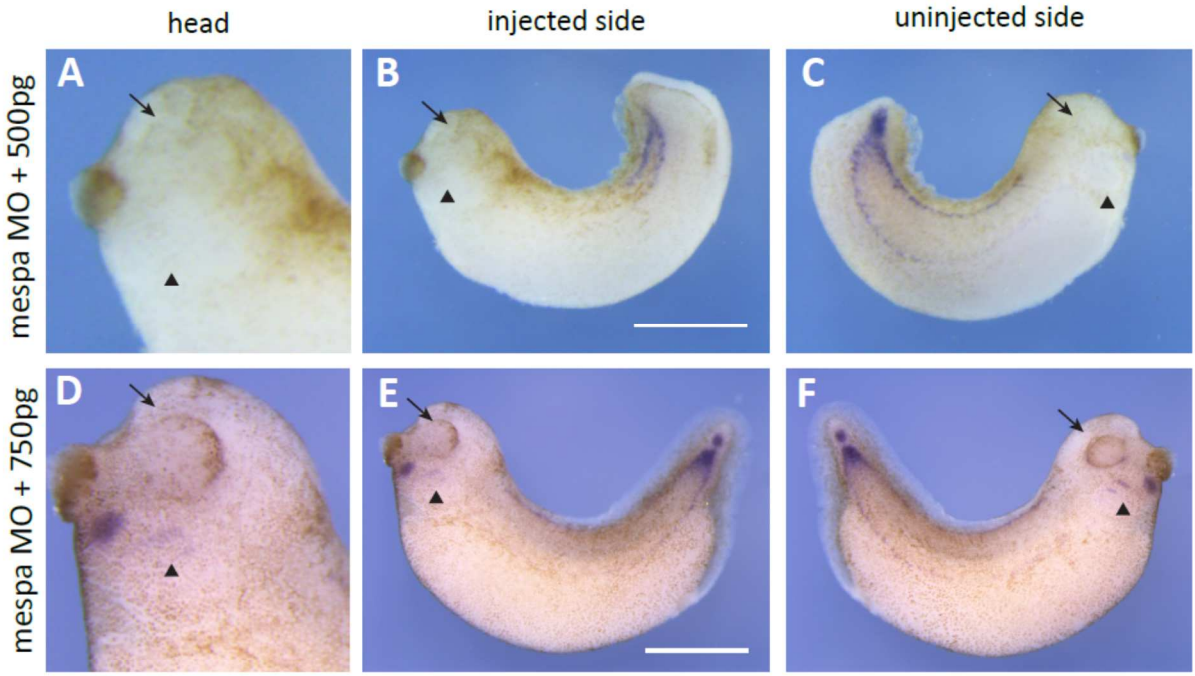

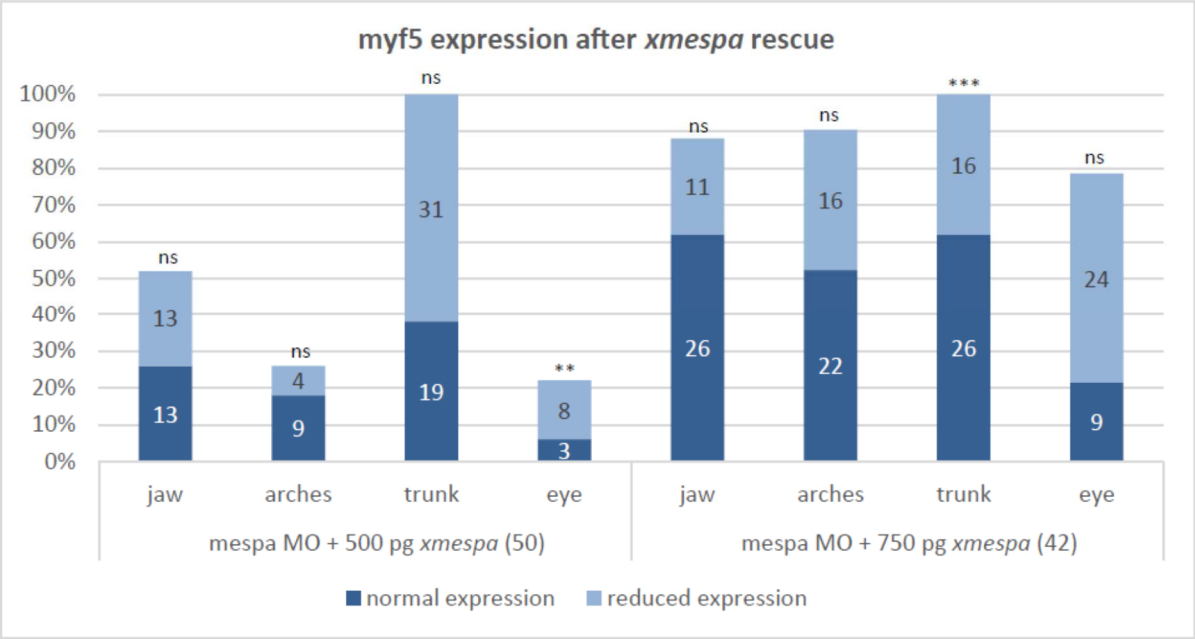

Figure 11: *Xmespa* mRNA has the power to rescue *myf5* expression of tadpoles dose-dependently
500pg and 750pg of morpholino insensitive *xmespa* mRNA were coinjected with 20ng of *mespa* MO. Embryos were cultivated until the tadpole stage, sorted and analysed by whole mount RNA *in situ* hybridisation. The rescue with 500pg mRNA is insufficient and embryos still exhibit big losses of *myf5* expression comparable to *mespa* MO alone. Coinjection of 750pg *xmespa* mRNA restores the *myf5* phenotype at least partially regarding length growth and expression in the trunk myotome. Additionally it increases importantly the rate of embryos expressing *myf5* due to the compensation of developmental delay. Arrowhead points at branchial arches. Arrow indicates eye region. **(A) + (D)** Magnifications of the head region. **(B) + (C) + (E) + (F)** Lateral view onto injected and uninjected side. **(G)** Differential *myf5* expression analysis in four distinct regions of the embryo. Significance was tested comparing expression of single domains of embryos under rescue conditions with those of *mespa* morphants. **, $p<0.01$; ***, $p<0.0001$; n=3 biological replicates; scale bar represents 1mm.

All in all, these experiments prove the specificity of the effect of *mespa* depletion regarding *myoD* and *myf5* expression in tadpoles. *Xmespa* mRNA was shown to have a dose-dependent capacity to restore normal expression patterns of myogenic markers, increase the number of somites to normal values, and salvage the linked elongation process. This indicates a requirement for *mespa* for normal myogenesis but also suggests an involvement of *mespa* in somitogenesis.

3.3.4 Overexpression of *xmespa* mRNA in whole mount embryos does not cause ectopic expression of myogenic transcription factors

To see whether *xmespa* is sufficient to induce ectopic expression of *myf5* and *myoD*, I injected *xmespa* mRNA into one blastomere at the two-cell stage and cultivated the embryos until the tadpole stage.

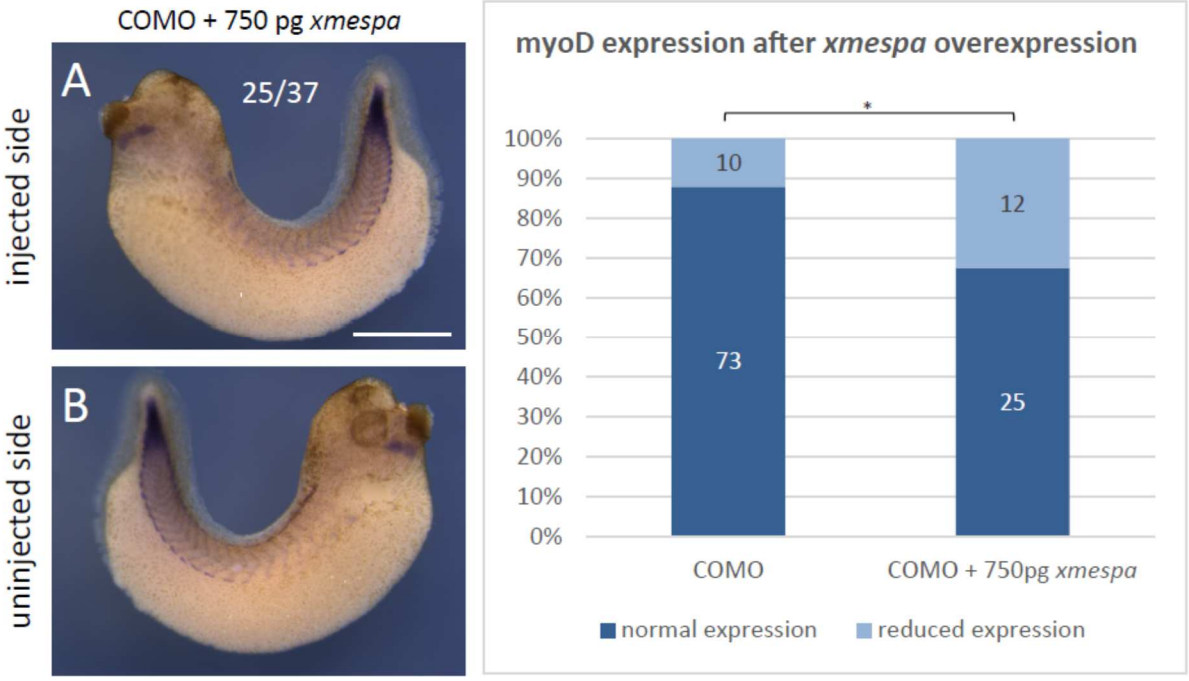

Figure 12: *Xmespa* overexpression leads to a significant reduction of *myoD* expression and no ectopic activation
20ng COMO and 750pg *xmespa* mRNA were injected into one blastomere at the two-cell stage. **(A) + (B)** Whole mount *in situ* hybridisations of tadpole embryos after early COMO + 750pg *xmespa* mRNA treatment. An overexpression of *xmespa* mRNA can also lead to the reduction of *myoD* expression and somite number, which was present in one third of

the population. **(C)** Chart shows phenotypic distribution of *myoD* expression patterns. n ≥ 3 biological replicates; *, $p<0.05$; Scale bar: 1mm.

I did not observe any ectopic expression of myogenic markers nor an enhancement of the stain. A significant proportion of embryos were physically shortened. Embryos developed four somites less on the injected side than they did on the uninjected side (Fig. 14). One third of embryos stained for *myoD* exhibited reduced expression (Fig. 12) ($p<0.05$). When analysed for *myf5* expression, embryos subjected to *xmespa* overexpression were of a similar phenotype as those stained for *myoD*, with slightly shortened body axes and no visible ectopic or enhanced staining. Their main deficits occurred in cranial structures of mesodermal origin like the extraocular muscles and the branchial arches (Fig. 12A, B).
In addition, *myf5*-expressing myogenic precursors of the trunk were depleted in about half of the embryos, which could be seen frequently in a bending of the embryo towards the injected side. *Myf5* expression was significantly reduced in all analysed subdomains ($p<0.0001$ or $p<0.01$; Fig. 13 C).
This experiment showed that *mespa* mRNA overexpression does not drive ectopic expression of myogenic markers *myoD* and *myf5* in vivo and cannot induce myogenesis on its own. However, embryos appeared posteriorised with a reduced expression of myogenic markers, shortened axes and perturbed formation of the head muscles. Since, in this assay, *xmespa* was also overexpressed in areas critical for cell migration like the neural crest, the phenotype after overexpression can be at least partially explained by disturbed migratory processes.

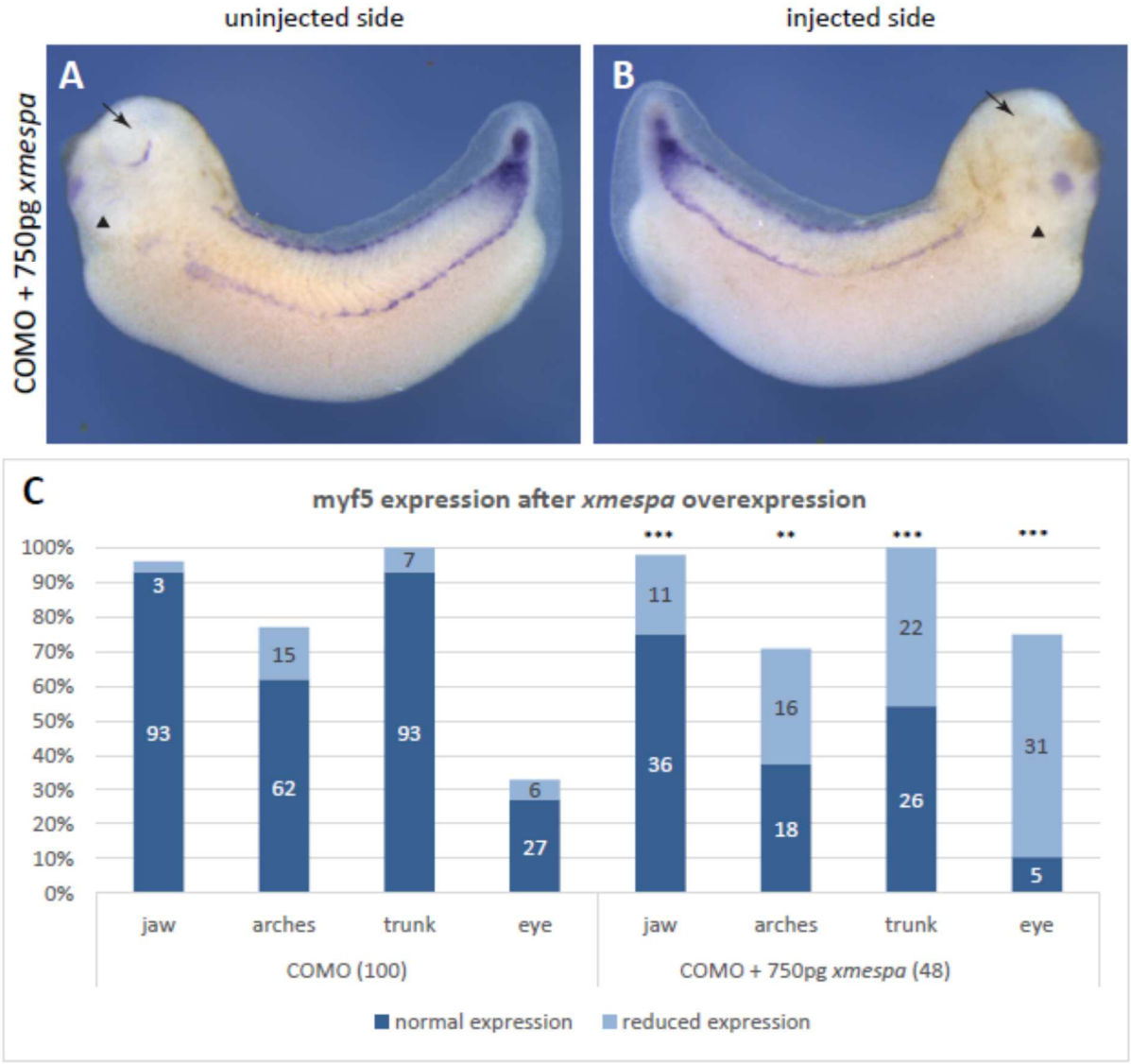

Figure 13: *xmespa* overexpression causes reduction of *myf5* expressing cranial structures
750pg *xmespa* mRNA were coinjected with with 20ng COMO. Embryos were cultivated until and sorted at the tadpole stage (around NF32). Subsequently whole mount RNA *in situ* hybridisation was performed to analyse *myf5* expression pattern. Embryos exhibited more likely a loss of jaw (not visible in the image above) and eye muscles, a reduction of the branchial arches and the ep- and hypaxial myotome in the trunk area. Lateral view onto uninjected **(A)** and injected side **(B). (C)** Analysis of *myf5* expression penetrance in COMO and *xmespa* overexpressed embryos. Statistical significance was tested for each subregion of *myf5* expression between control group and treated group. Chart displays differential *myf5* expression in distinct areas. Total number of analysed individuals in brackets. Black arrow points at eye region. Black arrowhead indicates branchial arches. **, $p<0.01$; ***, $p<0.0001$; n≥3 biological replicates; scale bar: 1 mm.

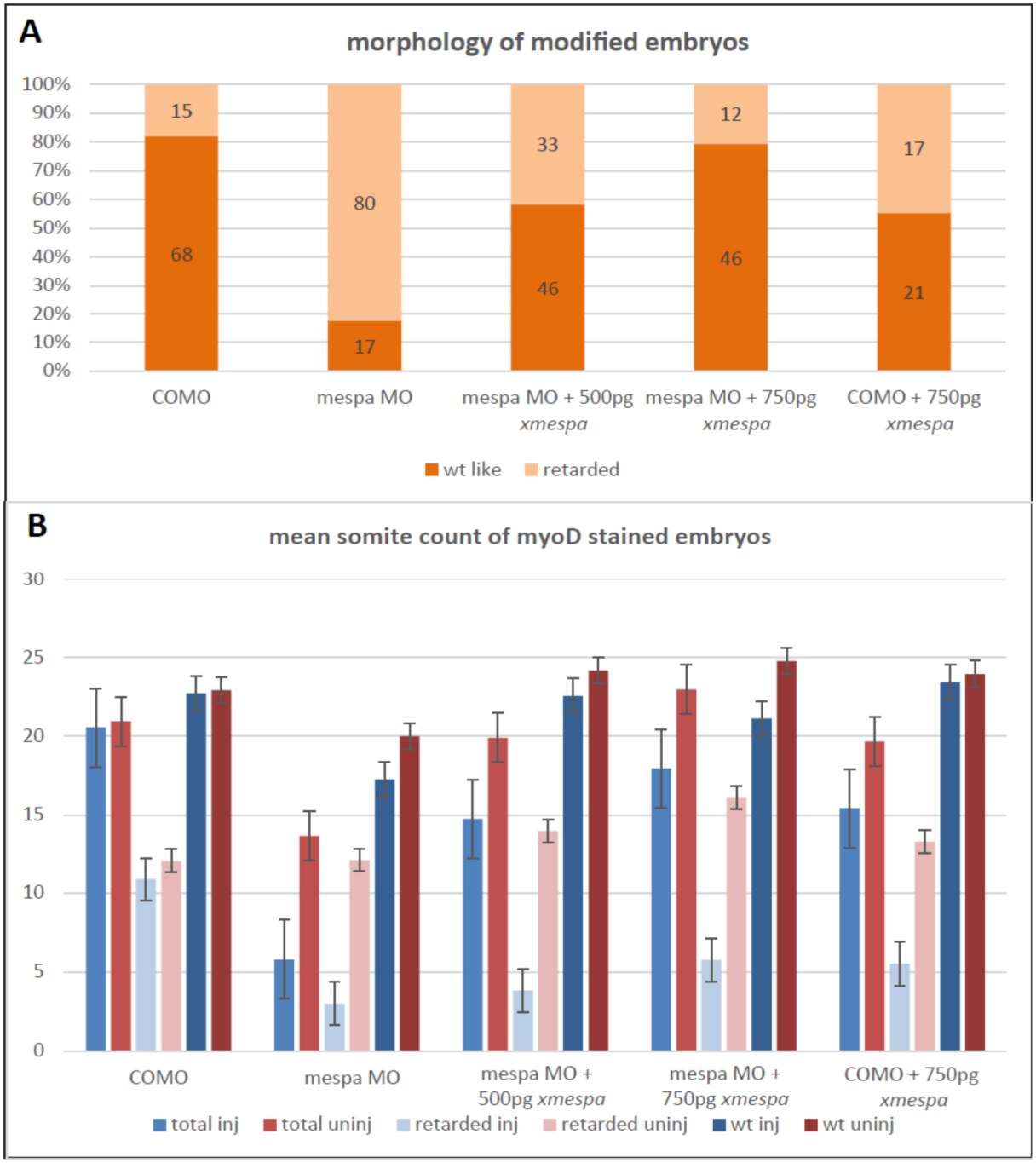

Figure 14: Somitogenesis is strikingly diminished in *mespa* depleted embryos and can be rescued by *xmespa*
(A) Morphology of *myoD* stained tadpole embroys. Due to their developmental progress, they were classified in retarded and wild-type like embryos. A strong developmental delay can be observed in *mespa* morphants, but also under rescue conditions with 500pg *xmespa* mRNA and after overexpression of *xmespa* (COMO + 750pg *xmespa* mRNA). **(B)** Analysis of somite count based on *myoD* expression pattern in half-sided modified tadpole embryos (NF 32). Somites were counted on injected and uninjected side. Diagram shows total count and separate numbers for embryos with retarded or wild-type morphology. n>3 biological replicates. Error bars represent standard error.

3.3.5 Overexpression of *xmespa* mRNA in ectopic tissue drives *eomes* and *xbra* expression during early development

Previous experiments by our group showed, that the overexpression of *mesp*-related genes in ectopic tissue leads to the activation of cardiac markers like *Nkx 2.5* or *Troponin*

(Kriegmair et al., 2013). To examine other potential direct or indirect downstream targets of *mespa*, we took advantage of the overexpression in animal cap explants. To this end, a total amount of 1ng of either *xmespa* mRNA or *myoD* mRNA was injected radially, i.e. into all blastomeres at the four-cell stage. At stage NF 8 (mid-blastula) the explantation of the animal caps was performed by selectively excising the central part of the animal pole while leaving the marginal zones intact (Fig. 15 A). The caps were cultivated until the siblings reached NF 11 (gastrula) or NF 14 (neurula). The siblings also served as a staining control during the procedure of RNA *in situ* hybridisation. Since *xmespa* knockdown experiments presented an important alteration of expression, the caps were stained for the myogenic markers *myf5* and *myoD* as well as for the T-box transcription factors *eomes* and *xbra*. Subsequently, they were compared to uninjected caps of the same age.

Animal caps stained for *xbra* (Fig. 15 F; 2/26 embryos) and *eomes* (see Fig. 15 G; 20/26) showed ectopic expression at the early gastrula stage, whereas myogenic transcription factors *myoD* and *myf5* were not detectable in gastrula-stage caps after injection of 1ng of *xmespa* mRNA (Figure 15 H, I). Since *eomes* is not expressed in the ectodermal tissue of animal caps (Ryan et al., 1996), the detection of *eomes* in explants of uninjected control caps (Fig. 15 C) might be ascribed to caps cut too large, sections of which may have received induction signals from the marginal zone. Except for *eomes*, uninjected controls did not show any expression at the gastrula or neurula stage. Interestingly, no induction of *eomes* was visible in neurula-stage caps (Figure 15 O, 0/24). The transient expression of *eomes* and its endogenous downregulaton at the neurula stage (NF 15) have to be considered and could be adduced as possible explanation (Xenbase). *Xmespa* mRNA managed to induce *xbra* expression in four out of 24 caps (Fig. 15 N). Neither *myoD* (Fig. 15 P) nor *myf5* expression (Fig. 15 Q) were activated by *xmespa* at NF 14. MyoD protein is known to autoactivate the transcription of the *myoD* gene (Steinbach et al., 1998).

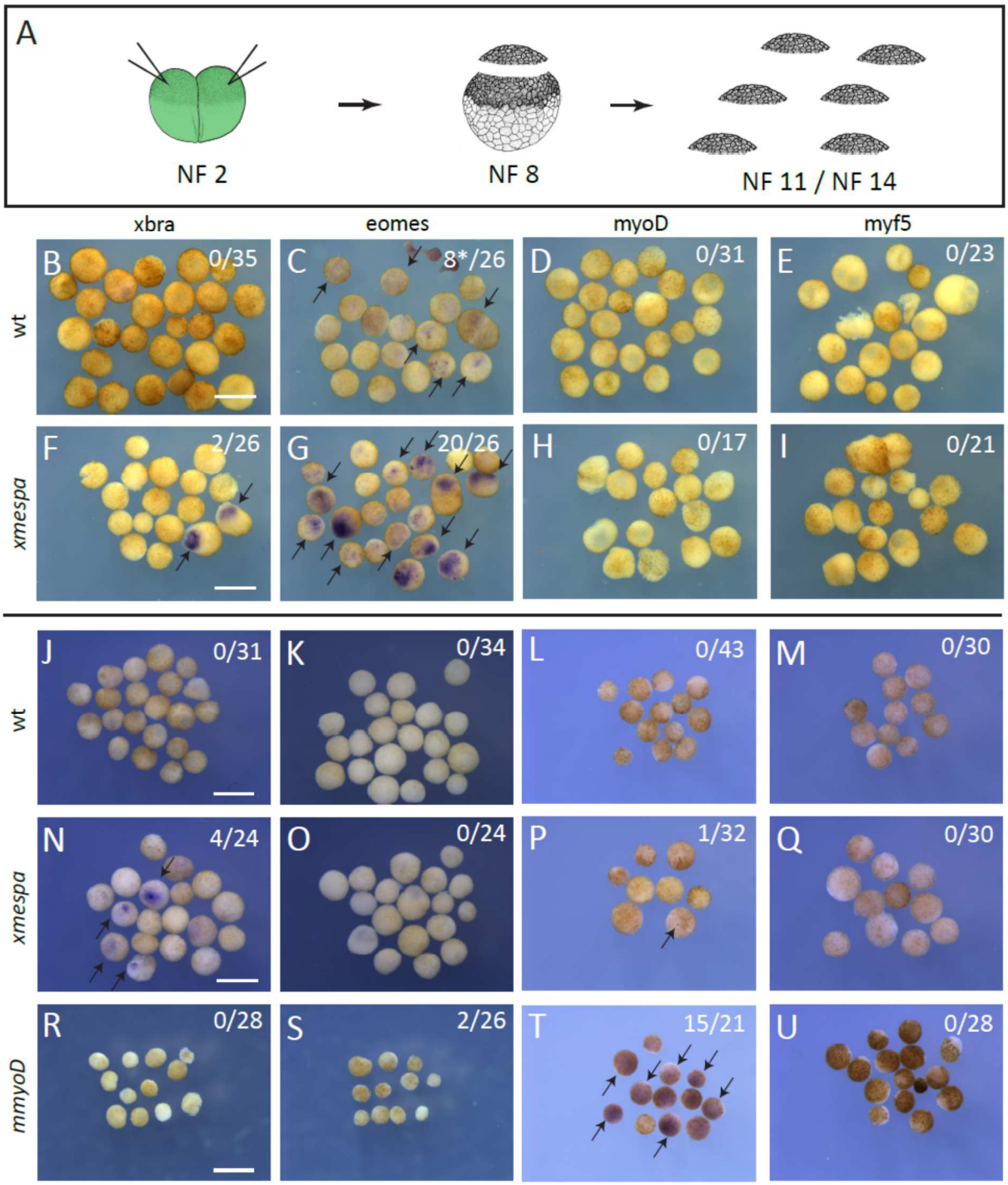

Figure 15: Overexpression of *xmespa* shows capacity to induce T-box transcription factors *eomes* and *xbra* in ectodermal tissue.
(A) Embryos were injected with a total of 1ng *xmespa* mRNA respectively *mmyoD* mRNA at the two-cell stage into both blastomeres. The animal caps were explanted at the mid blastula stage (NF 8), cultivated until gastrula **(B - I)** and neurula respectively **(J - U)** and analysed by subsequent RNA *in situ* hybridisation. In gastrula stage caps *xmespa* overexpression leads to the induction of *eomes* **(G)** and in lower extent of *xbra* **(F)**. *Xmespa* mRNA injected caps exhibit *xbra* expression at the neurula stage **(N),** whereas no *eomes* stain was visible. **(T)** Image shows autocatalytical potential of *myoD* mRNA and serves as positive control. Diagrams depict quantities of *eomes* **(V)**, *xbra* **(W)**, *myoD* **(X)** and *myf5* **(Y)** expressing animal caps for each analysed condition. *, $p<0.05$; *** $p<0.0001$; n = 3 biological replicates; arrows indicate ectopically induced animal caps. Scale bar indicates 1 mm.

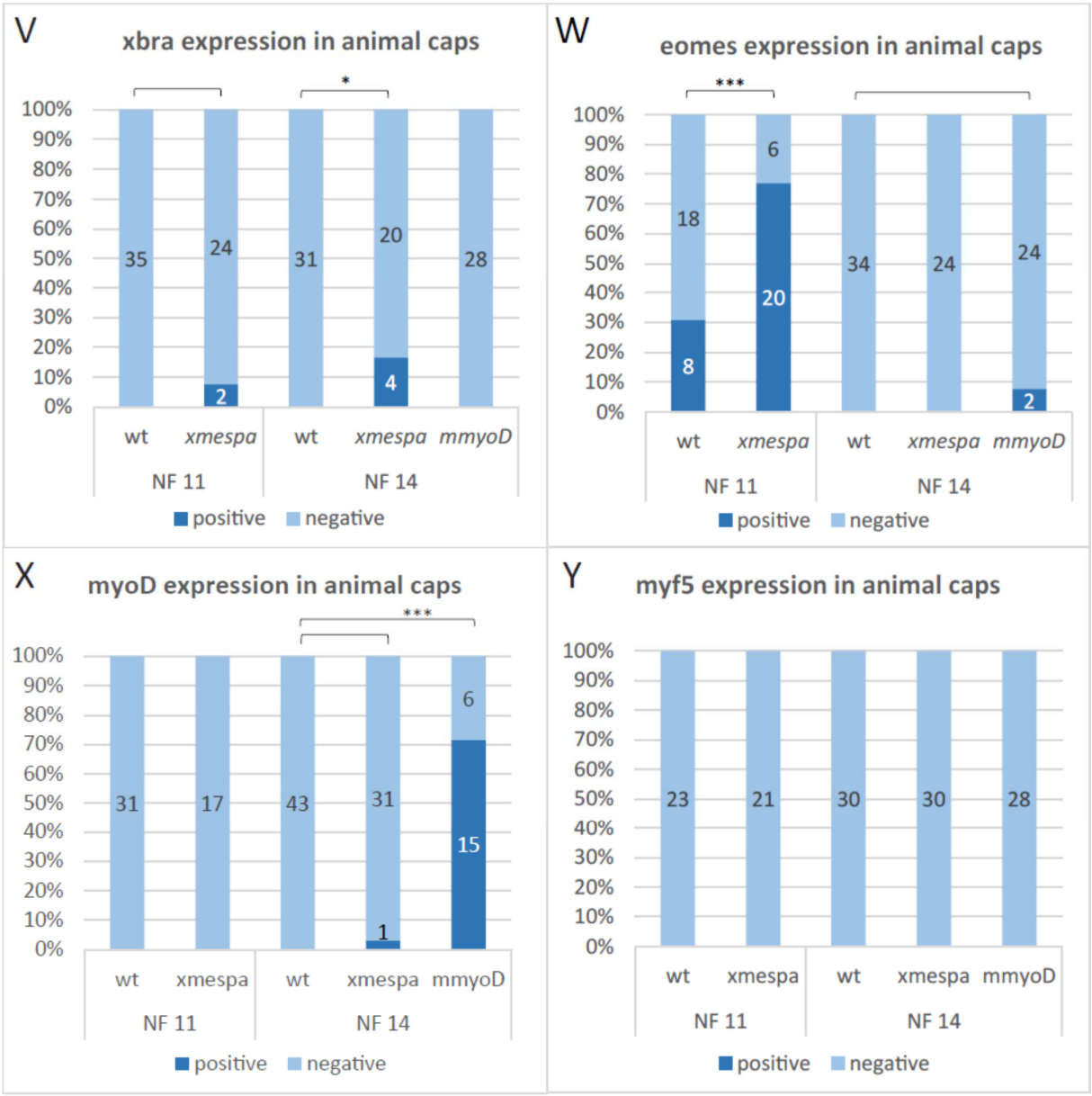

In agreement with this finding, injected *mmyoD* mRNA activated endogenous *myoD* transcription in 15 out of 21 caps (Fig. 15 S). In order to detect not the injected mRNA, but the induced one, the injected *mmyoD* mRNA was constructed to avoid interference with the mRNA dig-probe used for *in situ* hybridisation. By containing only the open reading frame of *mmyoD*, the injected mRNA can induce endogenous *myoD*, but cannot be target by the dig-probe. This experiment showed that *xmespa* has also the potency to induce and drive the expression of panmesodermal markers *eomes* and *xbra*, which indicates a broader functional spectrum of *xmespa*. Seeing as we have proven the necessity of *mespa* for skeletomyogenesis, the synopsis with this data suggests that *mespa* is required, but not sufficient to induce myogenic transcription factors in and of itself. These results only refer to inducing activity during gastrulation and neurulation.

3.4 Vasculogenesis

Cells fated to become endothelium do not manage to depart from the primitive streak in homozygotically *mesp1*-deficient mice (Saga et al., 1999). Moreover, it has been reported that almost all cardiovascular progenitors are derived from *mesp1*-expressing cells (Saga et al., 2000), indicating an important contribution of *mesp1* to the vascular lineage. Subsequent studies of Bondue et al. (2008); (2011) provided deeper insight into target genes and regulatory mechanisms which resulted in the conclusion that *mesp1* may be an evolutionarily conserved master regulator for the specification of multipotent cardiovascular progenitors. In one important step of this mechanism, *mesp1* patterns cardiovascular precursors by *Dkk1*-mediated blocking of canonical Wnt-signalling (David et al., 2008). Clonal analysis confirmed that cells from the first heart field (FHF) and cells from the second heart field (SHF) arise from *mesp1*$^{+}$ cells and contribute to the formation of vasculature (Lescroart et al., 2014).

However, it remains to be fully elucidated how *mesp*-homologues contribute to vasculogenesis in other organisms. This study serves as an in vivo approach to investigate the interaction of *Xenopus mespa* and the endothelial receptor *aplnr* (apelin receptor).

It was first described in human stem cells as *APJ*, with a close similarity to the Angiotensin receptor (AT1) and possessing G-protein-coupled activity (O'Dowd et al., 1993). As an important angiogenic factor, the ligand *apelin* is crucial for normal vascular development in *Xenopus* (Cox, D'Agostino, Miller, Heimark, & Krieg, 2006; Inui, Fukui, Ito, & Asashima, 2006) and zebrafish (Tucker et al., 2007). Cardiovascular deformations caused early death in *APJ* double knockout lines in mice (Kang et al., 2013), which indicates a central role in normal embryonic vasculogenesis. Moreover, *aplnr* was found to be upregulated in brain tumours, proving an involvement in pathological angiogenesis (Kalin et al., 2007; Kidoya & Takakura, 2012; Kidoya et al., 2008).

The following chapter details how I examined whether MO-based *mespa* knockdown alters *aplnr* expression patterns in *Xenopus* tadpoles.

3.4.1 *Mespa* knockdown has striking effects on vasculogenesis

Aplnr was examined as a representative for mesodermal lineages involved in vasculogenesis in tadpole embryos. In line with former studies (Devic, Paquereau, Vernier, Knibiehler, & Audigier, 1996), *aplnr* gene expression analysis proved its presence

in the retinal artery, the anterior cardinal vein, aortic arches and ventral aorta in the head, the posterior cardinal vein, the dorsal aorta, the intersomitic veins, vitelline arteries and the vitelline network which we call ventral vascular plexus (Fig. 16).

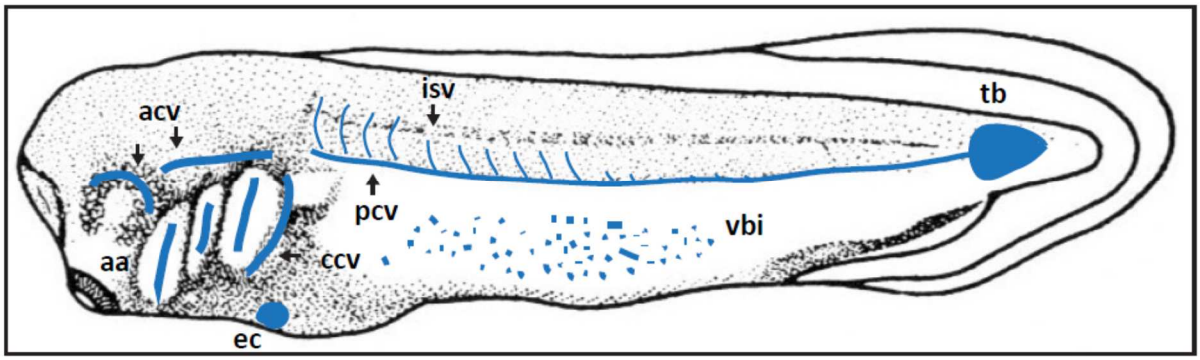

Figure 16: *Aplnr* expression pattern at the tadpole stage (NF 32)
Aplnr expression analysis revealed presence in all major vessels. From rostal to caudal: **acv:** anterior cardinal vein, **aa:** aortic arches, **ec:** endocard, **ccv:** commun cardinal vein, **pcv:** posterior cardinal vein, **isv:** intersomitic veins, **vbi:** ventral blood islands (vascular plexus), **tb:** tailbud. dorsal aorta not shown (Adapted from: Mills, Kruep, and Saha (1999))

To address the question of interaction between *mespa* and *aplnr*, embryos were injected unilaterally with 20ng of MO at the two-cell stage and cultivated up until the tadpole stage (NF 32) as in previous knockdown experiments (Fig. 17). Due to the complex expression pattern of *aplnr* being present in the epithelium of major vessels, I subdivided the stain into five distinct domains: the cardinal and intersomitic vessels, the aortic arches, the ventral vascular plexus and the periocular vessels. The periocular vessels comprise the retinal artery and the anterior cardinal vein. The dorsal aorta was not investigated in this study, since it is not externally visible.

More than half of the *mespa*-deficient embryos, but only 25% of control embryos showed a retarded development, meaning that *mespa* knockdown causes an important developmental delay which can last up to the tadpole stage, depending on the constitution of the embryos concerned (Fig. 17 H). As shown in Figure 17 D and E, knockdown of *mespa* leads to a significant reduction or even the absence of the cardinal and intersomitic veins (white arrows), the aortic arches (dotted circle) and the periocular vessels. The cells lining the aortic arches and also the cardinal and intersomitic veins, were very often disarranged. *Aplnr* expression in the tail bud and in the ventral vascular plexus were not affected by the intervention and showed no specific up- or downregulation.

These experiments indicate that *mespa* is required for *aplnr* expression. According to Xenbase, *aplnr* transcription commences at NF 10, thus it overlaps with *mespa* transcription temporally, offering another clue pointing towards a possible link.

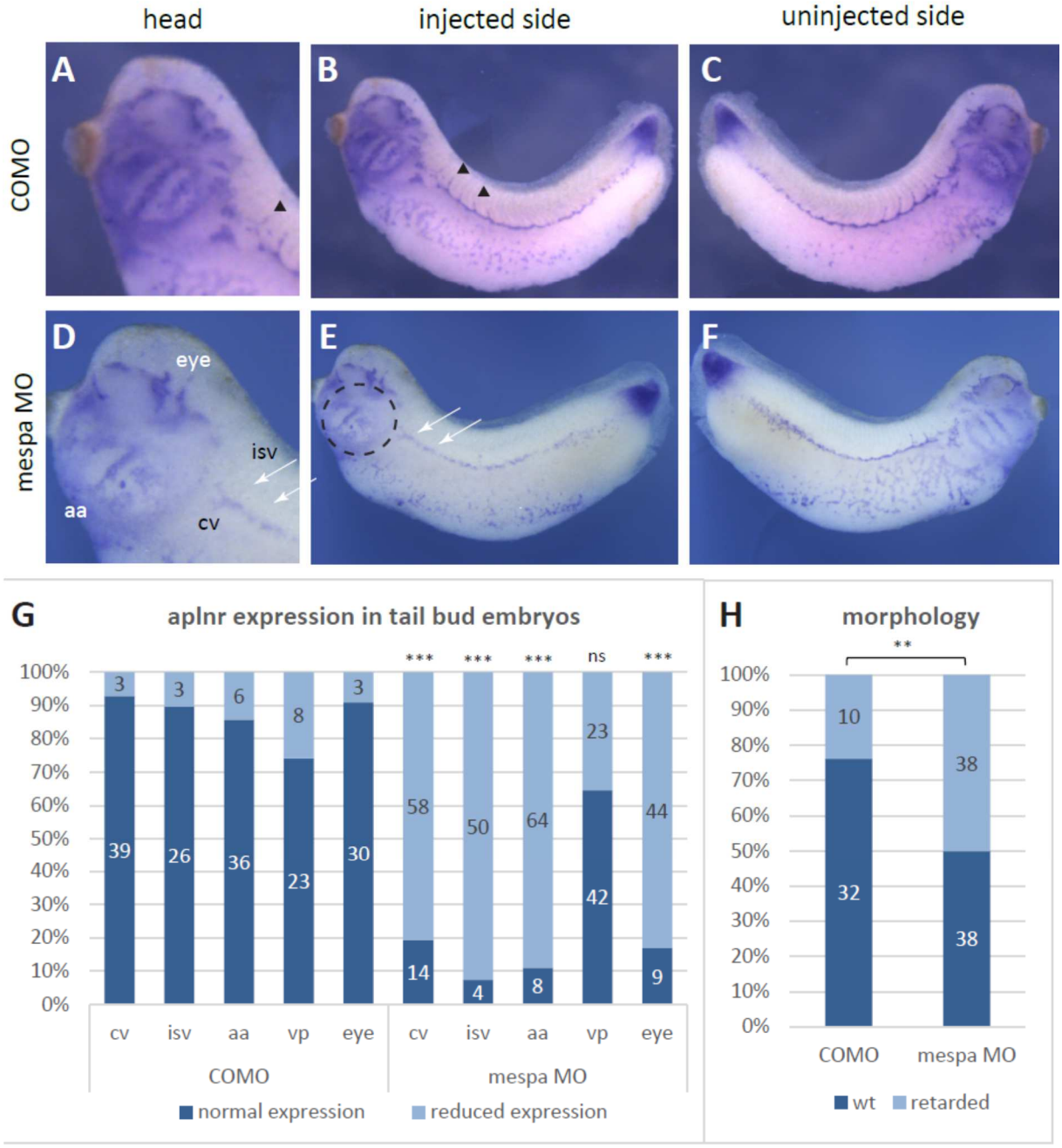

Figure 17: *Mespa* knockdown affects vasculogenesis remarkably
20ng of morpholino were injected into one blastomere of two-cell-stage embryos and *aplnr* expression was examined at the tadpole stage by whole mount RNA *in situ* hybridisation (NF 32). Five differently affected areas can be distinguished of which the cardinal and intersomitic veins as well as the aortic arches and eye vessels were most intensely compromised. **(A) + (D)** Magnification of head region. Lateral view onto control **(B) + (C)** or *mespa* morphant **(E) + (F)**. **(G)** Analysis of phenotypic penetrance of *aplnr* expression in tadpoles in three independent biological repeats; Statistical test were performed comparing expression of each subdomain in control and *mespa* morphant. **(H)** Regarding the morphology embyros were categorised into 'wild-type like' (wt) and 'retarded'. Black arrowheads point at sprouting intersomitic veins in control embryos. White arrows indicate lacking intersomitic veins and thinned cardinal vein in mespa deficient embryos. Dotted circle highlights the disturbed formation of aortic arches. **cv** cardinal vein, **isv** intersomitic veins, **aa** aortic arches, **vp** ventral vascular plexus, **eye** vascular plexus surrounding the eye. **ns,** not significant; **, p<0,01; ***, p<0,0001; n≥3 biological replicates; scale bar is 1 mm.

3.4.2 *Xmespa* is capable of restoring disrupted *aplnr* expression

Subsequently, rescue experiments enabled us to assess whether the observed morphological alterations of *aplnr* expression are specifically caused by *mespa* knockdown. To uncover a possible dose-dependent rescue, a low (500pg) and a high dose (750pg) of *xmespa* mRNA were coinjected with *mespa* MO. The injected side was traced by fluorescent Alexa 488.

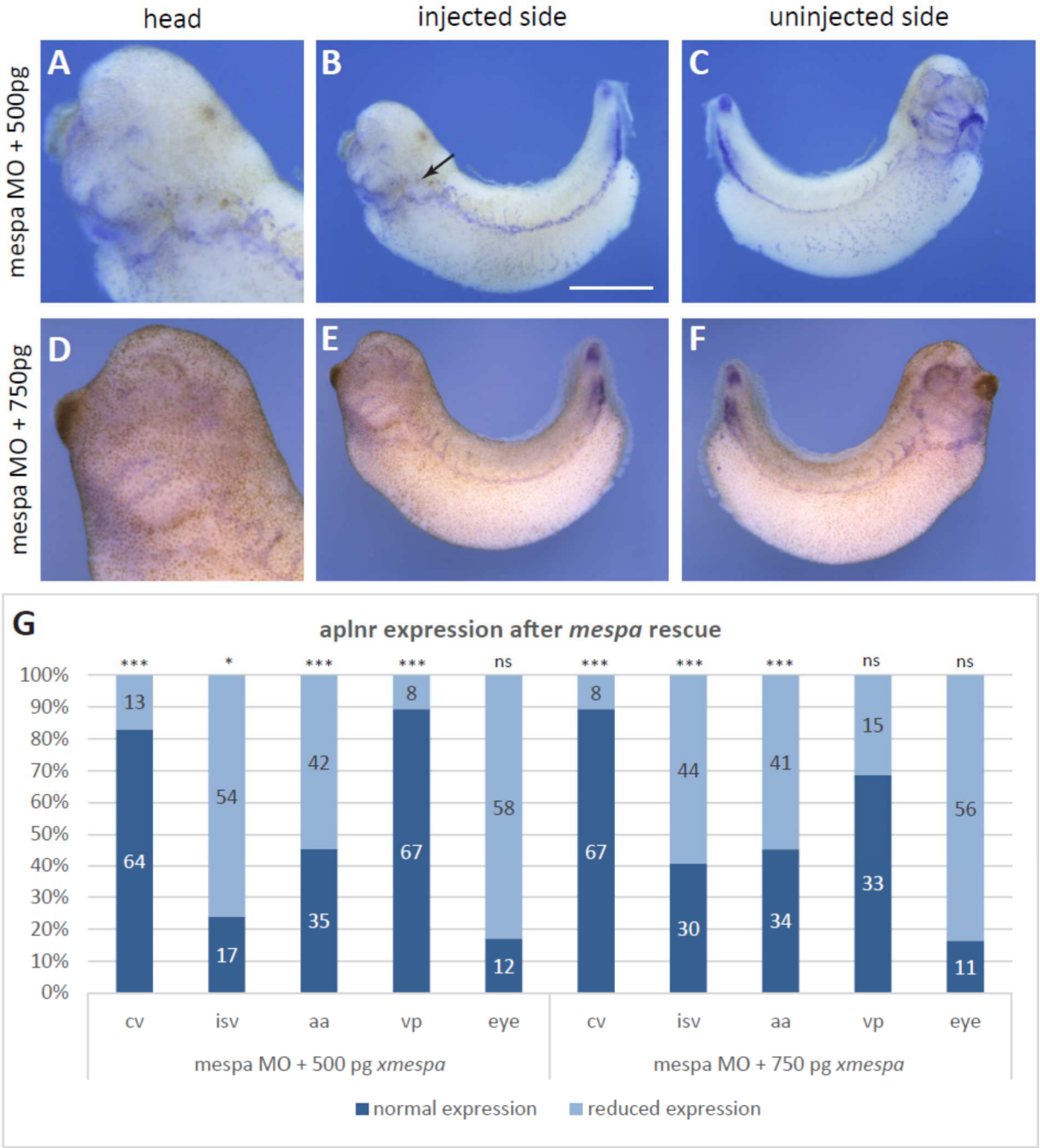

Figure 18: *Xmespa* is capable to restore disturbed *aplnr* expression
500pg respectively 750pg morpholino insensitive *xmespa* mRNA were coinjected with 20ng of *mespa* MO. Embryos were cultivated until and sorted at the tadpole stage NF 32 in order to proceed them to whole mount RNA *in situ* hybridisation. Analogously to the knockdown experiment alterations in five areas of the vascular system can be distinguished. Partial rescue of the *aplnr* phenotype can be observed especially in the aortic arches, the cardinal vein

and the intersomitic veins, with a certain disarrangement of *aplnr* expressing cells in rescue with 500pg *xmespa* mRNA (black arrow) and a dose dependence for intersomitic veins. **(A) + (D)** Magnification of head region. **(B) + (C) + (E) + (F)** Lateral view. **(G)** Analysis of phenotypic penetrance of *aplnr* expression in tadpoles. Statistical test compared expression in each subdomain of *mespa* morphants and rescue embryos. **cv** cardinal vein, **isv** intersomitic veins, **aa** aortic arches, **vp** ventral vascular plexus, **eye** vascular plexus surrounding the eye. **ns**, not significant; * $p<0,05$; ***, $p<0,0001$; n≥3 biological repeats; scale bar is 1 mm.

In both cases, the phenotype was partly rescued and just 18% of *mespa* morphants presented a retarded morphology, comparable to that seen in controls (Fig. 18). Retarded morphology in this context means that the individual developmental speed of the embyros was remarkably slower than the overall average. This implies that the observed expression patterns correspond to an earlier developmental stage. As depicted in Figure 18, *aplnr* expression in cardinal veins reached normal levels in 64 out of 77 embryos rescued with 500pg, and in 67 out of 75 embryos rescued with 750pg of *xmespa*. While the amount of embryos with normal intersomitic veins stayed under 25 % in the low dose group, while approximately 40 % of embryos in the high dose group attained this level. Hence, *xmespa* appeared to rescue the transcription of the endothelial marker *aplnr* dose-dependently in intersomitic veins. Both sets of rescue conditions resulted in comparable and significantly increased rates of normal *aplnr* expression in the aortic arches. *Aplnr* transcription in the endothelium of forming cranial vessels could not be rescued by *xmespa*. This approach indicates that the reduction of *aplnr* expression in tadpole embryos is specifically caused by *mespa* knockdown.

3.4.3 Overexpression of *xmespa* results in disarrangement of *aplnr* expressing cells involved in vasculogenesis

With the aforementioned effects of *mespa* knockdown in mind, I investigated *aplnr* alterations in *mespa*-overexpressed whole mount embryos. Analogously, 750pg of *xmespa* were coinjected with 20ng of COMO and Alexa 488 into one blastomere at the two-cell stage (Fig. 19).

Interestingly, *xmespa* overexpression does not expand domains of *aplnr* transcription or forced vasculogenesis in the sense of additional or ectopic expression, but leads to reduced and perturbed arrangements of *aplnr*$^{+}$ cells. More than 70% of intersomitic veins were reduced in size. Only 60% of the modified embryos exhibited normal aortic arches, but they frequently displayed abnormalities regarding the arrangement of said arches. *Xmespa* overexpressed embryos presented broadened or distended cardinal veins. About

80% of the embryos had attenuated periocular vessels (anterior cardinal vein and retinal artery).

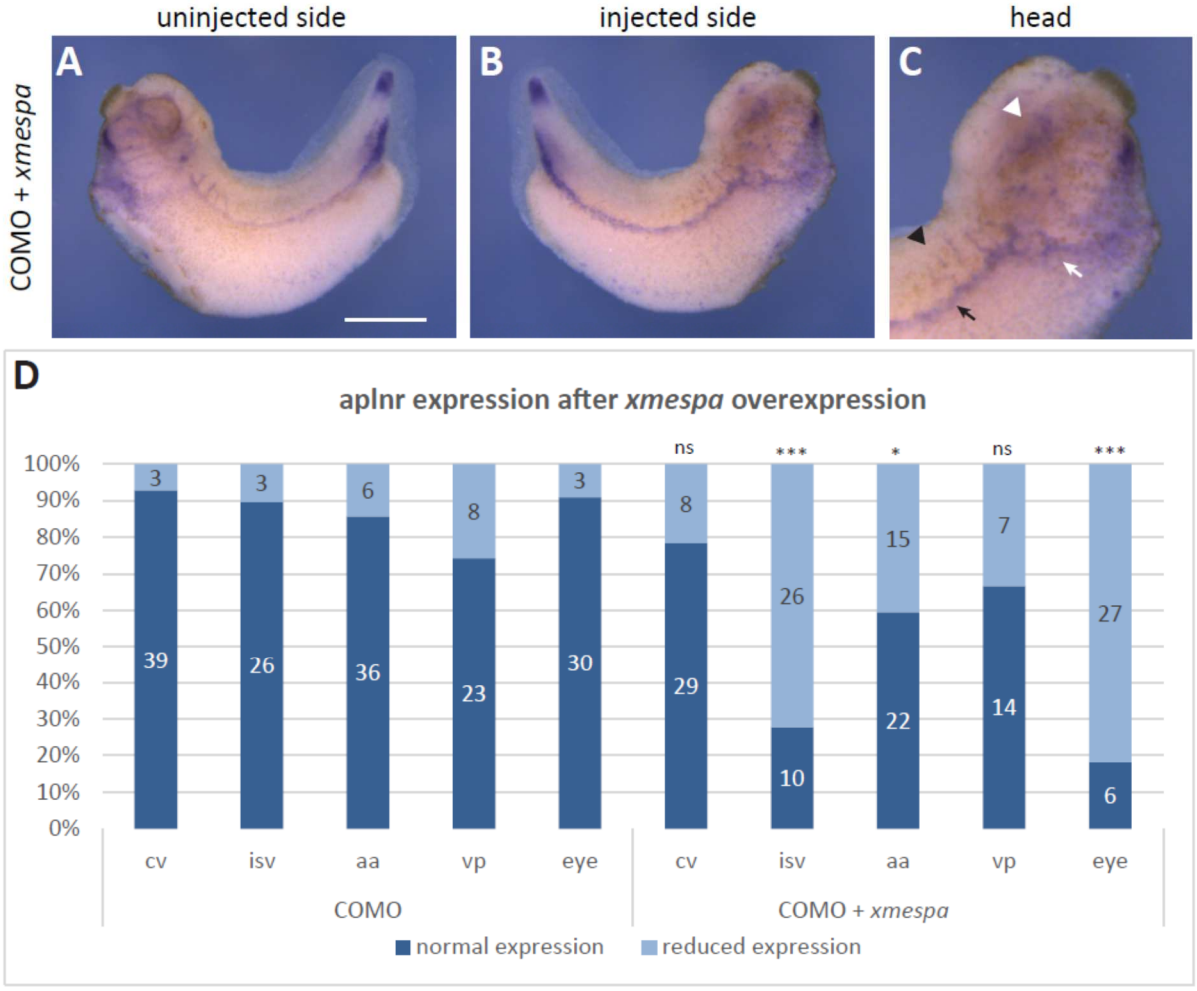

Figure 19: Disarrangement of the vascular system after *xmespa* overexpression
750pg of *xmespa* mRNA were coinjected with 20ng of COMO and Alexa 488 into one blastomere at the two-cell stage. Subsequently sorted at the tadpole stage NF 32 and whole mount RNA *in situ* hybridisation was performed to analyse *aplnr* expression. It is characterised by distension of the cardinal vein (cv), reduction or loss of intersomitic veins (isv), disarrangement of cells contributing to aortic arches (aa) and a reduction of periocular vessels (eye). **(A) + (B)** Lateral view. **(C)** Magnification of the head region. **(D)** Phenotypic analysis of *aplnr* expression in *xmespa* overexpressed tadpoles. black arrowhead: isv, black arrow: cv, white arrowhead: eye vessels, white arrow aa; **cv** cardinal vein, **isv** intersomitic veins, **aa** aortic arches, **vp** ventral vascular plexus, **eye** vascular plexus surrounding the eye. **ns**, not significant; *, $p<0,05$; ***, $p<0,0001$; n = 3 biological replicates. Scale bar is 1mm.

Taken together, these experiments uncovered an important interaction between *mespa* and the endothelial marker *aplnr*. *Mespa* protein knockdown altered the spatial distribution of *aplnr*$^{+}$ cells, especially in the aortic arches and the cardinal and intersomitic veins. Morphants exhibited truncated cardinal veins, while intersomitic veins were absent or strongly limited in their sprouting. These findings provide greater insight into the relevance of *mespa* during normal vasculogenesis. However, the overexpression assay showed no inducibility of the endothelial marker *aplnr* in whole mount embryos.

3.5 Effects on embryonic haematopoiesis

Early precursors of blood and vasculature derive from a common cell source called definitive haemangioblast, which originates in dorsolateral plate mesoderm (Ciau-Uitz, Pinheiro, Kirmizitas, Zuo, & Patient, 2013). Haematopoietic precursor cells form the ventral blood islands (VBI), which can be subdivided into anterior and posterior VBI domains (Ciau-Uitz, Walmsley, & Patient, 2000): They derive from different blastomeres of the 32-cell fate map plan, which are located on opposite sides. Putative anterior VBI (aVBI) precursors derive from dorsal blastomeres (C1, D1), while posterior VBI precursors (pVBI) are descendants of ventral blastomeres (D4). Lane and Smith (1999) and Kumano, Belluzzi, and Smith (1999) indicated that a circular band of cells of the vegetal-most marginal zone forms the ventral blood islands. Further fate mapping studies revealed that cells from the marginal zone contribute to the formation of this haematopoietic structure in a caudal to rostral order (Lane & Sheets, 2006). The expression of *mespa* in the dorsolateral mesoderm establishes the possibility that this gene could play a role in the specification of haematopoietic precursor cells.

Although previously proclaimed as master regulator of cardiovascular differentiation and migration, two recent reports have attributed to *mesp1* a haematopoiesis-inducing activity in mesodermal cells (Chan et al., 2013; Komada et al., 2012). According to Chan et al. (2013), *mesp1* promotes haematopoietic development, under the following conditions: *mesp1* needs to be activated in an early responsive window, in the absence of Wnt-signalling, but in presence of *mesp1* as a protein complex with E12.

3.5.1 *Mesp*-genes are required for embryonic haematopoiesis

To examine the influence of *mespa* in *Xenopus* haematopoiesis, we chose *α-globin (hba1)* as a definitive marker for erythropoiesis. The outcome of the resulting experiments on erythropoiesis cannot be seen as being directly transferrable to other haematopoietic cell lines, such as myeloid and lymphatic precursors. However, all haematopoietic cell lines originate from a common stem cell, the so-called haemangioblast. As *hba1* is a component of the oxygen-binding haemoglobin, which is first synthesised around NF 25. To avoid the bias caused by the *mespa*-MO-based retardation in development observed in my previous experiments, and to establish coherence with the other experiments, I chose the tadpole stage around NF 32 as the time of analysis.

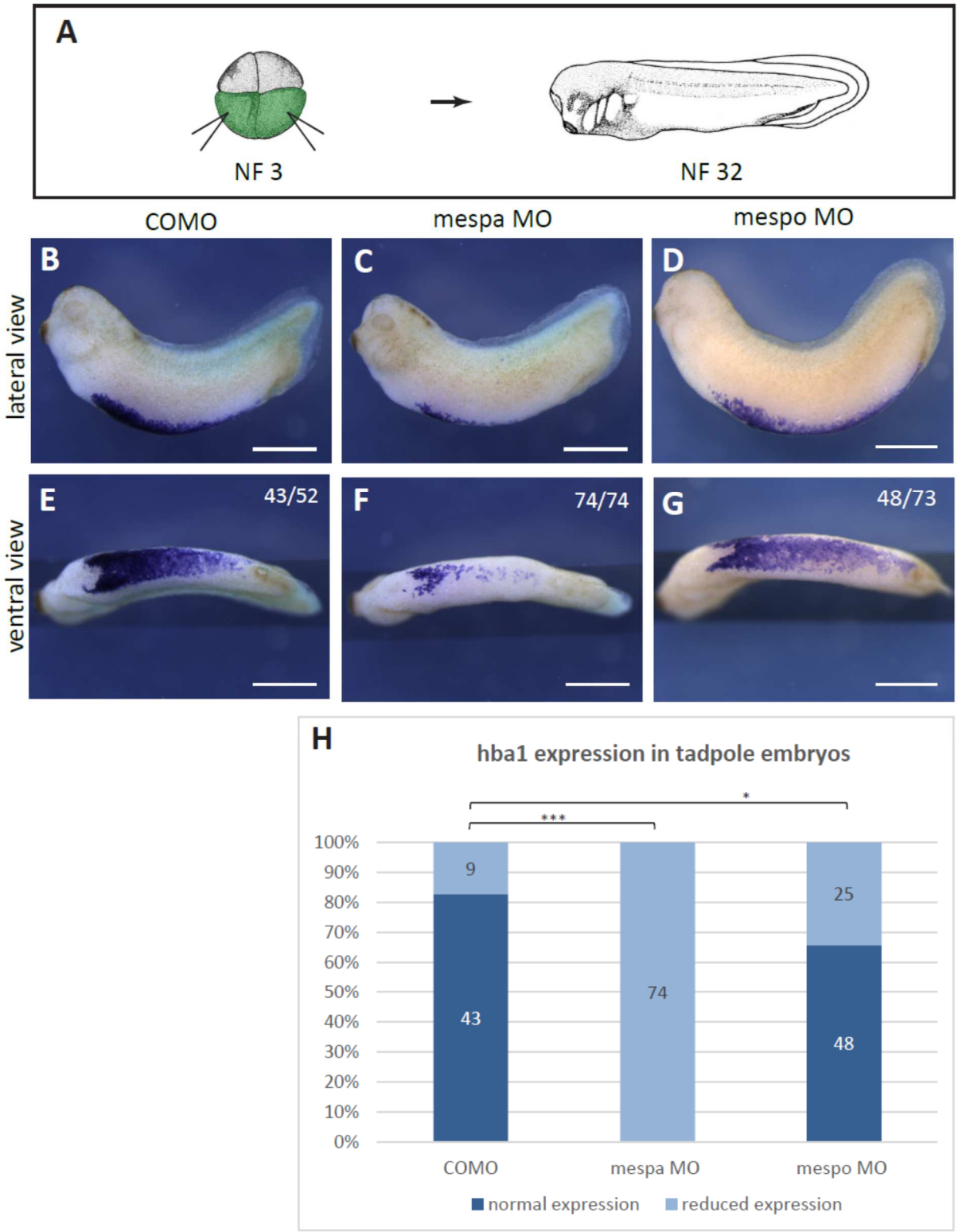

Figure 20: *Mespa* and *mespo* are both required for normal *hba1* expression
20ng of morpholino were injected into the two ventral blastomeres at the four-cell stage **(A)**. *hba1* domains were analysed by subsequent RNA *in situ* hybridisation. Embryos were cultivated until the tadpole stage. *hba1* expression is sharply reduced in *mespa* morphants. *Mespo* morphants exhibited only a slightly reduced phenotype. **(B) + (C) + (D)** Lateral view. **(E) + (F) + (G)** Ventral view, anterior to the left. **(H)** Phenotypic distribution o**f** *hba1* expression in tadpole embryos. *, $p<0.05$, *** $p<0.0001$; n≥4 biological replicates; scale bar: 1mm.

Since the *hba1* expression is located along the ventral midline in a y-shaped pattern, whose branching "opens" towards the head structure, it is not possible to definitively tell

from which side the *hba1*$^{+}$ cells in half-side injected embryos had derived. In case of unilateral depletion, cells could have possibly migrated across the midline from the contralateral side to compensate.

Hence, for the subsequent experiments, I changed the injection scheme and injected 20ng of morpholino into the two ventral blastomeres at the four-cell-stage, taking advantage of the distinct origins of the anterior and posterior VBIs (Fig. 20 A). Thereby, I addressed the posterior part of the *hba1* expression domain on both sides, which enabled me to better detect the presence of *hba1*. In three biological replicates of ventral injection of *mespa* MO, *hba1* expression was reduced or extinguished in the posterior ventral domain in all analysed tadpoles.

The depletion of *mespo* also led to an attenuation of the *hba1* stain in 25 out of 73 embryos, which constitutes a statistically significant reduction. The remaining 48 embryos appeared wild-type-like. The majority (43 of 52) of control MO embryos showed a normal stain, but nine showed *hba1* domains reduced in size, intensity or density. The different patterns in control morphants are reminiscent of the natural, age-dependent variation in hba1 expression, which is observed in unmanipulated embryos.

3.5.2 Loss of *hba1* expression is specific for *mespa* as proven by mRNA rescue

To examine the specificity of the findings of *mesp*-related gene knockdown, rescue experiments were performed by simultaneously injecting MO and MO-insensitive mRNA. Hence, the transcription of the injected mRNA was not blocked by the MO and mRNA could be translated to a biologically active protein. The rescue was performed by coinjecting 20ng of *mespa* MO and 750pg of *xmespa* mRNA into the two ventral blastomeres at the four-cell-stage (Fig. 21 A). Since a dose of 750pg of *xmespa* provided better rescue results. Coinjections with 500pg of *xmespa* were not performed in this experiment.

Xmespa mRNA managed to restore normal expression of *hba1* in 40% of the embryos. Figure 21 C shows the main phenotype of a still partly reduced stain. Whereas the wild-type expression pattern was usually a condensed and contiguous ribbon, rescue embryos more frequently exhibited a cloudy or scattered stain. The domains were split into anterior and posterior fields in four cases. Coinjection of MO and mRNA also partly restored the embryos' elongation.

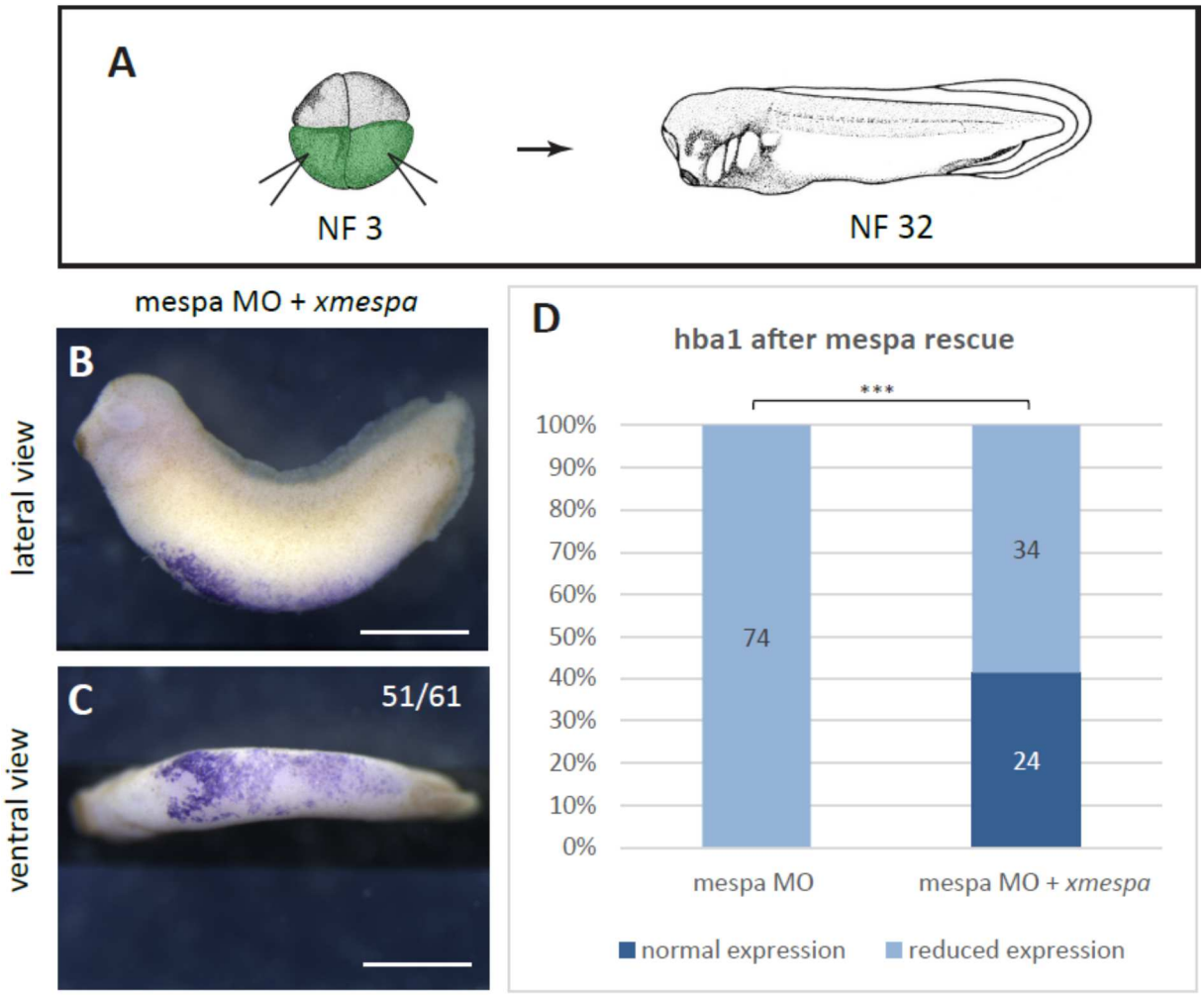

Figure 21: *xmespa* mRNA reestablishes *hba1* expression after morpholino-based *mespa* knockdown
Rescue was performed by coinjecting 750pg of morpholino insensitive *xmespa* mRNA with 20ng of *mespa* morpholino into the two ventral blastomeres at the four cell stage **(A)**. The images depict tadpole embryos after whole mount RNA *in situ* hybridisation for *hba1*. A partial restoration of *hba1* expression could be observed, which demonstrates the specificity of the phenotype after *mespa* knockdown. **(B)** Lateral view. **(C)** Ventral view, anterior left. **(D)** Penetrance of hba1 phenotype in tadpole embryos (NF 32). ***, $p<0.0001$; n = 3 biological replicates; Scale bar: 1mm.

3.5.3 *Mespa* overexpression does not enhance *hba1* expression

In a third step, I had a closer look at the effect of *xmespa* overexpression on haematopoiesis. In line with previous overexpression experiments, I injected 750pg of *xmespa* mRNA together with 20ng of COMO into the two ventral blastomeres of four-cell-stage embryos (Fig. 22 A). Interestingly, I did not find the enhancement of the *hba1* expression pattern I had expected, but rather a slight reduction of the stain in 35% of the analysed embryos compared to 18% in controls (Fig. 22 F). Thus, more embryos resembled a retarded developmental stage or inappropriate length. Moreover, in about a quarter of the embryos the *hba1* domain was split into two separate fields reminiscent of the distinct anterior and posterior VBIs, while the pattern was contiguous in all controls ($p<0.01$).

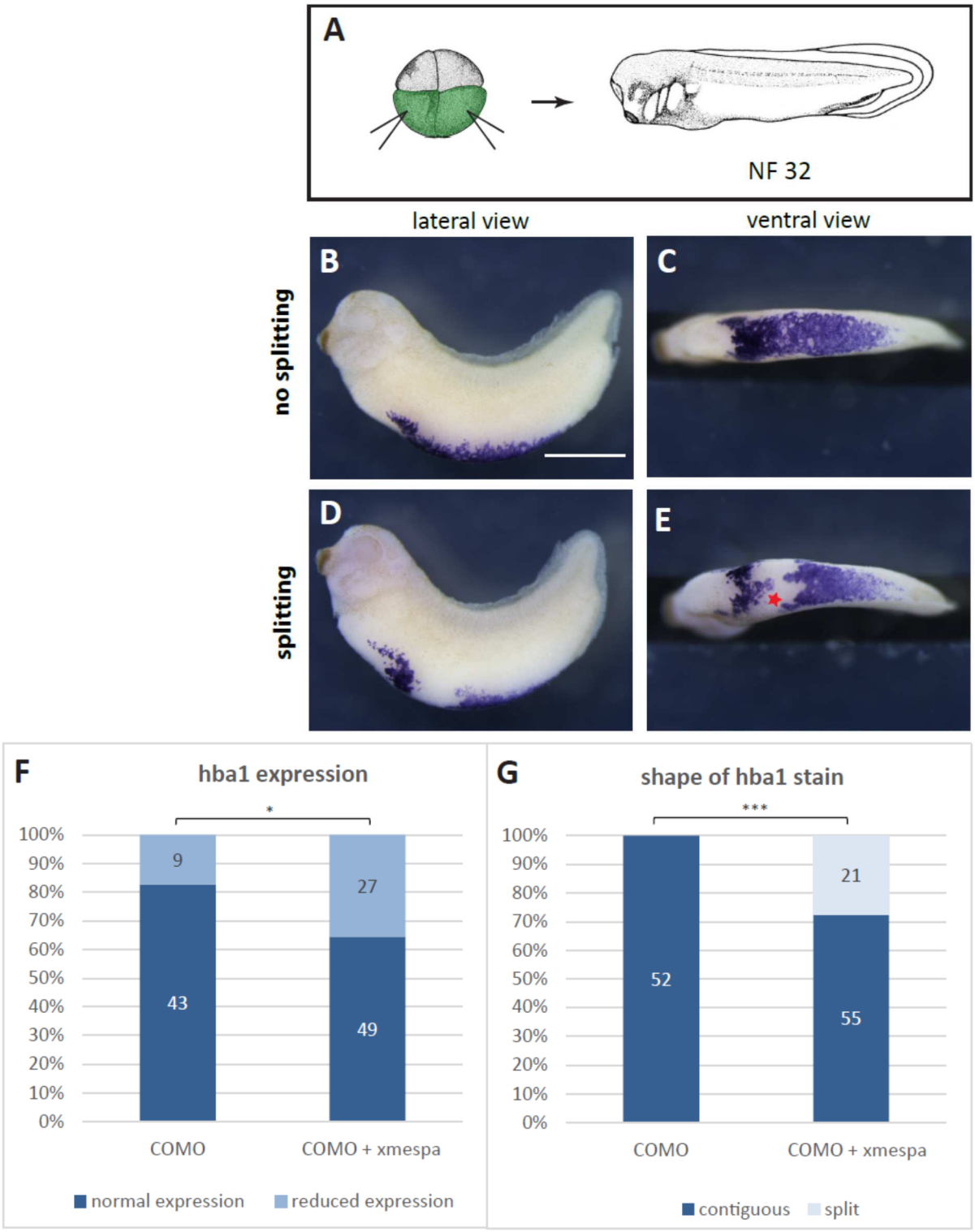

Figure 22: *xmespa* overexpression provokes reduction and splitting of the *hba1* expression domain.
750pg of *xmespa* mRNA were coinjected with 20ng of COMO into the two ventral blastomeres at the 4-cell stage **(A)**. Embryos were analysed by whole mount RNA *in situ* hybridisation at NF 32. **(B) + (D) L**ateral view. **(C) + (E)** Ventral view, anterior left in all images. **(F)** Analysis of phenotypic penetrance of *hba1* expression. **(G)** Chart illustrates quantity of embryos with contiguous vs. split shape of the *hba1* expression domain. *, $p< 0.05$; ***, $p<0.0001$; Red star indicates the cleft between the anterior and posterior domain. n=3 independent biological repeats; Scale bar: 1mm.

These studies showed that *mespa,* and to a lesser extent *mespo,* are crucial for *hba1* expression in tadpole embryos. In contrast, *mespa* overexpression did not lead to an enhancement of *hba1* expression, but reduced and split the haematopoietic domain.

These results suggest a transient requirement for *mespa* in formation of the erythroid cell lineage, which is sensitive to an experimentally induced increase or temporal extension of *mespa* expression. Altogether, these data suggest that *mespa* plays an important regulatory role in embryonic haematopoiesis.

3.6 Nephrogenesis

Nephrogenesis proceeds in tight coupling with vasculogenesis and embryonic haematopoiesis, as the endothelium of the glomus derives from the ventral wall of the dorsal aorta (Nieuwkoop & Faber, 1994). It describes the formation of the most primitive renal structure in vertebrates, i.e. the pronephron. The pronephric anlagen derive from lateral and intermediate mesoderm progenitors (Brandli, 1999). This field of mesodermal derivatives lies adjacent to paraxial mesoderm and the forming most anterior somites, which are required for pronephric development (Mitchell, Jones, Weeks, & Sheets, 2007). The intermediate mesoderm consists of two layers: the splanchnic layer on the endodermal side, which gives rise to the pronephric capsule anlage, while the overlying somatic layer forms the pronephric anlage itself, consisting of pronephric tube, pronephric duct and interstitial cells. Since progenitor cells of intermediate mesoderm receive inducing signals from the paraxial mesoderm, which is patterned by *mespa*, I investigated, whether *mespa* also drives the development of the kidney, as another organ arising from mesodermal progenitors.

In the beginning, I tested, whether *pax2* expression in tadpole embryos is sensitive to *mespa* perturbation. *Pax2,* also named *paired box2,* belongs to a family of transcription factors involved in organogenesis. It plays an important role during kidney development and differentiation, as it contributes to the formation of pronephric tubule and duct epithelia and the cerebral compartments of the nervous system such as the mid- and the hindbrain and the sensory organs (Carroll et al., 1999; Heller & Brandli, 1997). Up to now, there has not been any investigation of the interaction of *mespa* and *pax2*.

3.6.1 *Mespa* affects the development of the pronephros

During the appr. 18 hours between stages NF 28 and 34, progenitors of the nephric mesenchyme, deriving from the intermediate mesoderm, undergo complex morphogenetic processes like the outgrowth of the outflow tract, the appearance and formation of the nephrostomes and the elongation and subsequent coiling of the pronephric tubule (Nieuwkoop & Faber, 1994). Due to the rapid speed of morphogenesis, slight retardations in development or minimal perturbations of these processes may elicit apparent morphological differences between the injected and uninjected sides.

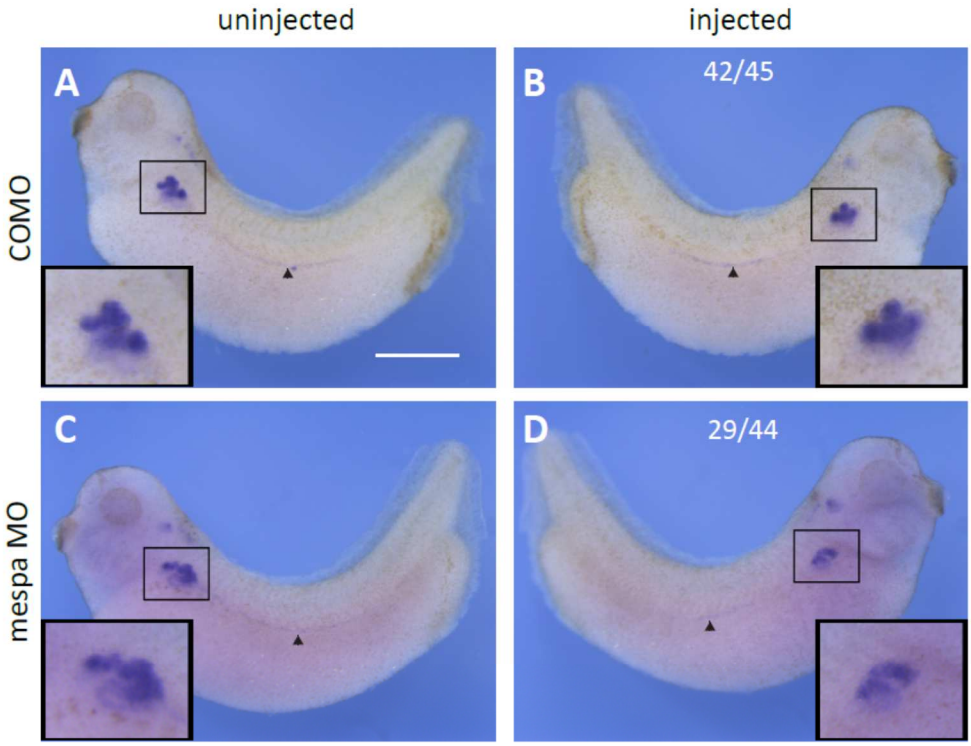

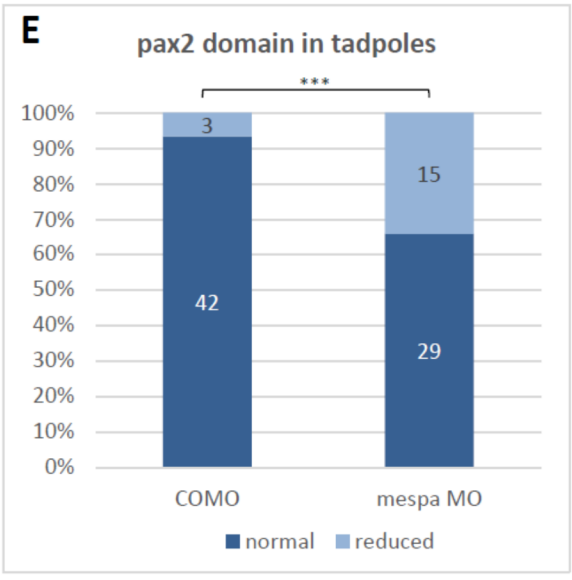

Figure 23: *Mespa* depletion diminishes the size of the pronephric anlagen
20ng of MO were injected at the two-cell stage and sorted due to their laterality at the tadpole stage. Whole mount RNA *in situ* hybridisation of tadpole embryos displays *pax2* expression domains. The images depict representative lateral views of both conditions. The arrowheads indicate the pronephric duct. The inserts show a magnification of pax2 expression domains of injected and uninjected side of control **(A) + (B)** or *mespa* morphant tadpoles **(C) + (D)**. *Mespa* morphants showed significantly downsized pronephric anlagen. **(E)** Phenotypic penetrance of size of *pax2* expression domain after *mespa* depletion. ***, p=0.0001; n=3 independent biological replicates. Scale bar: 1mm.

Two-cell-stage *Xenopus* embryos were injected with 20ng of either *mespa* MO or COMO into one blastomere and cultivated up until the tadpole stage. As shown in Figure 23 *mespa* deficient embryos always exhibited the pronephric anlagen on the manipulated and the wild-type side in a manner comparable to the corresponding controls. Interestingly, a significant number of *mespa* morphants exhibited a pronephron of diminished size (15/44; p<0.0001) which appeared to be less coiled than in control embryos. Neither the intensity nor the shape of the *pax2*-expressing cells, which form the collecting tube, was changed.

These data suggest that *mespa* is not responsible for *pax2*-expression per se. The extent of renal development rather depends on the progression of morphogenesis and differentiation downstream of *pax2*, which depend on *mespa*.

3.7 Epithelial-to-Mesenchymal-Transition

Cell migration is one of the key processes during embryogenesis. Besides being able to perform direct patterning and differentiation of mesodermal tissues, *mespa* was reported to possess the striking capacity to direct cell migration. Mesodermal cells, and more specifically cardiovascular precursors, do not manage to depart properly from the primitive streak of *mesp1*-knockout mice in order to contribute to the formation of the heart tube (Saga et al., 1999).

Cells obtain the ability to migrate by epithelial-to-mesenchymal transition (EMT), a process extensively studied in developmental biology, particularly with regard to its clinical importance in tumour development and metastatic dissemination. Lindsley et al. (2008) showed that *mesp1* is capable of binding to cis-regulatory DNA elements of *snai1* and *twist1* genes, thus inducing their transcription. These two transcription factors are known to control EMT, e.g. in differentiating ES cells during gastrulation regarding cardiovascular development. Both markers exhibit dual expression: in the mesoderm during the process of gastrulation and in the ectoderm-derived neural fold and neural crest (NC) at later stages of development. Since NC cells also contribute to the formation of the heart, they might follow the migratory movements of mesodermal progenitors.

Moreover, it was reported that NC can be induced by paraxial mesoderm which is also patterned by *mespa* (Monsoro-Burq, 2003). With this study, we expand our understanding of *mespa* during EMT, migration and patterning of NC in *Xenopus laevis*.

3.7.1 *Snai1* expression analysis

To get new insights into the role of *mespa* during EMT, its influence on *snai1* expression was observed. *Snai1* belongs to a family of DNA-binding zinc finger proteins and is known as one of the key factors in the complex process of EMT (Carver, Jiang, Lan, Oram, & Gridley, 2001; Thiery & Sleeman, 2006). It incorporates a crucial function in mesodermal layer formation and migratory movements by repressing the transcription of the cell adhesion protein E-cadherin. Early *snai1* expression first emerges in the dorsal marginal zone and subsequently extents ventrally to complete a ring around the blastopore. Hence, *snai1* follows the formation of the blastopore lip, which starts at the dorsal side of the embryo where involution is initiated. When the mesoderm starts to ingress during gastrulation, one can still observe a thin margin between the *snai1* expression domain and the blastopore on the ventral side. After involution, *snai1* expression is downregulated in mesodermal derivatives, but activated in the neural fold migrating anteriorly (Essex, Mayor, & Sargent, 1993). *Snai1*$^{+}$ cells also contribute to the formation of the NC and neural plate during neurulation. At the tadpole stage, *snai1*-expressing cells were found in the cranial NC in the branchial arches and the head region.

3.7.2 *Mespa* knockdown does not affect *snai1* expression throughout *Xenopus* development

I addressed the question of possible interaction between *snai1* and *mespa* with *mespa* knockdown experiments, injecting 20ng of *mespa* MO into one of two blastomeres of two-cell stage embryos, and observing *snai1* expression at the following end points: gastrula (NF 11), neurula (NF 14) and tadpole stage (NF 32). During gastrulation, 91% of *mespa*-deficient embryos showed normal expression of *snai1* compared to 100% of control embryos, as illustrated by Figure 24 A and B. Only a small fraction of *mespa*-depleted embryos presented a reduced expression pattern. This fraction might represent *mespa* morphants that fail to gastrulate.

During neurulation, two out of 32 control embryos and five out of 28 *mespa*-depleted embryos exhibited a reduced expression. In each of the groups, the majority of embryos presented a normal phenotypic pattern (Fig. 24 C, D). These changes in the *mespa*-depleted group seem to constitute unspecific alterations, since they did not differ significantly from the controls.

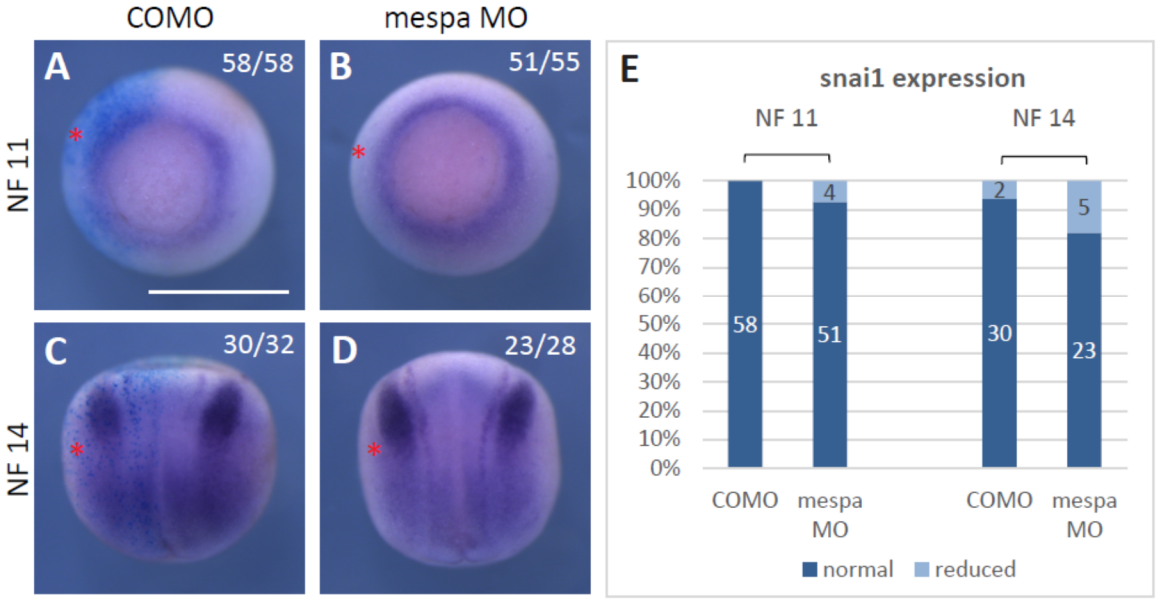

Figure 24: *Snai1* expression is not affected by *mespa* knockdown
Embryos were injected into one blastomere at the two-cell stage with 20ng of morpholino and analysed by whole mount RNA *in situ* hybridisation at the gastrula stage (NF 11) and the neurula stage (NF 14). The expression pattern shows no significant alteration after *mespa* knockdown compared to control injections. **(A) + (B)** Gastrula; view from posterior onto the blastopore, dorsal uppermost. **(C) + (D)** Neurula, dorsal view, anterior uppermost. **(E)** Penetrance of phenotypes of the embryos in n≥3 biological repeats. $p>0.05$; Scale bar represents 1mm.

Mespa knockdown in tadpole-stage embryos showed comparable results. As depicted in Figure 25, 88% of the modified embryos and 98 % of controls did not exhibit an altered *snail1* expression pattern. 12% of *mespa*-deficient embryos presented an attenuated stain in the head region and branchial arches ($p>0.05$). Since *mespa* is not expressed in (neuro)ectoderm as *snai1* does in this developmental stage, only a paracrine mechanism would have explained an interaction.

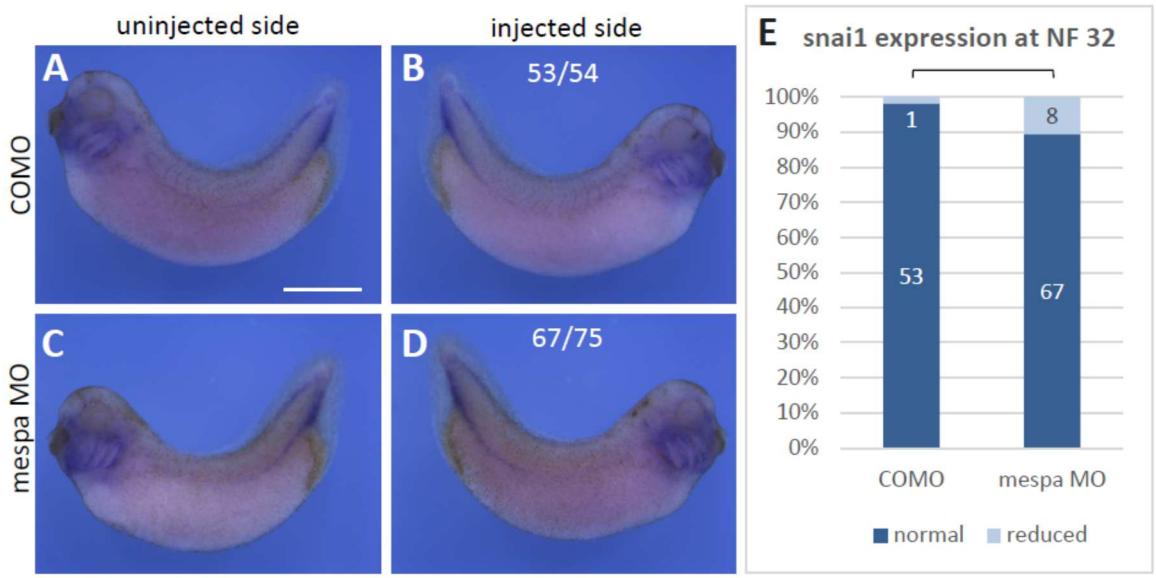

Figure 25: *Mespa* depletion does not impair expression of EMT marker *snai1* in tadpole stage embryos
20ng of morpholino were injected into one blastomere of two-cell stage embryos. *Snai1* expression was detected by whole mount RNA *in situ* hybridisation. **(A - D)** Lateral view onto the embryos (NF 32) on either injected or uninjected side. *Snai1* expressing cells are especially located in the area of jaw, branchial arches and in the hyp- and epaxial posterior lines along the tailbud. **(E)** Phenotypic penetrance of *snai1* expression in tadpole stage NF 32. $p>0.05$; n = 3 biological replicates, scale bar indicates 1 mm.

In conclusion, I did not observe a significant alteration of the *snai1* expression pattern after *mespa* knockdown at any of the three developmental stages. In this study, we could neither prove the regulatory interaction between *mespa* and *snai1* in *Xenopus* during gastrulation (NF 11) previously described in ES cells, nor uncover an indirect regulatory interaction between mesodermal *mespa* and *snai1* in the NC at the neurula and tadpole stages.

3.7.3 *Twist1* expression and function

The second EMT marker, which I investigated, is *twist1*, a bHLH transcription factor that was first cloned as a cDNA related to the Drosophila gene *twist* (Hopwood, Pluck, & Gurdon, 1989). Activated after mesodermal induction, *twist1* is initially exclusively expressed in mesodermal cells including the notochord and the lateral plate mesoderm. As development proceeds, *twist1* gets activated independently in the neural crest, yet with a temporal delay compared to *snai1* (Linker, Bronner-Fraser, & Mayor, 2000).

In addition to its important role in gastrulation (Thiery & Sleeman, 2006), the bHLH transcription factor *twist1* has been found to have a major influence in the process of the specification of cranial structures, since its loss disrupts the formation of the viscerocranium (H. Bildsoe et al., 2013). It has to be considered that the branchial arches, from which cranial structures largely arise, are a construct of mesodermal and ectodermal origin. While the neural crest contributes to the formation of cartilage and bone of the face

(Mayor, Yaung, & Vargas, 1999), recent publications have brought to light that head muscles and cardiovascular progenitors share a common mesodermal origin patterned by *mesp1* (Lescroart et al., 2010).

Here, I take a closer look at the changes of *twist1* expression patterns after *mespa* knockdown at vital developmental stages of *Xenopus* embryos to elucidate a potential interaction between *xmespa* and *twist1*-expressing cells.

3.7.4 Expression of EMT marker *twist1* depends on early *mespa* activation

MO-based knockdown experiments were performed at the two-cell stage with a unilateral injection of 20ng of *mespa* MO (Fig. 26), while tracing the injected side with *lacZ* staining. During early neurulation, *twist1* is restricted to the mesoderm, being expressed in the notochord and in two distinct cell patches, which contribute to the head mesoderm.

At NF 16, *twist1* expression emerges in the neural fold (Linker et al., 2000). Interestingly, at the early neurula stage (NF 14) *mespa* knockdown caused a partial loss of the anterior *twist1*$^{+}$ cell patch in 75% of the embryos (Fig. 26 B). The notochord appeared broadened and twisted. Although one third of control embryos also exhibited this reduction of the lateral anterior patch, the alterations in the expression pattern of *mespa*-depleted embryos was statistically significant ($p<0.01$).

To observe the dynamic process during development, the experiment was repeated for the tail bud (NF 25) and tadpole stages (NF 32). At stage NF 25, *mespa* knockdown resulted in a reduction and migratory delay of *twist1*-expressing cells in the neural, hyoid and branchial crest in 68% of *mespa*-deficient embryos, being compatible with the findings at the neurula stage (Fig. 26 I, J) ($p<0.0001$).

The analysis of *twist1* expression in *mespa*-blocked tadpole embryos (NF 32) provided a phenotype consistent with the aforementioned early developmental stages (Fig. 27). About 49% of the embryos showed a reduced and disarranged *twist1* expression in the area of the branchial arches (Fig. 27 E, F). The paraxial expression in the posterior hyp- and epaxial cell lineages was unaffected.

These knockdown studies of *mespa* on *twist1* expression showed a persistent reduction of *twist1* expression throughout the sequence of early development.

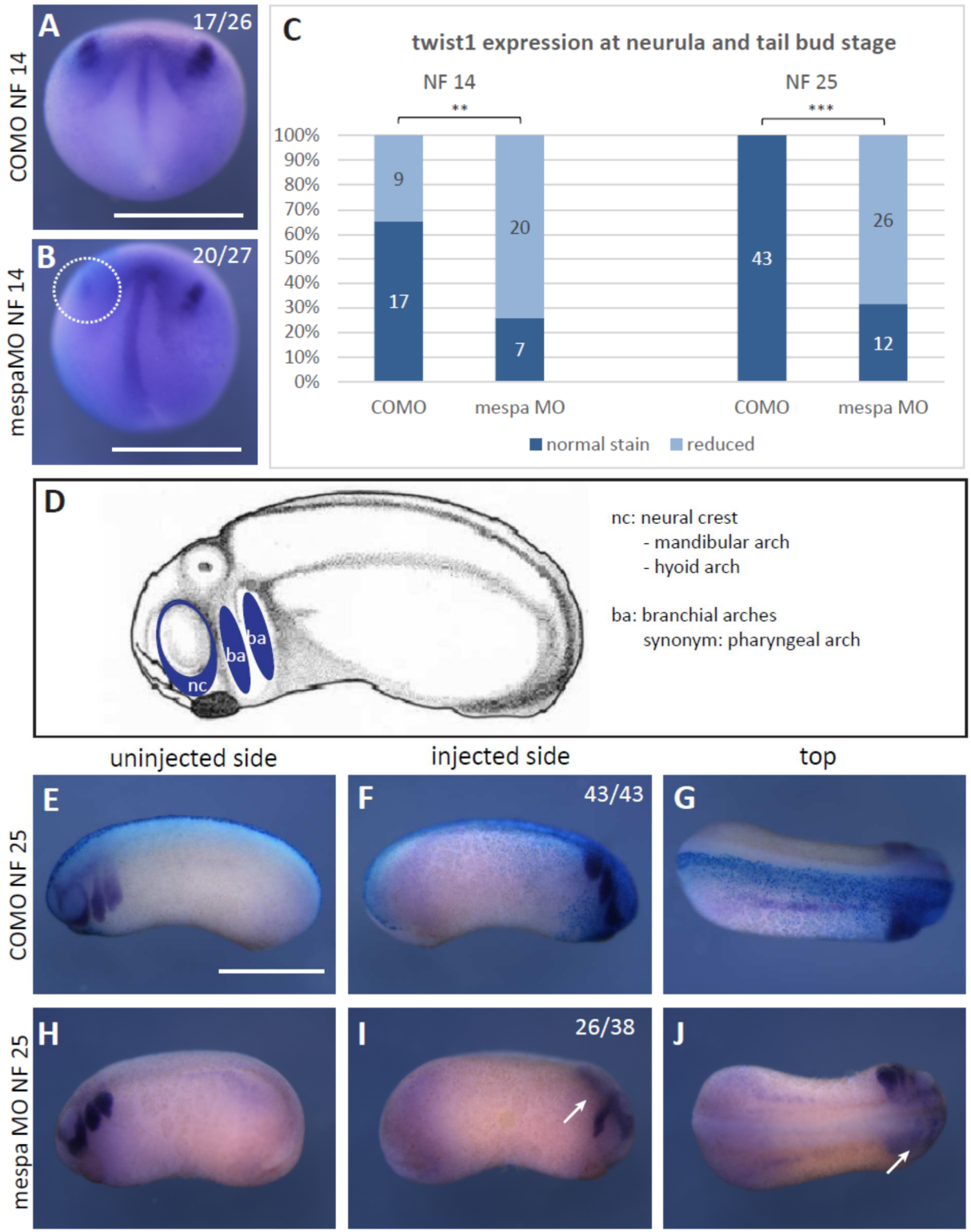

Figure 26: Expression of EMT marker *twist1* depends on early *mespa* activation
20ng of morpholino were injected unilaterally at the two-cell-stage and embryos were cultivated until the neurula stage and the ail bud stage respectively. Subsequently embryos were proceeded to whole mount RNA *in situ* hybridisation. A reduction of expression was observed in the branchial arches from neurula to tail bud stage after morpholino based *mespa* knockdown. White dashed circle and white arrows point out the loss of *twist1* stain in *mespa*-depleted embryos. **(A) + (B)** View from dorsal, anterior on top, posterior on the bottom. **(C)** Distribution of *twist1* expression pattern in neurula (NF 14) and tail bud stage (NF 25) embryos. **(D)** Illustration of *twist1* expressing cranial structures in tail bud embryo (NF 25). **(E) + (H)** Lateral view , anterior left**. (F) + (I)** Lateral view onto the injected side, anterior right. **(G) + (J) V**iew from the top, anterior right. n≥3 biological replicates, **, $p<0.01$; ***, $p<0.0001$; scale bar indicates 1 mm

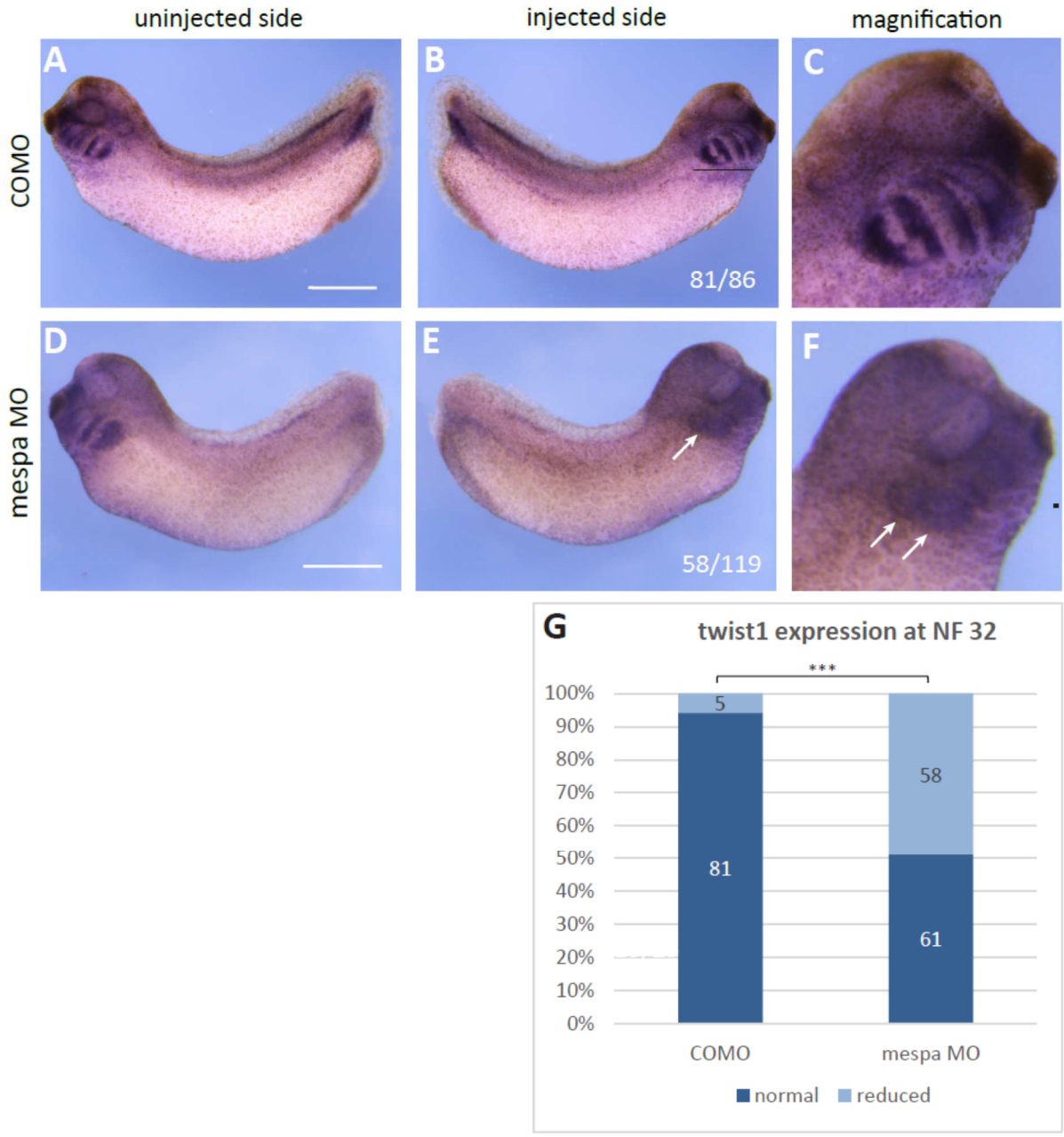

Figure 27: Deterioration of *twist1* expression in *mespa* depleted embryos persists until the tadpole stage
20ng of morpholino were coinjected with Alexa 488 and sorted according to their injected side. The images show embryos after whole mount RNA *in situ* hybridisation. Diminished *twist1* expression can be seen in the branchial arches and rarely in the hyp- and epaxial lines. **(A) + (B)** Control MO. **(D) + (E)** *mespa* MO; **(C) + (F)** Images depict magnifications of the head of the injected side. White arrows point at missing branchial arches. All images show lateral views. **(G)** Phenotypic penetrance of *twist1* expression in tadpole embryos (NF 32)**;** n≥3 biological replicates; ***, $p<0.0001$; Scale bar represents 1mm.

3.7.5 *xmespa* mRNA rescue and overexpression cause defects of facial structures

To prove the specificity of the effect of *mespa* MO knockdown, one-sided coinjections with 750pg of *xmespa* mRNA were performed at the two-cell-stage. Cultivation was done up until the tadpole stage NF 32 with exchange of buffer on a daily basis.

Surprisingly, embryos under rescue conditions with 750pg of mRNA exhibited even heavier defects of the *twist1* expression of facial structures compared to *mespa*

morphants, especially in the branchial arches (Fig. 28 B, C). 58 out of 119 *mespa* MO injected embryos exhibited a reduced *twist1* expression pattern versus 38 out of 55 embryos injected with *mespa* MO plus *xmespa* mRNA (Fig. 28 D). *Twist1*$^{+}$ cells were disarranged and spread over the head region, with the exception of their natural location in the branchial arches. Hence, *xmespa* coinjection could not restore the normal *twist* pattern, but reduced the expression domain.

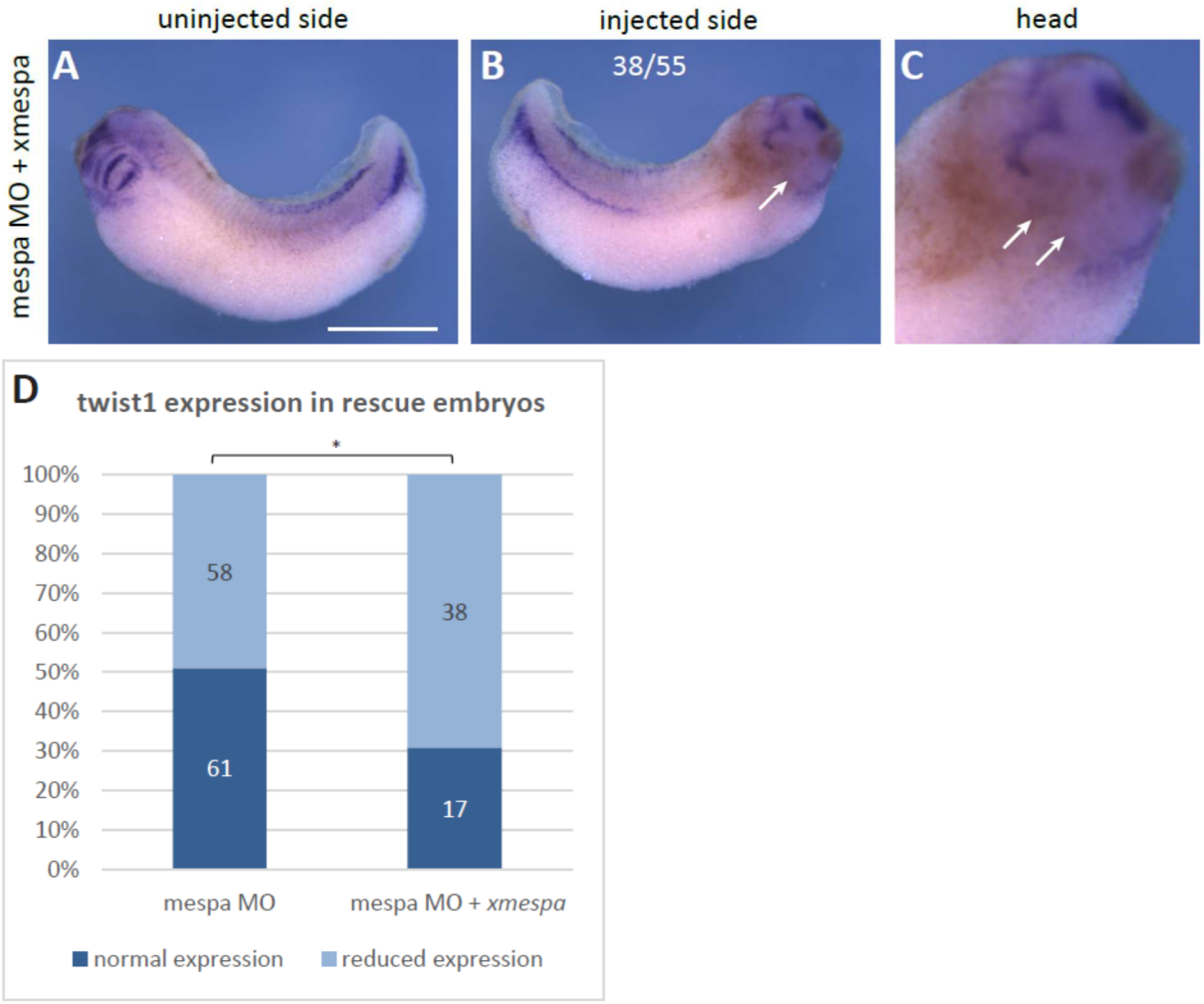

Figure 28: *xmespa* mRNA cannot rescue *twist1* expression in the head region of *mespa* depleted tadpoles
20ng of *mespa* MO were coinjected 750pg *xmespa* mRNA and Alexa 488. Embryos were sorted according to their injected side in NF 32. Whole mount RNA *in situ* hybridisation was perfomed to evaluate *twist1* expression. Simultaneous injection of *mespa* MO and *xmespa* mRNA does not rescue the normal *twist1* phenotype but compound the loss of cranial *twist1* expression. **(A) + (B)** Lateral view. **(C)** Magnification of the head. **(D)** Phenotypic penetrance of *twist1* expression in tadpoles after rescue injection (*mespa* MO + 750pg *xmespa* mRNA). White arrows point out the localisation of the branchial arches. n≥3 biological repeats. *, $p<0.05$; scale bar represents 1mm.

To complete my investigations of the influence of *mespa* on *twist1* expression, I injected 20ng of COMO together with 750pg of *xmespa* mRNA into one half of two-cell-stage embryos (Fig. 29). The overexpression of x*mespa* led to a reduction of the *twist1* stain, predominantly in the branchial arches, in 50% of the modified embryos (Fig. 29 B, C, D, $p<0.0001$). *Twist1*-expressing cells contributing to other facial structures were present,

but not appropriately located. The observed perturbed and disarranged *twist1* patterns in *xmespa*-overexpressed embryos were comparable to those in rescue embryos.

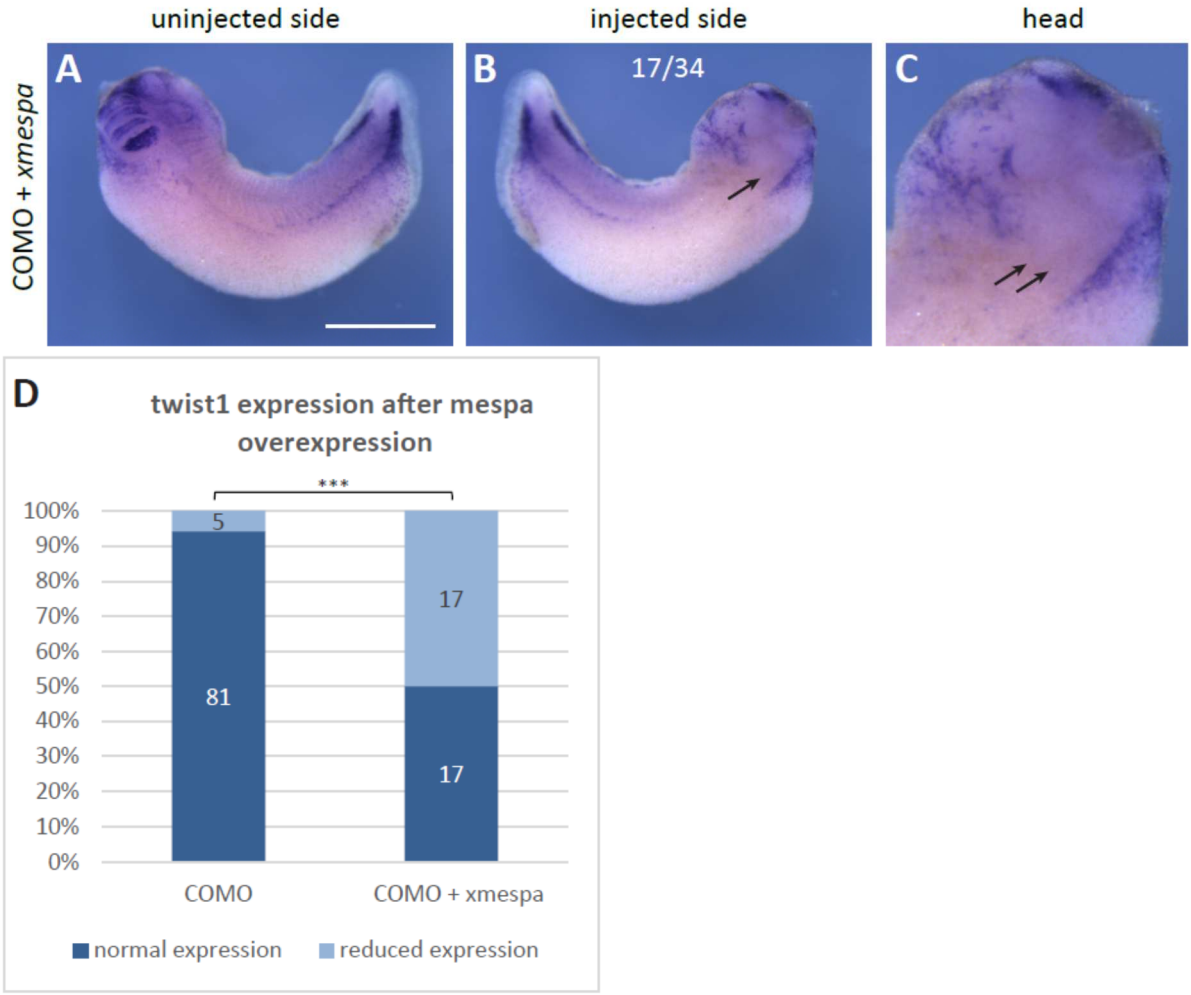

Figure 29: Overexpression of *xmespa* mRNA leads to reduced and disarranged *twist1* expression in the head region
20ng of COMO were coinjected with 750pg *xmespa* mRNA and Alexa 488. Embryos were sorted according to their injected side. Images show embryos after whole mount RNA *in situ* hybridisation. Overexpression of *xmespa* mRNA provokes a striking reduction and disarrangement of cranial *twist1* expression especially in the branchial arches. **(A) + (B)** Lateral view. **(C)** Magnification of the head. **(D)** Penetrance of *twist1* expression in tadpoles. Arrows indicate the natural localisation of the branchial arches. n≥3 independent biological repeats; ***, $p<0.0001$; Scale bar: 1mm.

In these experiments, I showed the interaction between *mespa* and the morphology of *twist1* expression at the neurula and tail bud stages in migrating mesodermal and NC cells and as a representative of facial structures of mesodermal origin at the tadpole stage. Depletion of *mespa* caused an important loss of mesodermal *twist1* expression at the neurula stage (Linker et al., 2000) and of the branchial arches at the tail bud and tadpole stages, which could not be rescued by the coinjection of *xmespa* mRNA and MO. This suggests that *mespa* is required, but not sufficient for *twist1* expression. The overexpression resulted in similar aberrations of the facial phenotype in modified embryos, which could indicate possible migratory defects of the mesodermal *twist1*-expressing cells, which usually contribute to the formation of the branchial arches.

4. Discussion

4.1 Mesoderm induction and differentiation

Mesoderm induction marks one of the most important steps during development since it is the basis for the formation of a large variety of tissues and organs and anterior-posterior patterning. The T-Box transcription factors *eomesodermin (eomes)* and *xbrachyury (xbra)* play pivotal roles during the initiation of mesodermal fate, maintenance and patterning (Gentsch, Monteiro, & Smith, 2017; Probst & Arnold, 2017). Since they can be directly induced by *activin*, *FGF* and *Wnt* signalling, they belong to the earliest signs of mesodermal lineage (Showell et al., 2004). In *Xenopus*, they are spatially and temporally coexpressed with *mespa* in the preinvoluted mesoderm during early gastrulation (compare Fig. 1). Early knockdown analysis on *mesp*-related genes revealed, that they are required for normal gastrulation and mesodermal patterning (Saga et al., 1999). Yet, the epistatic relationships of these factors and their differential function during early development still need to be fully elucidated. Here, I have addressed the question of whether *mespa* is needed for the induction or maintenance of *eomes* and *xbra.*

As Showell et al. (2004) revealed, *eomes* is activated prior to *xbra* and functionally located at the junction of endodermal and mesodermal lineage. The distinct patterning happens in a context-dependent manner. According to a recent report, low Nodal concentrations seem to activate *eomes* in order to give rise to mesodermal progenitors, or more specifically *mesp1*$^{+}$ cardiovascular progenitors, whereas high levels of Nodal guide endodermal and notochord development (Costello et al., 2011). Thus, *eomes* contributes to anterior-posterior axis formation and mesoderm migraton (Arnold, Hofmann, Bikoff, & Robertson, 2008). Another study supports this hypothesis of *eomes* acting upstream of *mesp1*, initiating the cardiogenic cascade by directly binding to *mesp1* promotor sequences in mice. However, van den Ameele et al. (2012) state that the induction of cardiac lineages depends on a temporal expression of *eomes* and on the absence of *activin*, while high *activin* levels promote endodermal fates and inhibit cardiac lineage.

As recently shown, the T-Box transcription factors *brachyury (T)* also plays a crucial role upstream of *mesp1* in mice. David et al. (2011) reported the potential of *brachyury (T),* the homologue of *xbra* in mice*,* to induce *mesp1,* thereby establishing colonies of cardiovascular progenitors in ES cells and in vivo. Moreover, they identified a direct

binding site upstream of the *mesp1* gene in mice. Previous studies showed that *brachyury(T)* is able to enhance cardiac development from a multipotent cardiovascular progenitor, but *eomes* is not (Kattman, Huber, & Keller, 2006).

Although these and other findings (Liu & Schwartz, 2014) suggest a clear hierarchy by which mesp*1* is downstream from *eomes* and *brachyury (T)*, recent Chromatin Immunoprecipitation Sequencing analysis showed, that both *brachyury (T)* and *eomes* can be targeted and induced by *mesp1* (Soibam et al., 2015). Taken together with the previous studies, this might indicate the existence of regulatory feedback loops between the T-Box transcription factors and *mesp1*.

For a better understanding of the regulatory interaction during the early mesodermal induction and patterning, I performed loss-of-function and gain-of-function experiments in *Xenopus laevis*. *Mespa* knockdown revealed that *mespa* is required for *xbra* expression at the early gastrula stage, since *xbra* staining was strongly reduced (Fig. 2 B). However, *mespa* did not seem to be the only inducer since knockdown experiments provided a reduction, but no complete loss of *xbra* expression at the gastrula stages. This is consistent with the fact that other inducers for *xbra* during mesoderm induction exist (Showell et al., 2004). This effect seems to be transient and only plays a role during early patterning processes. Moreover, it has to be considered that the *mespa* MO does not target the dorsal mesoderm, which results in an unaffected expression pattern in the organiser at the gastrula stage. Therefore, *xbra* might be controlled by *mespa* in the non-organiser region only. A possible mechanism of regulation in axial mesoderm is proposed by Latinkic and Smith (1999): According to their findings, negative control by *gsc* restricts *xbra* in the organiser region. Moreover, promoter analysis demonstrated the differential regulation of *xbra* in the organiser region / axial mesoderm and the non-organiser mesoderm (Lerchner, Latinkic, Remacle, Huylebroeck, & Smith, 2000).

At the neurula stage, *xbra* expression was partly restored, but still compromised by the lack of blastopore closure and the gastrulation defects. In line with previous findings by Soibam et al. (2015), *mespa* seems to be an inducer of *xbra*, since ectopic *xbra* expression was observed in animal cap explants at the gastrula stage (Fig. 15 F) and to a significant extent at the neurula stage (Fig. 15 N). After this initiation of mesoderm induction and commitment to specific fates, *mespa* seems to influence migration of mesodermal progenitors including *xbra*$^{+}$ cells and control correct gastrulation and formation of the posterior mesoderm by *xbra*-expressing cells. During mesoderm induction, *xbra*

expression is maintained by a positive feedback mechanism based on FGF activation (Kimelman, 2006). My data suggest that *mespa* might also possess a comparable function for *xbra* maintanence.

Moreover, the gastrulation defects are possibly reflecting the reduction in *xbra* expression, similar to Conlon and Smith (1999), who injected *Xbra*-En^{R}, a construct which inhibits *xbra* induction using the repressor element from Drosophila engrailed replacing the activation domain of *xbra*. In embryos injected with Xbra-En^{R}, gastrulation did not occur appropriately, due to the lack of convergent extension, and the blastopore did not close properly. However, according to Gentsch et al. (2013) *xbra* morphant embryos do not show a gastrulation phenotype. This might be due to the compensation by remaining T-Box TFs, like *eomes* or *vegT*, which share overlapping binding sites with *xbra*. As shown, T-Box TFs contribute to a gene regulatory network maintaining neuromesodermal bipotent stem cells and the loss-of-function of these genes favors neural development (Gentsch et al., 2013).

The unpaired tail bud blastema did not permit to distinguish precisely the effects of the knockdown and the difference between the left and right side of the embryo with regards to *xbra* expression. Hence, I focused on early interactions, for which the experiments were likely to generate more detailed information. In conclusion, *mespa* and *xbra* might be connected through a positive feedback loop to keep the expression of *xbra* and its activation of *mespa* constant in order to enhance cardiovascular fate. The missing effect of *mespa* on *xbra* expression after knockdown in tadpole embryos also supports this theory. At this developmental stage *xbra* expression still remains in the tail bud blastema for the outgrowth of the tail, which does not seem to be controlled by *mespa*. *Xbra* expression persists in bipotential neuromesodermal progenitors of the chordoneural hinge and the posterior wall of the neurenteric canal, where *mespa* is not expressed (Gentsch et al., 2017).

My investigations with *mespo* provided further information on this topic**.** After *mespo* knockdown, the domain of *xbra*$^{+}$ cells appeared slightly broadened at the gastrula and neurula stages (Fig. 2 D, G). This could be explained by the two processes of direct induction and the lacking progress of migration. *Mespo*-deficient embryos still contain *mespa* (Kriegmair et al., 2013). *Mespa* can thus induce *xbra*, while *mespo*-deficient cells are slightly prevented from physiological involution due to the migratory deficit caused by the lack of *mespo.* These *mespo*-deficient cells pile up and create a broader stain.

Alternatively, *mespo* might influence the EMT cassette during involution, since gastrulation is considered an EMT-like process, while *mespa* is needed for migration of the anterior edge mesoderm. As shown by Gentsch et al. (2013) that in *xbra* deficient embryos the anterior most somites are generated under the influence of *vegT* and *eomes*. In this context, *mespa* might also play an important role being expressed in the leading edge mesoderm (Kriegmair et al., 2013). The anterior and posterior separation of *mespa* and *mespo* expression during gastrulation might be part of the separation of head and trunk somites, with *mespo* being involved in the segmentation of trunk and tail somites.

However, in zebrafish, it was reported that *mespo* is located downstream of *ntl*, the zebrafish homologue of *xbra* (Goering et al., 2003). In conclusion, *mespo* has no influence on *xbra* transcription, while *mespa* can induce *xbra* expression in non-organiser mesoderm of *Xenopus* at early developmental stages. This indicates potential involvement of *xbra* in a common regulatory feedback loop.

In contrast to *xbra, mespa* and *mespo* knockdown have only marginal effects on *eomes* transcription (Fig. 3 B + C). It remains possible that the *mespa*/*xbra* feedback loop ensures the correct number of *eomes* expressing cells in preinvoluted mesoderm. Interestingly, in the naïve pluripotent cells of animal caps *mespa* can induce the *eomes* gene in ectopic manner (Fig. 15). This suggests that, in line with the recent findings in ESC by Soibam et al. (2015), it is also possible for *eomes* to be directly targeted by *mespa* in *Xenopus*. This is particularly interesting considering that *eomes* is the earliest-expressed marker of mesoderm induction (compare Showell et al. (2004)). One explanation might be that depending on the surroundings in which *mespa* expression takes place or the level of *eomes* transcription, *mespa* can either induce or limit *eomes*.

At later stages beyond the tail bud stage, *eomes* is not affected by *mespa* as the cells in the neural tissue of the telencephalon in which *eomes* is reactivated, are not related by lineage to *mespa*-derived mesoderm. Hence, the mutual interaction is only restricted to early mesodermal induction and patterning until the downregulation of *eomes* in mesoderm.

This study proves the involvement of *mespa* in early mesoderm induction and patterning of non-committed mesodermal progenitors, more likely supporting the idea of a regulatory network instead of the concept of rigid epistatic activation. Moreover, these considerations suggest that binding of *mespa* to *xbra* and *eomes* gene regulatory regions is regulated in a context-dependent manner.

4.2 Skeletomyogenesis

Research in developmental biology has provided great insight into the regulatory mechanisms driving skeletal muscle formation as a major step in the process of mesodermal differentiation and specification. An increasing amount of evidence indicates that myogenesis in cranial and trunk muscles have distinct regulatory programmes and arise from distinct cell populations (Kelly, 2012; Tajbakhsh, 2009; Tzahor, 2009). Several studies in mice suggest that trunk muscles originate from the somites, a development assisted by *pax3/7*, whereas head muscles come from the anterior paraxial mesoderm and prechordal plate (Buckingham, 1992; Chal & Pourquie, 2017). Furthermore, investigations of myogenesis have identified a common source of cardiac and craniofacial myogenic progenitors (Tzahor, 2009), which could indicate a role of *mespa* in skeletomyogenesis.

My experiments concerning the interplay of *mespa* and the myogenic regulatory factors (MRFs) *myoD* and *myf5* mainly addressed the question of how *mespa* influences skeletomyogenesis during early developmental stages and in the process of development. At later developmental stages in *Xenopus*, MRFs and especially *myf5* are not only expressed in skeletal muscle of the trunk, but also in distinct or overlapping groups of head muscles as shown in this work and by Della Gaspera et al. (2012).

Chan et al. (2013) showed that *mesp1* is able to induce paraxial mesodermal fate and myogenic progenitors expressing *myf5* and *myoD* in serum-absent conditions. These progenitors contribute particularly to the formation of cranial muscles, but also, albeit to a lesser extent, to trunk and limb muscles. As recently confirmed, cardiac and skeletal myogenic progenitors of the head region arise from a common *mesp1*$^{+}$ origin. Certain factors in the serum are capable of driving cardiac fate, while down-regulating skeletal muscle fate (Chan et al., 2016). *TGFß1/activin*-inhibition and the stimulation of *BMP2/4* facilitate development in a cardiogenic direction. Hence, depending on the environment, *mesp1*$^{+}$ cells have the ability to transdifferentiate into distinct fates. Reflecting the close proximity of cardiac and myogenic lineages, their findings preferentially cover the myogenic origin of head structures, which will be discussed later.

Addressing the topic of myogenic regulation, differences between myogenesis in *Xenopus* and myogenesis in mammals and avian species caused by metamorphosis have to be considered (Della Gaspera et al., 2012). In *Xenopus*, it is possible to delineate three myogenic waves: The first one occurs before dermatomyotome formation, i.e. at the

gastrula and neurula stages, and probably disappeared in higher vertebrates. The second wave happens during somitogenesis, while the third and last wave takes place after metamorphosis. The differential expression of MRFs in these three phases suggests distinct myogenic programmes, which might even be regulated epigenetically. However, which role does *mespa* play during these three waves of myogenesis?

Due to temporal and spatial overlap, we expected a regulatory interaction of *mesp*-related genes, i.e. *mespa* and *mespo*, and the two myogenic regulatory factors *myoD* and *myf5*. At early developmental stages when mesodermal patterning takes place during gastrulation, they exhibit comparable expression domains in the marginal zone, except for the prospective notochord (Fig. 1). In contrast to our observations, *myf5* is reported to be restricted to the dorsolateral portion of the marginal zone (Sabillo et al., 2016). Since this portion has also been fatemapped as the origin of the prospective heart anlagen, coexpression of *mespa* and *myf5*/*myoD* suggests a common progenitor cell for cardiac and skeletomyogenic lineages, whose final fate decision depends on environmental cues.

In my investigations, a striking *mespa*-dependence of myogenic regulatory factors *myoD* and *myf5* expression could be observed throughout embryonic development. Knockdown experiments with *mesp* genes revealed that *mespa* is required for *myoD* (Fig. 5 and 7) and *myf5* expression (Fig. 6 and 9). This proves for the first time that *Xenopus mespa* is not only crucial during specification at the gastrula stage, as shown by Frenz (2017), but also for normal myogenesis at the neurula stage, when the organisation of paraxial mesoderm occurs, and at the tadpole stage. Interestingly, *mespo*, as a downstream target of *mespa*, exhibited a similar involvement in myogenesis. Yet this involvement was restricted to gastrulation, since myogenic gene expression in *mespo* morphants recovered to normal levels by neurula stage, suggesting a compensatory mechanism.

However, animal cap assays (Fig. 15) and *mespa* overexpression approaches (Fig. 12 and 13) did not display direct inducibility or ectopic expression of *myoD* and *myf5*. This is consistent with recent findings from ChIP Seq analysis in murine ES cells, which also did not observe a direct induction of myogenic transcription factors *myoD*, *myf5* or *myogenin* by *mesp1* (Soibam et al., 2015). This matches the results of my animal cap assay in which I found no direct inducibility in ectopic tissue. However, the interaction has to be assessed differentially: *Mespa* might have a distinct impact on myogenesis, regulating the first and second, but not the third wave of muscle formation. Since the first two phases represent indirect development before metamorphosis in *Xenopus*, mammals undergo direct

myogenesis, corresponding to the third wave, while the other waves have been lost during evolution (Sabillo et al., 2016). Furthermore, differences of genetic properties between amniote and frog homologues of *myoD* have been described. In *Xenopus*, a differential localisation of overexpressed myc-tagged *xmyoD* protein was found in different regions of the embryo: At the animal pole, *xmyoD* is mainly expressed in cytoplasm, but can also be expressed in the nucleus in the marginal zone, hence in regions where mesoderm induction takes place. Mouse *myoD* is constitutively nuclear (Rupp, Snider, & Weintraub, 1994). This might also indicate the presence of different regulatory relations in frogs and mammals.

In fact, there might be several reasons, why *mespa* cannot activate the early myogenic genes. First, the effect of *mespa* interference could be dose-dependent, which means that *mespa* only activates myogenic markers at high doses. However, overexpression experiments probably leads to supraphysiological concentrations.

Second, as we have observed in recent reports, the specification into certain lineages differs based on the surroundings, coexpressed factors and the timepoint of activation (Chan et al., 2013). As demonstrated by Chan et al. (2016), muscle differentiation also depends on Rho-kinase inhibition in *mesp*$^{+}$ progenitors. Since *mespa* as a bHLH transcription factor acts via hetero- or homodimerisation (Chan et al., 2013; Lindsley et al., 2008), its role in skeletomyogenesis could be transmitted by binding partners like E-proteins, which facilitate a much more efficient binding to promoter regions. As animal cap assays are conducted in ectopic tissue, they may not provide a sufficient amount of the aforementioned binding partners that to replicate the natural conditions found during mesodermal patterning. Hence, simply overexpressing *mespa* in unphysiologically high amounts of mRNA is not sufficient to drive myogenesis, neither in the animal cap assay nor in the whole mount approach. In contrast, constitutive expression of *mespa* favours cardiac differentiation instead of skeletomyogenesis (Chan et al., 2013).

The lack of induction or specification of mesoderm by *mespa* at early timepoints in knockdown animals has a prolonged impact on myogenic differentiation, which can be seen during the second myogenic wave (Fig. 5, 6, 7, 9). The development of trunk muscles is dependent on correct somitogenesis and the formation of the dermatomyotome in *Xenopus*. The homologues *mesp1* and *mesp2* in mice, or *mespa* and *mespb* in lower vertebrates like *D. rerio* and *X. laevis*, play essential roles in these processes. *Mesp2* is responsible for rostro-caudal patterning, whereas *mesp1* facilitates epithelialisation

(Morimoto, Kiso, Sasaki, & Saga, 2006; Takahashi et al., 2005; Takahashi, Yasuhiko, Kitajima, Kanno, & Saga, 2007). *Mesp1/2* double-knockout mice exhibit a completely disrupted somite formation (Saga et al., 1997).

In *Xenopus*, *mespb* is concerned to play similar roles as *mesp2* in mammals (Kriegmair et al., 2013). By mediating normal somitogenesis in cooperation with *mespb*, *mespa* supports the process of appropriate dermatomyotome formation. In accordance with my loss-of-function experiments, *mespa* is crucial for trunk expression of *myoD* in the stacked myocytes of differentiating somites and *myf5* in the hyp- and epaxial myotome, representing the ventral and dorsal borders of the dermatomyotome. The missing direct inducibility of myogenic progenitors in the animal cap assay and the lack of a direct binding of *mesp1* to myogenic promotor regions (Soibam et al, 2015) support this notion of an indirect influence of *mespa* on trunk myogenesis. This stays in line with the low contribution of *mesp1*$^{+}$ cells to the formation of trunk and limb formation (Chan et al., 2013).

The perturbed somitogenesis and the control of migration via *RasGRP3* explain the impaired elongation of *mespa*-deficient embryos (Chiapparo et al., 2016). Another possible mediator in somitogenesis could be *mespo*, also known as *pMesogenin1*, acting downstream of *mespa* (Kriegmair et al., 2013). This *mesp*-related bHLH transcription factor is considered to be crucial for segmentation in somitogenesis and trunk muscle formation (Tazumi, Yabe, Yokoyama, Aihara, & Uchiyama, 2008; Wang et al., 2007; Yoon & Wold, 2000), since *mespo* depletion in mice leads to the complete loss of both somite formation and the segmentation of trunk and tail.

In my investigations, I was able to demonstrate that *mespa* is required, but not sufficient to induce myogenic regulatory factors during early *Xenopus* development. Further distinctions of regulatory mechanisms by Chromatin Immunoprecipitation Sequencing (ChIP-Seq), conditional gain-of-function experiments using glucocorticoid inducible fusion proteins or specific gene knockout by Crispr/Cas9 might be suitable approaches to gain a deeper insight into the impact of *mespa* on myogenesis.

4.3 Vasculogenesis

Vasculogenesis describes the developmental process of *de novo* formation of blood vessels from undifferentiated mesodermal progenitor cells. Vasculogenesis has to be clearly distinguished from the term angiogenesis, which means the growth or sprouting of new vessels from already existing vascular structures (Drake, 2003). Vasculogenesis occurs concomitantly with haematogenesis due to a common precursor cell, the so-called haemangioblast (Drake, 2003). Likewise, close developmental relations between the heart and the vascular system have been revealed. Lineage tracing studies by Kattman et al. (2006) identified multipotent progenitors of the cardiovascular lineage expressing *Flk1*, i.e. vascular endothelial growth factor receptor 2 (*VEGFR2*). These multipotent progenitors possess the potential to differentiate into either cardiac, endothelial or smooth muscle lineages.

Despite extensive *in vitro* studies, vasculogenesis is still not completely understood *in vivo*. To examine the role of *mespa* during the process of vasculogenesis in *Xenopus*, I investigated its influence on the expression of the endothelial receptor *aplnr*. First discovered as *APJ* in human cells by O'Dowd et al. (1993), the *Xenopus* homologue is termed *aplnr* or *xmsr*, i.e. *Xenopus* mesenchyme associated serpentine receptor. This small G-Protein-coupled receptor was found to be located in the inner layer of endothelium during heart tube formation and vasculogenesis (Devic et al., 1996).

Early investigations on the function of *mesp1* in mice uncovered a small population of mesodermal *mesp1*-expressing cells as the major source of almost all vascular progenitors, including those giving rise to the endothelium of the dorsal aorta and intersomitic and cranial vessels (Saga et al., 2000). By directly binding to regulatory gene domains, *mesp1* acts as the master activator of the transcriptional programme for cardiovascular development in early mesodermal differentiation (Bondue et al., 2008). In this context, *mesp1* specifically promotes common multipotent cardiovascular progenitors (MCPs) from which cardiac and vascular precursor cells arise. A dual reporter strain of human ES cells confirmed the potential of *mesp1*-expressing cells to undergo multiple fates (Den Hartogh et al., 2015). Several lines of evidence proved an increase of vascular or endothelial markers like *Flk1* or *Pecam-1* after *mesp1* overexpression in ES cells (David et al., 2008; Lindsley et al., 2008). Recently, Eskildsen et al. (2019) confirmed the impact of *mesp1* on vasculogenesis in hiPSC by showing that the specific knockdown of *mesp1* by CRISPRi system leads to a decrease of genes involved in vascular cell

determination, like *kdr/vegfr2*. Moreover, microarray data of *mesp1*-expressing cells showed an upregulation of *alpnr* in ES cells during E6.5 and E7.5 after transient activation of *mesp1* (Bondue et al., 2011; Lescroart et al., 2014). Furthermore, they uncovered the direct binding of *mesp1* to the *aplnr* promotor region by Chromatin-Immunoprecipitation Sequencing analysis (ChIP-Seq) and a strong coexpression in single-cell-PCR. These data favour the notion that *mespa* also acts upstream of *aplnr* in *Xenopus*.

The MO-based knockdown experiments of this study focused on the analysis of the *mespa*-dependence of *aplnr* at the tadpole stage, which merely reflects one timepoint during organogenesis. The experiments revealed that *mespa* is essential for normal *aplnr* expression in major vessels like the cardinal and intersomitic veins, the aortic arches and periocular vessels in *Xenopus* tadpoles (Fig. 17 D, E). The specificity of this effect was proven by the partial rescue of the normal *aplnr* phenotype (Fig. 18), particularly concerning the expression of *aplnr* in the cardinal and intersomitic veins and aortic arches. This is in line with the epistatic findings of *mespa* and *aplnr* in ES cells in previous studies. Poole and Coffin (1989) demonstrated that the major vessels are subjected to distinct processes. While the cardinal vein, dorsal aorta and aortic arches are generated de novo by vasculogenesis, intersomitic veins arise from angiogenic sprouting, as confirmed by transplantation experiments. My results suggest that *mespa* is required for vasculo- and angiogenesis.

In contrast to previous investigations, the one-sided overexpression of *mespa* mRNA in two-cell-stage embryos did not result in an enhancement or ectopic *aplnr* expression as shown by the Dox-inducible approach in ESC (Lescroart et al., 2014) or in *Xenopus* animal cap assays by Frenz (2017). The overexpression approach in one blastomere at the two-cell-stage (Fig. 19) and probably also the high *xmespa* mRNA dose of 750pg in the rescue experiment implies that *mespa* reached areas where it is usually not expressed. This may have led to a disorganisation of cell migration and subsequently to a disarranged and attenuated phenotype as depicted in Figure 19. Due to its essential role in migratory processes, the expression of *mespa* in the NC could be particularly critical in this regard.

Various studies have provided great insight into the function of *aplnr*. Interestingly, they reported a remarkable role of *aplnr* in cardiogenesis in several model organisms. As described in *Xenopus*, *aplnr* and its ligand *apelin* are required for the expression of cardiac genes of the contractile apparatus like *cTnI* (Inui et al., 2006). In comparison, *Apelin/APJ* deficient zebrafish embryos exhibited a severely reduced number of cardiac progenitors

(Zeng, Wilm, Sepich, & Solnica-Krezel, 2007). A possible explanation for the contribution of *apelin*/*APJ* to cardiogenesis was suggested by D'Aniello et al. (2009). They proposed that *apelin/APJ* as a downstream target of *Cripto* participates in cardiac differentiation. Similar to the embryonic lethality of *mesp1*/*mesp2* double-knockout in mice, the majority of *APJ*-/- homozygous mutants died due to cardiovascular malformations in utero (Kang et al., 2013). Surprisingly, the most recent study in zebrafish highlighted that *aplnr* mutant embryos exhibited a delayed expression of *mespaa*/*ab* during early cardiovascular development (Deshwar, Chng, Ho, Reversade, & Scott, 2016), proposing an inverse epistasis of *aplnr* and *mespaa/ab*. Taken together, *aplnr* plays an essential role during cardiovascular development by regulating the migration of cardiac progenitors.

In line with the whole set of investigations performed on the interaction between *mespa* and *aplnr* during vasculo- and cardiogenesis, this study suggests a clear epistatic interaction of *mespa* and *aplnr*. Since the expression of both starts at NF 9, i.e. immediately after zygotic genome activation, it is difficult to distinguish which one is upstream of the other. Since *mespa* expression emerges with delay, but still reaches full intensity after *aplnr* depletion in zebrafish, *aplnr* might merely provide an augmenting, but not an inducing, effect on *mesp* expression. Taken together with the finding of direct binding sites of *mespa* at the *aplnr* promotor, this clearly supports the idea that *mespa* is a major vascular regulator.

4.4 Haematopoiesis

The onset of adult haematopoiesis is closely linked to that of vasculogenesis, since both differentiation programmes derive from a common progenitor of lateral plate mesoderm (LPM), the so-called definitive haemangioblast (DH). In the Endothelial-to-Haematopoietic Transition (EHT), haematopoietic stem cells arise from haemogenic endothelium of the ventral wall of the nascent dorsal aorta (DA) (Ciau-Uitz & Patient, 2016). The DA is formed from cell colonies emerging from both sides of the DLP and fusing in the embryo's midline (Cleaver & Krieg, 1998). Definitive haemangioblasts constitute the first adult haematopoietic stem cells and thus represent the source of all adult blood cells. These lineage specifications occur during intraembryonic haematopoiesis. When addressing the subject of haematopoiesis, evolutionary differences between organisms,

like the shift towards in utero development in amniotes, need to be considered. While the zebrafish and the African claw frog develop extracorporally, they do not exhibit a yolk sac, which, in amniotes, is responsible for primitive blood formation, i.e. embryonic (extraembryonic) haematopoiesis. Its correlate in *Xenopus* and zebrafish is located in the so-called ventral blood islands in the ventral yolky part of the embryo. To date, the nomenclature and definitive origin of certain lineages have been discussed controversially. Lineage tracing analysis shed light on the origin of haematopoietic lineage, revealing that both DLP and posterior ventral blood islands derive from the ventral marginal zone, yet from different blastomeres (DLP from C3 and pVBI from D4), while anterior ventral blood islands originate from dorsal blastomeres (C1 and D1) of the marginal zone (Ciau-Uitz et al., 2000).

The influence of *mesp1* on haematopoiesis has been discussed controversially in the past. Several studies reported a direct suppression of haematopoiesis by *mesp1* in ES cells in mice, but also found Wnt-signalling to be a requirement (Bondue et al., 2008; Bondue et al., 2011; Lindsley et al., 2008). Up to now, several mechanisms suggesting the contribution of *mesp1* to haematopoiesis have been proposed.

Cai et al. (2012) showed that *mesp1* drives the expression of *Meis1* and *Meis2* in haemogenic endothelium. *Meis*, which refers to myeloid ectopic viral integration site, mediates the proliferation of haematopoietic progenitors, and facilitates megakaryocyte development.

Recent investigations in zebrafish and mice revealed *Trf3* and *Taf3* as upstream activators of *mespa* or *mesp1,* respectively, and showed a disrupted haematopoiesis after depletion either by MO injection in zebrafish embryos or RNA interference in mice. Chromatin Immunoprecipitation experiments uncovered a direct binding in the *mespa* promotor region. *Mespa* mRNA overexpression rescued normal expression of *gata1* and *hbbe1* involved in haematopoiesis (Hart, Raha, Lawson, & Green, 2007; Hart, Santra, Raha, & Green, 2009). Since neither *Trf3*- nor *mespa*-depleted embryos exhibited *cdx4* in their haematopoietic lineage, Hart et al. suggested a *Trf3* – *mespa* – *Cdx4* pathway. The *cdx4* gene encodes a protein also involved in haematopoiesis and is a possible downstream target of *mespa*.

Furthermore, temporal mapping via doxycycline-mediated *mesp1* pulse induction experiments showed a commitment of *mesp1*$^{+}$ mesodermal progenitors to haematopoietic lineage instead of cardiac lineage. In this context, it was found that the

heterodimer of *mesp1* and E12 binds to the *Tal1/Scl* enhancer in order to generate cells that undergo haematopoietic differentiation (Chan et al., 2013). *Tal1/Scl* marks the bipotent haemangioblasts, since it is also expressed in endothelium, but in contrast to its central role in haematopoiesis, *Tal1/Scl* is not essential for vascular development (Gering, Rodaway, Gottgens, Patient, & Green, 1998; Porcher et al., 1996). These findings indicate that binding partners like E-Proteins are necessary to confer fate to developping cells. This could be one mechanism to explain the contribution of *mespa* to haematopoietic lineage specification. Interestingly, a previous study showed that the presence of *Tal1/Scl* is sufficient to drive early mesodermal cells into haematopoietic fate in a cell-autonomous manner (Ismailoglu, Yeamans, Daley, Perlingeiro, & Kyba, 2008).

Recently, *Mesp1*-YFP-marked progenitor cells have been reported to contribute to haematopoietic lineages and subsequent ChIP-Seq data showed an upregulation of genes involved in blood formation like *Gata1, Lmo2, Tal1, Hbb-bh1, Hbb-y* (Soibam et al., 2015). My experiments revealed a striking impact of *mespa* on early ventral blood formation in *Xenopus* tadpoles, taking advantage of *α-globin (hba1)* as a distinct marker for erythropoiesis. Furthermore, we were able to prove a morphological reversibility of the phenotype by *xmespa* mRNA coinjection. However, knockdown of *mespa* caused a striking impairment of *α-globin (hba1)* expression in the VBI, site of primitive haematopoiesis and equivalent to the amniote yolk sac. By injecting into the two ventral blastomeres at the four-cell-stage, I preferentially targeted the prospective VMZ and therefore the pVBI and the DLP. Since the tube of the dorsal aorta is formed at NF 34, this approach precluded assessment of adult haematopoiesis deriving from haemangioblasts (Ciau-Uitz et al., 2000). From these results, I can draw a line to previous findings concerning the influence of *mespa* homologues in zebrafish or mouse. Interestingly, lineage tracing by Chan et al. (2013) proved that, in mice, the majority of yolk sac and an important part of adult haematopoietic cells originated from *mesp1+* progenitors. Therefore, I can conclude that, depending on the timepoint of *mespa* activation and the surrounding of the cells, mesodermal cells can undergo haematopoietic development.

A weak spot of the typical *Xenopus* approach - injection of mRNA at two-cell stage – is represented by the temporally uncontrolled production of the protein of interest. While a short period of *mespa* activity during gastrulation is known to be essential for development, our approach leads to a precocious and probably also prolonged expression of *mespa*. This could be one reason, why the rescue worked only partially and

overexpression caused a reduction of expression and led to retarded development. Injection of inducible *mespa* protein variants, e.g. fusion proteins with hormone binding domains from steroid hormone receptors (Hollenberg, Cheng, & Weintraub, 1993; Kolm & Sive, 1995) may provide an elegant and more physiological solution to this problem.
Ill-controlled timing of *mespa* overexpression may also account for another phenotype of my experiments, i.e. the separation of anterior and posterior ventral blood islands, since *mesp1* has the capacity to determine the speed and polarity of cell migration (Chiapparo et al., 2016). Thus, precursors of the anterior and posterior ventral blood islands, which derive from opposite sides of the pregastrula *Xenopus* embryo, cannot meet properly at the ventral side of the embryo at the early neurula stage NF 14 (Ciau-Uitz et al., 2000; Walmsley, Cleaver, & Patient, 2008).
This study was the first to analyse the influence of *Xenopus mespa* on embryonic haematopoiesis. The knockdown and rescue experiments together revealed that *mespa* and even *mespo* are indispensable for early blood formation. Based on our observations of these early developmental stages, we were not able to assess the extent to which *mespa* plays a role in adult haematopoiesis, as this process starts significantly later.

4.5 Nephrogenesis

Nephrogenesis is initiated by the formation of the intermediate mesoderm in the course of gastrulation. The anterior portion of the intermediate mesoderm forms the glomerular blood filter, while the posterior intermediate mesoderm contributes to the formation of the tubule system after epithelialisation (Naylor, Qubisi, & Davidson, 2017). Unlike in amniotes, the pronephron of lower vertebrates like *Xenopus* and zebrafish is a functional organ. In mammals, the pronephron undergoes sequential specification towards meso- and metanephros. Neighbouring mesodermal tissues develop in close relation to the pronephron and give rise to anterior somites (paraxial mesoderm) and the vascular system (dorsolateral mesoderm), notably including the DA (Desgrange & Cereghini, 2015). Progenitors forming the glomerular endothelium emerge from the DA. During pronephrogenesis, precursor cells of the intermediate mesoderm receive diverse induction and patterning signals. First, the intermediate mesoderm is segmented in a rostral to caudal manner, which contributes to the subdivision of the tubule system into

the proximal convoluted tubule (PCT), proximal straight tubule (ST), distal early (DE) and distal late tubule (DL) along the somites and the DA. Investigations by Seufert, Brennan, DeGuire, Jones, and Vize (1999) and Mitchell et al. (2007) suggested that intermediate mesoderm receives inductive signals from anterior somites, since a disruption of somitogenesis prevented early kidney development. The identity of these signals remained elusive for a long time. Recent studies have proposed *Wnt11* and *Wnt11b* as possible pronephric inducers (Tetelin & Jones, 2010).

The amphibian pronephron of zebrafish and *Xenopus* comprises two nephrons. Each nephron consists of a blood filter, the glomerulus, and a tubular system, which guarantee homeostasis of the organism by regulation of reabsorption and secretion of soluble agents and electrolytes. This reflects the close links between pronephrogenesis and the development of the vascular system (Ciau-Uitz & Patient, 2016).

To assess the influence of *mespa* on pronephrogenesis, I investigated *pax2* expression in tadpole embryos. *Pax2*, i.e. paired box2, is one of the earliest markers of intermediate mesoderm and exerts pivotal influence on pronephrogenesis along with *pax8* (Buisson, Le Bouffant, Futel, Riou, & Umbhauer, 2015). While *pax8* establishes the pronephric anlage in the first steps of kidney development by controlling the proliferation of pronephric progenitors, *pax2* contributes to further differentiation by directly activating downstream target genes.

Expressed in pronephric tubule and duct epithelia (Carroll et al., 1999; Heller & Brandli, 1997), *pax2* serves for analysis of the *mespa* effect on pronephrogenesis. Up to now, the influence of *mespa* on kidney development has not been examined properly. Our knockdown approach showed diminished pronephron size and reduced tubule coiling in *mespa*-depleted embryos (Fig. 23). While the pronephron appears less organised, the underlying cause of this phenotype remains elusive.

Soibam et al. (2015) listed gene ontology data of genes enriched in *mesp1*$^{+}$ embryonic stem cells. Some of these genes are essential for kidney development, although Soibam and coworkers did not mention this fact. Their uncommented finding supports our hypothesis that *mespa* is needed for kidney development. In future, ChIP Seq analysis would be needed to establish potential epistatic relationships between mespa and pronephrogenic genes.

However, non-cell autonomous functions could also be involved in this process. According to current models, the intermediate mesoderm receives inductive signals from anterior

somites (Mitchell et al., 2007; Seufert et al., 1999). Since *mespa* plays an important role in the early rostro-caudal patterning of the somites and in the epithelialisation during somitogenesis, disrupted anterior somite formation might impair the specification of the intermediate mesoderm and subsequently impair pronephrogenesis (Morimoto et al., 2006; Takahashi et al., 2005). In light of this scenario, *mespa* fulfills at least an indirect regulatory function by patterning the paraxial mesoderm.

Moreover, the phenotype observed after *mespa* knockdown could be the result of the impairment of the formation of the vascular system and the DA (see chapter 'Vasculogenesis'). Since the glomerular endothelium is formed from progenitors of the DA, a lack of vascular and haematopoietic structures during pronephrogenesis could result in a less organised and reduced morphology of the glomeruli in the pronephric anlage, as *pax2* expression per se was present.

Finally, retarded kidney development in *mespa*-deficient embryos might be a result of perturbed mesodermal progenitor migration and patterning, including the intermediate mesoderm, since recent publications revealed that *mespa* controls the speed of mesodermal migration (Chiapparo et al., 2016). Ergo, mesodermal progenitors of the intermediate and lateral mesoderm might have been prevented from appropriate involution and migration by the lack of *mespa*.

In summary, a comprehensive model for *mespa* involvement in pronephrogenesis remains elusive. Therefore, the underlying gene regulatory networks of lineage specification and migratory movements need to be assessed more profoundly by ChIP Seq analysis. Yet, even though we could not establish a direct epistasis, my investigation has shown that various developmental processes of the pronephron and the vascular system are closely linked and early changes in *mespa* levels can lead to an impairment of expression patterns.

4.6 EMT

The Epithelial-to-Mesenchymal Transition (EMT) is one of the pivotal processes that drive migratory cell movements during development. EMT and genes involved in these processes have been extensively studied during gastrulation and neural crest migration (Shook & Keller, 2003), since they contribute to the formation of germ layers and the organisation of tissues within the embryo. Massive gastrulation defects in *mespa*-deficient embryos reflect the perturbation of normal EMT. Saga et al. (1999) showed at the very

beginning of *mesp1* characterisation in mice that mesodermal cells of *mesp1*-deficient embryos were not able to emerge from the primitive streak and thus revealed a role of *mesp1* in migration of cardiovascular progenitors. In *Xenopus*, the formation of the blastopore lip and involution do not proceed properly after *mespa* knockdown (my data). Recently, Wen and Winklbauer (2017) indicated that an ingression-like cell migration, which requires fibronection and c-cadherins, is reminiscent of EMT and underlies endoderm internalisation during gastrulation.

Gene expression analysis in ES cells revealed the striking impact of *mesp1* on EMT through the induction and regulation of *snai1* and *twist1* (Bondue & Blanpain, 2010; Lindsley et al., 2008). *Snai1* and *twist1* represent two key regulators in Epithelial-to-Mesenchymal Transition (Carver et al., 2001; Thiery & Sleeman, 2006). By downregulation of cadherins and detachment from laminins of the basal membrane, cells lose their apico-basal polarity, gain mesenchymal proteins and obtain the ability to migrate. Moreover, cells start to express *snai1* as they involute and contribute to the formation of the mesodermal mantle (Essex et al., 1993). Single-cell-based qRT-PCR revealed a striking coexpression of *mesp1* and *snai1* throughout almost the entire embryonic development (Lescroart et al., 2014). Further ChIP Seq analysis by Soibam et al. (2015) confirmed *snai1* and *twist1* genes as direct targets of *mesp1* in the orchestra of EMT in mice.

Our MO-based knockdown experiments on *mespa* did not confirm these findings in *Xenopus* embryos at any of the analysed developmental stages, since we could not observe a significant alteration in expression patterns (Fig. 24, 25). It has to be considered that *mespa* and *snai1* are spatially coexpressed only at the gastrula stage. Starting at the neurula stage, *snai1* is activated in the neural fold, to which *mespa* is not related by lineage (Linker et al., 2000). As an indispensable developmental process, EMT, represented by *snai1,* could be regulated by a wide range of mechanisms. One of these mechanisms, the *mespa*-pathway, might be specific to a certain group of progenitor cells. In the case of *mespa* knockdown, another pathway could be upregulated to achieve compensation. The Notch Intracellular domain, LOXL2, NF-κB, HIF-1α, IKKα, SMAD, HMGA2, Egr-1, PARP-1, STAT3, MTA3, and Gli1 have the capacity to directly bind to the *snai1* promotor region and regulate *snail1* expression (Kaufhold & Bonavida, 2014). The animal cap assay would have been a conceivable option to prove inducibility of *snai1* by *mespa* in vivo, but has not been performed yet. Therefore, from my set of data I cannot confirm that *mespa* is

required for normal expression and function of *snai1,* even though *mesp1* might have the capacity to induce *snai1* In ES cells.

Snai1 knockout was found to be early embryonic lethal and *snai1*-deficient embryos do not undergo gastrulation (Carver et al., 2001). Considering the fact that *mesp1* was reported to induce *snai1* in EMT, gastrulation defects in my experiments could have been caused by insufficient activation of *snai1* transcription. The death of embryos with severe gastrulation defects constitutes a negative selection, which might have prevented the revelation of the relation between *mespa* and *snai1* in this MO-based knockdown approach. Therefore, the small fraction of embryos exhibiting a reduced *snai1* expression after *mespa* knockdown, might represent a regulatory interaction between the two transcription factors (Fig. 24). Regarding the half-side depleted embryos that survived gastrulation, various possible mechanisms that may have helped them compensate for the lack of *mesp* genes can be discussed. Among these are paracrine induction from the contralateral side, the overlapping function of other *mesp* homologues like *mespb* as reported by Lindsley et al. (2008), and, conceivably, other EMT-regulating pathways.

Most recent studies by Chiapparo et al. (2016) focused on functional commonalities of and differences between *mesp1* and *mesp2*. They revealed a functional overlap of *mesp1* and *mesp2*, especially regarding the specification of cardiovascular progenitors (CP), cardiovascular differentiation and EMT, including the direct activation of *snai1* and *twist1*. Moreover, Chiapparo and coauthors highlighted the particular capacity of *mesp1* to influence the polarity and speed of cell migration. By activation of *Prickle1,* which is involved in the regulation of PCP (Planar cell polarity), *mesp1* is able to guide progenitor cells unidirectionally, thereby facilitating the processes of convergence (the medial condensation of cells) and extension (elongation of the body axis) during embryogenesis. RasGRP3 as a direct target of *mesp1* mediates the speed of migratory movements.

All these aspects shed light on the crucial involvement of *mesp* genes in migratory mechanisms and cell movements.

4.7 The interplay of mesoderm and neural crest in head formation

The development of the head constitutes one of the great evolutionary advantages of vertebrates, and is conserved in a wide range of organisms. While cells from the neural crest (NC) form the skull and cartilage, head muscles originate from cranial paraxial mesoderm (Harel et al., 2009).

An increasing amount of evidence appears to suggest that the genetic programmes responsible for the development of the trunk and craniofacial muscles differ significantly (Grifone & Kelly, 2007; Noden & Francis-West, 2006; Tzahor, 2009). The bipotent myogenic lineage of cardiopharyngeal mesoderm (CPM) has been reported to be the origin of head muscles and the second heart field (SHF) in mice, with relations between muscles derived from the first arch (temporalis and masseter), and right-ventricule myocardium, as well as between face muscles, derived from the second branchial arch, and OFT myocardium (Chan et al., 2016; Lescroart et al., 2010). Diogo et al. (2015) have reviewed the recently developed concept of a cardiopharyngeal field that gives rise to progenitors of the right ventricule, the outflow tract and branchiomeric muscles. Lineage analysis enhanced this model by revealing that, notably, facial and masseter muscles derive from *mesp1*$^{+}$ precursors (Chan et al., 2013).

Within the precise architecture of branchial arches, cells of the CPM are surrounded by cells from the NC (Harel et al., 2009). Nathan et al. (2008) found that CPM contributes to the proximal part of the branchial arch, which in turn develops into the mandibular adductor muscles, whereas the splanchnic mesoderm (SpM) sends cells to the distal region to form the intermandibular muscles.

This study focused on certain aspects of head formation regarding muscle specification, but also on the development of bones and cartilage. As revealed in the analysis of myogenic marker *myf5* at the tadpole stage, we were able to prove a participation of *myf5*-expressing cells in head muscle formation (Fig. 9 C). *Mespa* is required for the normal development of head myoblasts, which then contribute to the establishment of branchiomeric, periocular and jaw muscles (Fig. 9 F), likely arising from the *mespa*-patterned CPM. It has to be considered that *myf5* expression in gastrula stage embryos is restricted to areas within the dorsolateral mesoderm corresponding to the patches from which the heart fields arise. Taken together with the fact, that *myf5* contributes importantly to craniofacial muscles, this supports the notion that cells, which were *myf5*$^{+}$ earlier, contribute to the SHF. The eye, mastication and tongue muscles are among the

derivatives, which coexpress *mesp1* and *myf5* in mice (Harel et al., 2009), while MRFs contribute to head muscles to a various degree (Della Gaspera et al., 2012). Head muscles derive from a common paraxial medioanterior field and coexpress *myoD* and *myf5*. A further differentiation takes place beyond the period of observation of these investigations, wherefore I could not prove a contribution in our experiments.

Interestingly, Hebrok et al. (1994) pointed out that *myf5*, as a representative for muscle differentiation, can be downregulated by constitutive *twist1* expression. This mechanism might help differentiate between myogenic and cartilage development in the head.

The bHLH transcription factor *twist1* is expressed in both lateral plate mesoderm and in NC cells (Hopwood et al., 1989) at different developmental stages. *Twist1* is activated in mesoderm during early gastrulation acting as a driver in EMT, comparable to *snai1*. Although both *snai1* and *twist1* are essential players in the process of EMT during gastrulation, they differ importantly with regard to their expression thereafter. While *snai1* is mainly located in NC, *twist* is expressed in the mesoderm at the initiation of neurulation (NF 14) (Linker et al., 2000) and increasingly activated in NC. This bipotent property of *twist1* made it particularly interesting for my investigations. The interaction between *mespa* and *twist1* at the neurula stage (NF 14) can be explained by the prolonged presence of *twist1* in mesoderm (compare Fig. 24 D and 26 B).

During the formation of head structures, mesoderm and cranial neural crest (CNC) develop in close anatomical relation especially in the branchial arches (Rinon et al., 2007), where myofibers of mesodermal origin attach to CNC derived skeletal structures. Mesodermal *twist1* function seems to be a necessary component for the migration and normal specification of the CNC, where *twist1* plays an essential role in the closure of the cephalic neural tube and the appropriate alignment of the branchial arches (Soo et al., 2002). Vice versa, the ablation of *twist1* expression in CNC cells results in a perturbed arrangement of the cranial expression of myogenic genes like *myoD* and *myf5*, while the early initiation of myogenesis was not affected (Rinon et al., 2007). There it was shown that CNC cells control the patterning of the anterior mesoderm and head muscles in an extrinsic, non-cell autonomous manner by *twist1*-mediated regulation the expression of cell-adhesion molecules like cadherins. Thus, *twist1* might represent a communicator between the cranial mesoderm and the CNC.

According to recent studies, *twist1*-null mice exhibit craniofacial malformations including a reduction of the frontonasal, sub-ocular and first branchial arch and the loss of certain

skeletal structures (Barnes & Firulli, 2009; H. Bildsoe et al., 2009). Evidently, these defects can be affiliated to an abnormal epithelialisation and deterioration in mesenchymal-to-epithelial-transition (MET) (H. Bildsoe et al., 2013). Further analysis of *twist1* ablation revealed a loss and malformation of cranial mesoderm derived skeleton, as well as an incomplete segregation of mesodermal and neural crest cells. To specify more precisely, *twist1*-expressing tissues contribute to the formation of the cranial mesoderm, the muscles of face and neck, endothelial cells, blood vessels and the bones of the neurocranium and the posterior skull base. The work of Heidi Bildsoe et al. (2016) deepened our understanding of the underlying mechanism. They showed a temporal and spatial coexpression of *mesp1* and *twist1* in the nascent mesoderm of mice suggesting an interaction of the two important players in craniofacial development. Moreover, they detailed that downstream targets of *twist1* are involved in the interaction of cells with extracellular matrix in order to acquire mesenchymal characteristics (Heidi Bildsoe et al., 2016). This supports the notion, that the bHLH transcription factor *twist1* is crucial in the development of craniofacial structures.

In this study, I have shown that m*espa* is required for normal *twist1* expression in the branchial arches in tail bud and tadpole embryos, particularly in the two posterior streams of the branchial arches (Fig. 26 I, J, Fig. 27 E, F). Cranial *twist1* expression was sharply reduced or disarranged after *mespa* knockdown, which suggests that *mespa* is an upstream regulator of *twist1*. Since bipotent *mespa* precursors also pattern the development of cranial mesodermal structures including head muscles, *twist1* could be a possible interaction partner responsible for directing cell migration and the patterning of cranial structures. The results of our knockdown experiments align with previous findings by confirming, that normal *twist1* expression requires *mespa* activation (Lindsley et al., 2008; Soibam et al., 2015). Since I analysed the interaction between *mespa* and *twist1* at stages from the neurula to the tadpole stage, the epithelial-to-mesenchymal transition during gastrulation was not covered by this study. Especially the investigations conducted in tail bud stage embryos imply that *mespa* influences *twist1* expression particularly in the two posterior streams of the branchial arches, containing the anterior mesoderm and not affecting the more rostrally located CNC (Fig. 26 I, J). With my rescue and overexpression approaches (Fig. 28, 29), I could not confirm the specificity or direct inducibility of *twist1* by *mespa* that had been shown in the aforementioned studies. Injecting high doses of *mespa* mRNA, coupled with prolonged expression of *mespa* protein

in the rescue and overexpression experiments might lead to a presence of *mespa* in and interference with tissues like the NC, which are critical for migration. The resulting interference with normal *mespa* expression might prevent migration, lead to a down-regulation of *twist1* expression in cardiopharyngeal mesoderm or commit cells to aberrant fates. Since *mespa* is not expressed in the neural crest, a paracrine effect can be suggested to regulate the expression at later developmental stages. Transplantation analysis of wt crest cells into *mespa* morphants will be helpful to assess the inducibility of *twist1*.

In a broader perspective, this analysis might also shed some light on the involvement of *mespa* in the regulatory network of congenital diseases. The probable genetic separation of limb muscles and craniofaciohumeral muscles could explain the phenotypes in certain congenital diseases like DiGeorge or Charge Syndrom (mutation in CHD7-gene) (Kong et al., 2014), which are characterized by heart defects and craniofacial abnormalities. Moreover, mutations in the *twist1* locus can cause the autosomal dominant Saethre-Chotzen-Syndrom, a condition of known to feature various degrees of facial and skeletal malformations (Howard et al., 1997). Bearing in mind the involvement and interaction of *mespa* and *twist1* in the patterning of craniofacial structures, this work, together with previous findings, might postulate a perturbed communication between NC and mesodermal cells as underlying mechanism of the respective malformations.

5. Abbreviations

AP	alkaline phosphatase
ATP	adenosine triphosphate
bHLH	basic-Helix-Loop-Helix
BMP	Bone morphogenetic protein
bp	basepair
CHD	congenital heart defect
ChIP-Seq	Chromatin-Immunoprecipitation Sequencing
CNC	Cranial neural crest
COMO	Control morpholino
CPM	cardiopharyngeal mesoderm
CRISPR	Clustered Regularly Interspaced Short Palindromic Repeats
CTP	cytidine triphosphate
DA	dorsal aorta
DE	distal early tubule
DEPC	diethylpyrocarbonate
dig	digoxigenin
DH	definitive haemangioblast
DL	distal late tubule
DLP	dorsal lateral plate
DNA	desoxyribonucleic acid
DTT	Dithiothreitol
EDTA	ethylenediaminetetraacetic acid
EHT	Endothelial-to-Haematopoietic Transition
EMT	Epithelial to mesenchymal transition
En^R	Drosophila engrailed repressor element
ES	embryonic stem
et al.	et alii, and others
FGF	Fibroblast growth factor
FHF	first heart field
GFP	Green fluorescent protein
GTP	guanosine triphosphate

h	hour/hours
I.e.	id est
IMZ	involuting marginal zone
IVTR	in-vitro-transcription
kbp	kilo basepairs
M	molar
l	liter
MAB	maleic acid buffer
MBS	m-maleimidobenzoyl-N-hydoxysuccinimide ester
MBT	mid-blastula transition
MCP	Multipotent cardiovascular progenitor
MET	mesenchymal-to-epithelial-transition
min	minute
ml	milliliter
mm	millimeter
mM	millimolar
MO	morpholino
MRF	myogenic regulatory factor
mRNA	messanger ribonucleic acid
NC	neural crest
NF	developmental stage according to Nieuwkoop & Faber, 1994
NIMZ	non-involuting marginal zone
nm	nanometer
NTP	nucleosidtriphosphate
OFT	outflowtract
PBS	Phosphate buffered saline
PCP	planar cell polarity
PCT	proximal convoluted tubule
pg	picogram
PGC	primordial germ cells
PSM	presomitic mesoderm
qRT PCR	quantitative reverse transcription polymerase chain reaction

RNA	ribonucleic acid
RT	room temperature
SHF	second heart field
SPM	splanchnic mesoderm
SSC	saline-sodium citrate
ST	proximal straight tubule
TF	transcription factor
TGFß	Transforming growth factor ß
u	unit
UTP	uridine triphosphate
UV	ultraviolet
VBI	ventral blood islands
WHO	World health organisation
WT	wild-type
ß-hCG	ß-human chorionic gonadotropin
µg	microgram
µl	microliter

6. References

Arnold, S. J., Hofmann, U. K., Bikoff, E. K., & Robertson, E. J. (2008). Pivotal roles for eomesodermin during axis formation, epithelium-to-mesenchyme transition and endoderm specification in the mouse. *Development, 135*(3), 501-511. doi:10.1242/dev.014357

Barnes, R. M., & Firulli, A. B. (2009). A twist of insight - the role of Twist-family bHLH factors in development. *Int J Dev Biol, 53*(7), 909-924. doi:10.1387/ijdb.082747rb

Beck, C. W., & Slack, J. M. (1998). Analysis of the developing Xenopus tail bud reveals separate phases of gene expression during determination and outgrowth. *Mech Dev, 72*(1-2), 41-52.

Beck, C. W., Whitman, M., & Slack, J. M. (2001). The role of BMP signaling in outgrowth and patterning of the Xenopus tail bud. *Dev Biol, 238*(2), 303-314. doi:10.1006/dbio.2001.0407

Bildsoe, H., Fan, X., Wilkie, E. E., Ashoti, A., Jones, V. J., Power, M., . . . Loebel, D. A. F. (2016). Transcriptional targets of TWIST1 in the cranial mesoderm regulate cell-matrix interactions and mesenchyme maintenance. *Dev Biol, 418*(1), 189-203. doi:https://doi.org/10.1016/j.ydbio.2016.08.016

Bildsoe, H., Loebel, D. A., Jones, V. J., Chen, Y. T., Behringer, R. R., & Tam, P. P. (2009). Requirement for Twist1 in frontonasal and skull vault development in the mouse embryo. *Dev Biol, 331*(2), 176-188. doi:10.1016/j.ydbio.2009.04.034

Bildsoe, H., Loebel, D. A., Jones, V. J., Hor, A. C., Braithwaite, A. W., Chen, Y. T., . . . Tam, P. P. (2013). The mesenchymal architecture of the cranial mesoderm of mouse embryos is disrupted by the loss of Twist1 function. *Dev Biol, 374*(2), 295-307. doi:10.1016/j.ydbio.2012.12.004

Birsoy, B., Kofron, M., Schaible, K., Wylie, C., & Heasman, J. (2006). Vg 1 is an essential signaling molecule in Xenopus development. *Development, 133*(1), 15-20. doi:10.1242/dev.02144

Bondue, A., & Blanpain, C. (2010). Mesp1: a key regulator of cardiovascular lineage commitment. *Circ Res, 107*(12), 1414-1427. doi:10.1161/CIRCRESAHA.110.227058

Bondue, A., Lapouge, G., Paulissen, C., Semeraro, C., Iacovino, M., Kyba, M., & Blanpain, C. (2008). Mesp1 acts as a master regulator of multipotent cardiovascular progenitor specification. *Cell Stem Cell, 3*(1), 69-84. doi:10.1016/j.stem.2008.06.009

Bondue, A., Tannler, S., Chiapparo, G., Chabab, S., Ramialison, M., Paulissen, C., . . . Blanpain, C. (2011). Defining the earliest step of cardiovascular progenitor specification during embryonic stem cell differentiation. *J Cell Biol, 192*(5), 751-765. doi:10.1083/jcb.201007063

Brandli, A. W. (1999). Towards a molecular anatomy of the Xenopus pronephric kidney. *Int J Dev Biol, 43*(5), 381-395.

Braun, T., Bober, E., Buschhausen-Denker, G., Kohtz, S., Grzeschik, K. H., & Arnold, H. H. (1989). Differential expression of myogenic determination genes in muscle cells: possible autoactivation by the Myf gene products. *EMBO J, 8*(12), 3617-3625.

Buckingham, M. (1992). Making muscle in mammals. *TIG, 8*(4), 144-149.

Buisson, I., Le Bouffant, R., Futel, M., Riou, J. F., & Umbhauer, M. (2015). Pax8 and Pax2 are specifically required at different steps of Xenopus pronephros development. *Dev Biol, 397*(2), 175-190. doi:10.1016/j.ydbio.2014.10.022

Cai, M., Langer, E. M., Gill, J. G., Satpathy, A. T., Albring, J. C., Kc, W., . . . Murphy, K. M. (2012). Dual actions of Meis1 inhibit erythroid progenitor development and sustain general hematopoietic cell proliferation. *Blood, 120*(2), 335-346. doi:10.1182/blood-2012-01-403139

Carroll, T. J., Wallingford, J. B., & Vize, P. D. (1999). Dynamic patterns of gene expression in the developing pronephros of Xenopus laevis. *Dev Genet, 24*(3-4), 199-207. doi:10.1002/(sici)1520-6408(1999)24:3/4<199::aid-dvg3>3.0.co;2-d

Carver, E. A., Jiang, R., Lan, Y., Oram, K. F., & Gridley, T. (2001). The mouse snail gene encodes a key regulator of the epithelial-mesenchymal transition. *Mol Cell Biol, 21*(23), 8184-8188. doi:10.1128/mcb.21.23.8184-8188.2001

Chal, J., & Pourquie, O. (2017). Making muscle: skeletal myogenesis in vivo and in vitro. *Development, 144*(12), 2104-2122. doi:10.1242/dev.151035

Chan, S. S., Hagen, H. R., Swanson, S. A., Stewart, R., Boll, K. A., Aho, J., . . . Kyba, M. (2016). Development of Bipotent Cardiac/Skeletal Myogenic Progenitors from MESP1+ Mesoderm. *Stem Cell Reports, 6*(1), 26-34. doi:10.1016/j.stemcr.2015.12.003

Chan, S. S., Shi, X., Toyama, A., Arpke, R. W., Dandapat, A., Iacovino, M., . . . Kyba, M. (2013). Mesp1 patterns mesoderm into cardiac, hematopoietic, or skeletal myogenic progenitors in a context-dependent manner. *Cell Stem Cell, 12*(5), 587-601. doi:10.1016/j.stem.2013.03.004

Chiapparo, G., Lin, X., Lescroart, F., Chabab, S., Paulissen, C., Pitisci, L., . . . Blanpain, C. (2016). Mesp1 controls the speed, polarity, and directionality of cardiovascular progenitor migration. *J Cell Biol, 213*(4), 463-477. doi:10.1083/jcb.201505082

Cho, K. W., Blumberg, B., Steinbeisser, H., & De Robertis, E. M. (1991). Molecular nature of Spemann's organizer: the role of the Xenopus homeobox gene goosecoid. *Cell, 67*(6), 1111-1120.

Ciau-Uitz, A., & Patient, R. (2016). The embryonic origins and genetic programming of emerging haematopoietic stem cells. *FEBS Lett, 590*(22), 4002-4015. doi:10.1002/1873-3468.12363

Ciau-Uitz, A., Pinheiro, P., Kirmizitas, A., Zuo, J., & Patient, R. (2013). VEGFA-dependent and -independent pathways synergise to drive Scl expression and initiate programming of the blood stem cell lineage in Xenopus. *Development, 140*(12), 2632-2642. doi:10.1242/dev.090829

Ciau-Uitz, A., Walmsley, M., & Patient, R. (2000). Distinct origins of adult and embryonic blood in Xenopus. *Cell, 102*(6), 787-796.

Cleaver, O., & Krieg, P. A. (1998). VEGF mediates angioblast migration during development of the dorsal aorta in Xenopus. *Development, 125*(19), 3905-3914.

Conlon, F. L., Sedgwick, S. G., Weston, K. M., & Smith, J. C. (1996). Inhibition of Xbra transcription activation causes defects in mesodermal patterning and reveals autoregulation of Xbra in dorsal mesoderm. *Development, 122*(8), 2427-2435.

Conlon, F. L., & Smith, J. C. (1999). Interference with brachyury function inhibits convergent extension, causes apoptosis, and reveals separate requirements in the FGF and activin signalling pathways. *Dev Biol, 213*(1), 85-100. doi:10.1006/dbio.1999.9330

Costello, I., Pimeisl, I. M., Drager, S., Bikoff, E. K., Robertson, E. J., & Arnold, S. J. (2011). The T-box transcription factor Eomesodermin acts upstream of Mesp1 to specify cardiac mesoderm during mouse gastrulation. *Nat Cell Biol, 13*(9), 1084-1091. doi:10.1038/ncb2304

Cox, C. M., D'Agostino, S. L., Miller, M. K., Heimark, R. L., & Krieg, P. A. (2006). Apelin, the ligand for the endothelial G-protein-coupled receptor, APJ, is a potent angiogenic factor required for normal vascular development of the frog embryo. *Dev Biol, 296*(1), 177-189. doi:10.1016/j.ydbio.2006.04.452

D'Aniello, C., Lonardo, E., Iaconis, S., Guardiola, O., Liguoro, A. M., Liguori, G. L., . . . Minchiotti, G. (2009). G protein-coupled receptor APJ and its ligand apelin act downstream of Cripto to specify embryonic stem cells toward the cardiac lineage

through extracellular signal-regulated kinase/p70S6 kinase signaling pathway. *Circ Res, 105*(3), 231-238. doi:10.1161/circresaha.109.201186

Dale, L., & Slack, J. M. (1987). Regional specification within the mesoderm of early embryos of Xenopus laevis. *Development, 100*(2), 279-295.

David, R., Brenner, C., Stieber, J., Schwarz, F., Brunner, S., Vollmer, M., . . . Franz, W. M. (2008). MesP1 drives vertebrate cardiovascular differentiation through Dkk-1-mediated blockade of Wnt-signalling. *Nat Cell Biol, 10*(3), 338-345. doi:10.1038/ncb1696

David, R., Jarsch, V. B., Schwarz, F., Nathan, P., Gegg, M., Lickert, H., & Franz, W. M. (2011). Induction of MesP1 by Brachyury(T) generates the common multipotent cardiovascular stem cell. *Cardiovasc Res, 92*(1), 115-122. doi:10.1093/cvr/cvr158

De Robertis, E. M., Larrain, J., Oelgeschlager, M., & Wessely, O. (2000). The establishment of Spemann's organizer and patterning of the vertebrate embryo. *Nat Rev Genet, 1*(3), 171-181. doi:10.1038/35042039

Della Gaspera, B., Armand, A. S., Sequeira, I., Chesneau, A., Mazabraud, A., Lecolle, S., . . . Chanoine, C. (2012). Myogenic waves and myogenic programs during Xenopus embryonic myogenesis. *Dev Dyn, 241*(5), 995-1007. doi:10.1002/dvdy.23780

Den Hartogh, S. C., Schreurs, C., Monshouwer-Kloots, J. J., Davis, R. P., Elliott, D. A., Mummery, C. L., & Passier, R. (2015). Dual reporter MESP1 mCherry/w-NKX2-5 eGFP/w hESCs enable studying early human cardiac differentiation. *Stem Cells, 33*(1), 56-67. doi:10.1002/stem.1842

Desgrange, A., & Cereghini, S. (2015). Nephron Patterning: Lessons from Xenopus, Zebrafish, and Mouse Studies. *Cells, 4*(3), 483-499. doi:10.3390/cells4030483

Deshwar, A. R., Chng, S. C., Ho, L., Reversade, B., & Scott, I. C. (2016). The Apelin receptor enhances Nodal/TGFbeta signaling to ensure proper cardiac development. *Elife, 5*. doi:10.7554/eLife.13758

Devic, E., Paquereau, L., Vernier, P., Knibiehler, B., & Audigier, Y. (1996). Expression of a new G protein-coupled receptor X-msr is associated with an endothelial lineage in Xenopus laevis. *Mech Dev, 59*(2), 129-140.

Diogo, R., Kelly, R. G., Christiaen, L., Levine, M., Ziermann, J. M., Molnar, J. L., . . . Tzahor, E. (2015). A new heart for a new head in vertebrate cardiopharyngeal evolution. *Nature, 520*(7548), 466-473. doi:10.1038/nature14435

Dohrmann, C. E., Kessler, D. S., & Melton, D. A. (1996). Induction of axial mesoderm by zDVR-1, the zebrafish orthologue of Xenopus Vg1. *Dev Biol, 175*(1), 108-117. doi:10.1006/dbio.1996.0099

Drake, C. J. (2003). Embryonic and adult vasculogenesis. *Birth Defects Res C Embryo Today, 69*(1), 73-82. doi:10.1002/bdrc.10003

Durbin, L., Sordino, P., Barrios, A., Gering, M., Thisse, C., Thisse, B., . . . Holder, N. (2000). Anteroposterior patterning is required within segments for somite boundary formation in developing zebrafish. *Development, 127*, 1703-1713.

Eisen, J. S., & Smith, J. C. (2008). Controlling morpholino experiments: don't stop making antisense. *Development, 135*(10), 1735-1743. doi:10.1242/dev.001115

Eskildsen, T. V., Ayoubi, S., Thomassen, M., Burton, M., Mandegar, M. A., Conklin, B. R., . . . Sheikh, S. P. (2019). MESP1 knock-down in human iPSC attenuates early vascular progenitor cell differentiation after completed primitive streak specification. *Dev Biol, 445*(1), 1-7. doi:10.1016/j.ydbio.2018.10.020

Essex, L. J., Mayor, R., & Sargent, M. G. (1993). Expression of Xenopus snail in mesoderm and prospective neural fold ectoderm. *Dev Dyn, 198*(2), 108-122. doi:10.1002/aja.1001980205

Frenz, S. (2017). Thesis. *personal communication*.

Gentsch, G. E., Monteiro, R. S., & Smith, J. C. (2017). Cooperation Between T-Box Factors Regulates the Continuous Segregation of Germ Layers During Vertebrate Embryogenesis. *Curr Top Dev Biol, 122*, 117-159. doi:10.1016/bs.ctdb.2016.07.012

Gentsch, G. E., Owens, N. D., Martin, S. R., Piccinelli, P., Faial, T., Trotter, M. W., . . . Smith, J. C. (2013). In vivo T-box transcription factor profiling reveals joint regulation of embryonic neuromesodermal bipotency. *Cell Rep, 4*(6), 1185-1196. doi:10.1016/j.celrep.2013.08.012

Gerhart, J. (2002). Changing the axis changes the perspective. *Dev Dyn, 225*(4), 380-383. doi:10.1002/dvdy.10198

Gering, M., Rodaway, A. R., Gottgens, B., Patient, R. K., & Green, A. R. (1998). The SCL gene specifies haemangioblast development from early mesoderm. *EMBO J, 17*(14), 4029-4045. doi:10.1093/emboj/17.14.4029

Gilboa, S. M., Salemi, J. L., Nembhard, W. N., Fixler, D. E., & Correa, A. (2010). Mortality resulting from congenital heart disease among children and adults in the United States, 1999 to 2006. *Circulation, 122*(22), 2254-2263. doi:10.1161/circulationaha.110.947002

Goering, L. M., Hoshijima, K., Hug, B., Bisgrove, B., Kispert, A., & Grunwald, D. J. (2003). An interacting network of T-box genes directs gene expression and fate in the zebrafish mesoderm. *Proc Natl Acad Sci U S A, 100*(16), 9410-9415. doi:10.1073/pnas.1633548100

Grifone, R., & Kelly, R. G. (2007). Heartening news for head muscle development. *Trends Genet, 23*(8), 365-369. doi:10.1016/j.tig.2007.05.002

Harel, I., Nathan, E., Tirosh-Finkel, L., Zigdon, H., Guimaraes-Camboa, N., Evans, S. M., & Tzahor, E. (2009). Distinct origins and genetic programs of head muscle satellite cells. *Dev Cell, 16*(6), 822-832. doi:10.1016/j.devcel.2009.05.007

Harland, R. (1988). Growth factors and mesoderm induction. *Trends Genet, 4*(3), 62-63.

Hart, D. O., Raha, T., Lawson, N. D., & Green, M. R. (2007). Initiation of zebrafish haematopoiesis by the TATA-box-binding protein-related factor Trf3. *Nature, 450*(7172), 1082-1085. doi:10.1038/nature06349

Hart, D. O., Santra, M. K., Raha, T., & Green, M. R. (2009). Selective interaction between Trf3 and Taf3 required for early development and hematopoiesis. *Dev Dyn, 238*(10), 2540-2549. doi:10.1002/dvdy.22083

Hebrok, M., Wertz, K., & Fuchtbauer, E. M. (1994). M-twist is an inhibitor of muscle differentiation. *Dev Biol, 165*(2), 537-544. doi:10.1006/dbio.1994.1273

Helde, K. A., & Grunwald, D. J. (1993). The DVR-1 (Vg1) transcript of zebrafish is maternally supplied and distributed throughout the embryo. *Dev Biol, 159*(2), 418-426. doi:10.1006/dbio.1993.1252

Heller, N., & Brandli, A. W. (1997). Xenopus Pax-2 displays multiple splice forms during embryogenesis and pronephric kidney development. *Mech Dev, 69*(1-2), 83-104.

Hitachi, K., Kondow, A., Danno, H., Nishimura, Y., Okabayashi, K., & Asashima, M. (2009). Molecular analyses of Xenopus laevis Mesp-related genes. *Integr Zool, 4*(4), 387-394. doi:10.1111/j.1749-4877.2009.00110.x

Ho, B., Loh, S., Chan, W., & Soh, B. (2018). In Vivo Genome Editing as a Therapeutic Approach. *International Journal of Molecular Sciences, 19*(9), 2721.

Hollenberg, S. M., Cheng, P. F., & Weintraub, H. (1993). Use of a conditional MyoD transcription factor in studies of MyoD trans-activation and muscle determination. *Proc Natl Acad Sci U S A, 90*(17), 8028-8032.

Hopwood, N. D., Pluck, A., & Gurdon, J. B. (1989). A Xenopus mRNA related to Drosophila twist is expressed in response to induction in the mesoderm and the neural crest. *Cell, 59*(5), 893-903.

Howard, T. D., Paznekas, W. A., Green, E. D., Chiang, L. C., Ma, N., Ortiz de Luna, R. I., . . . Jabs, E. W. (1997). Mutations in TWIST, a basic helix-loop-helix transcription factor, in Saethre-Chotzen syndrome. *Nat Genet, 15*(1), 36-41. doi:10.1038/ng0197-36

Inui, M., Fukui, A., Ito, Y., & Asashima, M. (2006). Xapelin and Xmsr are required for cardiovascular development in Xenopus laevis. *Dev Biol, 298*(1), 188-200. doi:10.1016/j.ydbio.2006.06.028

Isaacs, H. V., Pownall, M. E., & Slack, J. M. (1994). eFGF regulates Xbra expression during Xenopus gastrulation. *EMBO J, 13*(19), 4469-4481.

Ismailoglu, I., Yeamans, G., Daley, G. Q., Perlingeiro, R. C., & Kyba, M. (2008). Mesodermal patterning activity of SCL. *Exp Hematol, 36*(12), 1593-1603. doi:10.1016/j.exphem.2008.07.005

Joseph, E. M., & Cassetta, L. A. (1999). Mespo: a novel basic helix-loop-helix gene expressed in the presomitic mesoderm and posterior tailbud of Xenopus embryos. *Mech Dev, 82*(1-2), 191-194.

Kalin, R. E., Kretz, M. P., Meyer, A. M., Kispert, A., Heppner, F. L., & Brandli, A. W. (2007). Paracrine and autocrine mechanisms of apelin signaling govern embryonic and tumor angiogenesis. *Dev Biol, 305*(2), 599-614. doi:10.1016/j.ydbio.2007.03.004

Kang, Y., Kim, J., Anderson, J. P., Wu, J., Gleim, S. R., Kundu, R. K., . . . Chun, H. J. (2013). Apelin-APJ signaling is a critical regulator of endothelial MEF2 activation in cardiovascular development. *Circ Res, 113*(1), 22-31. doi:10.1161/circresaha.113.301324

Kattman, S. J., Huber, T. L., & Keller, G. M. (2006). Multipotent flk-1+ cardiovascular progenitor cells give rise to the cardiomyocyte, endothelial, and vascular smooth muscle lineages. *Dev Cell, 11*(5), 723-732. doi:10.1016/j.devcel.2006.10.002

Kaufhold, S., & Bonavida, B. (2014). Central role of Snail1 in the regulation of EMT and resistance in cancer: a target for therapeutic intervention. *J Exp Clin Cancer Res, 33*, 62. doi:10.1186/s13046-014-0062-0

Kavka, A. I., & Green, J. B. (2000). Evidence for dual mechanisms of mesoderm establishment in Xenopus embryos. *Dev Dyn, 219*(1), 77-83. doi:10.1002/1097-0177(2000)9999:9999<::aid-dvdy1025>3.0.co;2-e

Kelly, R. G. (2012). The second heart field. *Curr Top Dev Biol, 100*, 33-65. doi:10.1016/b978-0-12-387786-4.00002-6

Kidoya, H., & Takakura, N. (2012). Biology of the apelin-APJ axis in vascular formation. *J Biochem, 152*(2), 125-131. doi:10.1093/jb/mvs071

Kidoya, H., Ueno, M., Yamada, Y., Mochizuki, N., Nakata, M., Yano, T., . . . Takakura, N. (2008). Spatial and temporal role of the apelin/APJ system in the caliber size regulation of blood vessels during angiogenesis. *EMBO J, 27*(3), 522-534. doi:10.1038/sj.emboj.7601982

Kiecker, C., Bates, T., & Bell, E. (2016). Molecular specification of germ layers in vertebrate embryos. *Cell Mol Life Sci, 73*(5), 923-947. doi:10.1007/s00018-015-2092-y

Kimelman, D. (2006). Mesoderm induction: from caps to chips. *Nat Rev Genet, 7*(5), 360-372. doi:10.1038/nrg1837

Kimelman, D., & Kirschner, M. (1987). Synergistic induction of mesoderm by FGF and TGF-beta and the identification of an mRNA coding for FGF in the early Xenopus embryo. *Cell, 51*(5), 869-877.

Kitajima, S., Miyagawa-Tomita, S., Inoue, T., Kanno, J., & Saga, Y. (2006). Mesp1-nonexpressing cells contribute to the ventricular cardiac conduction system. *Dev Dyn, 235*(2), 395-402. doi:10.1002/dvdy.20640

Kitajima, S., Takagi, A., Inoue, T., & Saga, Y. (2000). MesP1 and MesP2 are essential for the development of cardiac mesoderm. *Development, 127*, 3215-3226.

Kliegman, Stanton, Geme, S., & Schor. (2016). Nelson Textbook of Pediatrics Edition 20. *Elsevier*.

Kolm, P. J., & Sive, H. L. (1995). Efficient hormone-inducible protein function in Xenopus laevis. *Dev Biol, 171*(1), 267-272. doi:10.1006/dbio.1995.1279

Komada, Y., Yamane, T., Kadota, D., Isono, K., Takakura, N., Hayashi, S., & Yamazaki, H. (2012). Origins and properties of dental, thymic, and bone marrow mesenchymal cells and their stem cells. *PLoS One, 7*(11), e46436. doi:10.1371/journal.pone.0046436

Kong, P., Racedo, S. E., Macchiarulo, S., Hu, Z., Carpenter, C., Guo, T., . . . Morrow, B. E. (2014). Tbx1 is required autonomously for cell survival and fate in the pharyngeal core mesoderm to form the muscles of mastication. *Hum Mol Genet, 23*(16), 4215-4231. doi:10.1093/hmg/ddu140

Kriegmair, M. C., Frenz, S., Dusl, M., Franz, W. M., David, R., & Rupp, R. A. (2013). Cardiac differentiation in Xenopus is initiated by mespa. *Cardiovasc Res, 97*(3), 454-463. doi:10.1093/cvr/cvs354

Krneta-Stankic, V., DeLay, B. D., & Miller, R. K. (2017). Xenopus: leaping forward in kidney organogenesis. *Pediatr Nephrol, 32*(4), 547-555. doi:10.1007/s00467-016-3372-y

Kumano, G., Belluzzi, L., & Smith, W. C. (1999). Spatial and temporal properties of ventral blood island induction in Xenopus laevis. *Development, 126*(23), 5327-5337.

Kumano, G., & Smith, W. C. (2002). Revisions to the Xenopus gastrula fate map: implications for mesoderm induction and patterning. *Dev Dyn, 225*(4), 409-421. doi:10.1002/dvdy.10177

Lane, M. C., & Sheets, M. D. (2002). Rethinking axial patterning in amphibians. *Dev Dyn, 225*(4), 434-447. doi:10.1002/dvdy.10182

Lane, M. C., & Sheets, M. D. (2006). Heading in a new direction: implications of the revised fate map for understanding Xenopus laevis development. *Dev Biol, 296*(1), 12-28. doi:10.1016/j.ydbio.2006.04.447

Lane, M. C., & Smith, W. C. (1999). The origins of primitive blood in Xenopus: implications for axial patterning. *Development, 126*(3), 423-434.

Latinkic, B. V., & Smith, J. C. (1999). Goosecoid and mix.1 repress Brachyury expression and are required for head formation in Xenopus. *Development, 126*(8), 1769-1779.

Lerchner, W., Latinkic, B. V., Remacle, J. E., Huylebroeck, D., & Smith, J. C. (2000). Region-specific activation of the Xenopus brachyury promoter involves active repression in ectoderm and endoderm: a study using transgenic frog embryos. *Development, 127*(12), 2729-2739.

Lescroart, F., Chabab, S., Lin, X., Rulands, S., Paulissen, C., Rodolosse, A., . . . Blanpain, C. (2014). Early lineage restriction in temporally distinct populations of Mesp1 progenitors during mammalian heart development. *Nat Cell Biol, 16*(9). doi:10.1038/ncb3024

Lescroart, F., Kelly, R. G., Le Garrec, J. F., Nicolas, J. F., Meilhac, S. M., & Buckingham, M. (2010). Clonal analysis reveals common lineage relationships between head muscles and second heart field derivatives in the mouse embryo. *Development, 137*(19), 3269-3279. doi:10.1242/dev.050674

Lindsley, R. C., Gill, J. G., Murphy, T. L., Langer, E. M., Cai, M., Mashayekhi, M., . . . Murphy, K. M. (2008). Mesp1 coordinately regulates cardiovascular fate restriction and epithelial-mesenchymal transition in differentiating ESCs. *Cell Stem Cell, 3*(1), 55-68. doi:10.1016/j.stem.2008.04.004

Linker, C., Bronner-Fraser, M., & Mayor, R. (2000). Relationship between gene expression domains of Xsnail, Xslug, and Xtwist and cell movement in the prospective neural crest of Xenopus. *Dev Biol, 224*(2), 215-225. doi:10.1006/dbio.2000.9723

Liu, Y., & Schwartz, R. J. (2014). Transient Mesp1 expression. *Transcription, 4*(3), 92-96. doi:10.4161/trns.24588

Maguire, R. J., Isaacs, H. V., & Pownall, M. E. (2012). Early transcriptional targets of MyoD link myogenesis and somitogenesis. *Dev Biol, 371*(2), 256-268. doi:10.1016/j.ydbio.2012.08.027

Marlow, F. L., & Mullins, M. C. (2008). Bucky ball functions in Balbiani body assembly and animal-vegetal polarity in the oocyte and follicle cell layer in zebrafish. *Dev Biol, 321*(1), 40-50. doi:10.1016/j.ydbio.2008.05.557

Mayor, R., Yaung, R., & Vargas, A. (1999). Development of Neural Crest in Xenopus. *Cur Top Dev Bio, 43*, 85 - 113.

Mills, K. R., Kruep, D., & Saha, M. S. (1999). Elucidating the origins of the vascular system: a fate map of the vascular endothelial and red blood cell lineages in Xenopus laevis. *Dev Biol, 209*(2), 352-368. doi:10.1006/dbio.1999.9245

Mione, M., Shanmugalingam, S., Kimelman, D., & Griffin, K. (2001). Overlapping expression of zebrafish T-brain-1 and eomesodermin during forebrain development. *Mech Dev, 100*(1), 93-97.

Mitchell, T., Jones, E. A., Weeks, D. L., & Sheets, M. D. (2007). Chordin affects pronephros development in Xenopus embryos by anteriorizing presomitic mesoderm. *Dev Dyn, 236*(1), 251-261. doi:10.1002/dvdy.21014

Monsoro-Burq, A. H. (2003). Neural crest induction by paraxial mesoderm in Xenopus embryos requires FGF signals. *Development, 130*(>14), 3111-3124. doi:10.1242/dev.00531

Montague, T. G., & Schier, A. F. (2017). Vg1-Nodal heterodimers are the endogenous inducers of mesendoderm. *Elife, 6*. doi:10.7554/eLife.28183

Moody, S. A. (1987). Fates of the blastomeres of the 32-cell-stage Xenopus embryo. *Dev Biol, 122*(2), 300-319.

Morimoto, M., Kiso, M., Sasaki, N., & Saga, Y. (2006). Cooperative Mesp activity is required for normal somitogenesis along the anterior-posterior axis. *Dev Biol, 300*(2), 687-698. doi:10.1016/j.ydbio.2006.08.043

Murre, C., McCaw, P. S., Vaessin, H., Caudy, M., Jan, L. Y., Jan, Y. N., . . . et al. (1989). Interactions between heterologous helix-loop-helix proteins generate complexes that bind specifically to a common DNA sequence. *Cell, 58*(3), 537-544.

Nathan, E., Monovich, A., Tirosh-Finkel, L., Harrelson, Z., Rousso, T., Rinon, A., . . . Tzahor, E. (2008). The contribution of Islet1-expressing splanchnic mesoderm cells to distinct branchiomeric muscles reveals significant heterogeneity in head muscle development. *Development, 135*(4), 647-657. doi:10.1242/dev.007989

Naylor, R. W., Qubisi, S. S., & Davidson, A. J. (2017). Zebrafish Pronephros Development. *Results Probl Cell Differ, 60*, 27-53. doi:10.1007/978-3-319-51436-9_2

Nieuwkoop, P. D., & Faber, J. (1994). Normal table of Xenopus laevis (Daudin) : a systematical and chronological survey of the development from the fertilized egg till the end of metamorphosis. New York :: Garland Pub.

Noden, D. M., & Francis-West, P. (2006). The differentiation and morphogenesis of craniofacial muscles. *Dev Dyn, 235*(5), 1194-1218. doi:10.1002/dvdy.20697

O'Dowd, B. F., Heiber, M., Chan, A., Heng, H. H., Tsui, L. C., Kennedy, J. L., . . . Nguyen, T. (1993). A human gene that shows identity with the gene encoding the angiotensin receptor is located on chromosome 11. *Gene, 136*(1-2), 355-360.

Okabayashi, K., & Asashima, M. (2003). Tissue generation from amphibian animal caps. *Curr Opin Genet Dev, 13*(5), 502-507.

Olson, E. N. (1990). MyoD family: a paradigm for development? *Genes Dev, 4*(9), 1454-1461.

Peterson, A. G., Wang, X., & Yost, H. J. (2013). Dvr1 transfers left-right asymmetric signals from Kupffer's vesicle to lateral plate mesoderm in zebrafish. *Dev Biol, 382*(1), 198-208. doi:10.1016/j.ydbio.2013.06.011

Poole, T. J., & Coffin, J. D. (1989). Vasculogenesis and angiogenesis: two distinct morphogenetic mechanisms establish embryonic vascular pattern. *J Exp Zool, 251*(2), 224-231. doi:10.1002/jez.1402510210

Porcher, C., Swat, W., Rockwell, K., Fujiwara, Y., Alt, F. W., & Orkin, S. H. (1996). The T cell leukemia oncoprotein SCL/tal-1 is essential for development of all hematopoietic lineages. *Cell, 86*(1), 47-57.

Probst, S., & Arnold, S. J. (2017). Eomesodermin-At Dawn of Cell Fate Decisions During Early Embryogenesis. *Curr Top Dev Biol, 122*, 93-115. doi:10.1016/bs.ctdb.2016.09.001

Rinon, A., Lazar, S., Marshall, H., Buchmann-Moller, S., Neufeld, A., Elhanany-Tamir, H., . . . Tzahor, E. (2007). Cranial neural crest cells regulate head muscle patterning and differentiation during vertebrate embryogenesis. *Development, 134*(17), 3065-3075. doi:10.1242/dev.002501

Rupp, R. A., Snider, L., & Weintraub, H. (1994). Xenopus embryos regulate the nuclear localization of XMyoD. *Genes Dev, 8*(11), 1311-1323.

Ryan, K., Butler, K., Bellefroid, E., & Gurdon, J. B. (1998). Xenopus eomesodermin is expressed in neural differentiation. *Mech Dev, 75*(1-2), 155-158.

Ryan, K., Garrett, N., Mitchell, A., & Gurdon, J. B. (1996). Eomesodermin, a key early gene in Xenopus mesoderm differentiation. *Cell, 87*(6), 989-1000.

Sabillo, A., Ramirez, J., & Domingo, C. R. (2016). Making muscle: Morphogenetic movements and molecular mechanisms of myogenesis in Xenopus laevis. *Semin Cell Dev Biol, 51*, 80-91. doi:10.1016/j.semcdb.2016.02.006

Saga, Y. (1998). Genetic rescue of segmentation defect in MesP2-deficient mice by MesP1 gene replacement. *Mech Dev, 75*, 53-66.

Saga, Y., Hata, N., Kobayashi, S., Magnuson, T., Seldin, M. F., & Taketo, M. M. (1996). MesP1: a novel basic helix-loop-helix protein expressed in the nascent mesodermal cells during mouse gastrulation. *Development, 122*, 2769-2778.

Saga, Y., Hata, N., Koseki, H., & Taketo, M. M. (1997). Mesp2: a novel mouse gene expressed in the presegmented mesoderm and essential for segmentation initiation. *Genes Dev, 11*(14), 1827-1839. doi:10.1101/gad.11.14.1827

Saga, Y., Kitajima, S., & Miyagawa-Tomita, S. (2000). Mesp1 Expression Is the Earliest Sign of Cardiovascular Development. *Trends Cardiovasc Med, 10*, 345-352.

Saga, Y., Miyagawa-Tomita, S., Takagi, A., Kitajima, S., Miyazaki, J., & Inoue, T. (1999). MesP1 is expressed in the heart precursor cells and required for the formation of a single heart tube. *Development, 126*, 3437-3447.

Sargent, T. D., Jamrich, M., & Dawid, I. B. (1986). Cell interactions and the control of gene activity during early development of Xenopus laevis. *Dev Biol, 114*(1), 238-246.

Sawada, A., Fritz, A., Jiang, Y.-J., Yamamoto, A., Yamasu, K., Kuroiwa, A., . . . Takeda, H. (2000). Zebrafish Mesp family genes, mesp-a and mesp-b are segmentally expressed in the presomitic mesoderm, and Mesp-b confers the anterior identity to the developing somites. *Development, 126*, 1691-1702.

Schulte-Merker, S., & Smith, J. C. (1995). Mesoderm formation in response to Brachyury requires FGF signalling. *Curr Biol, 5*(1), 62-67.

Seufert, D. W., Brennan, H. C., DeGuire, J., Jones, E. A., & Vize, P. D. (1999). Developmental basis of pronephric defects in Xenopus body plan phenotypes. *Dev Biol, 215*(2), 233-242. doi:10.1006/dbio.1999.9476

Shook, D., & Keller, R. (2003). Mechanisms, mechanics and function of epithelial-mesenchymal transitions in early development. *Mech Dev, 120*(11), 1351-1383.

Showell, C., Binder, O., & Conlon, F. L. (2004). T-box genes in early embryogenesis. *Dev Dyn, 229*(1), 201-218. doi:10.1002/dvdy.10480

Smith, J. C. (1987). A mesoderm-inducing factor is produced by Xenopus cell line. *Development, 99*(1), 3-14.

Soibam, B., Benham, A., Kim, J., Weng, K. C., Yang, L., Xu, X., . . . Liu, Y. (2015). Genome-Wide Identification of MESP1 Targets Demonstrates Primary Regulation Over Mesendoderm Gene Activity. *Stem Cells, 33*(11), 3254-3265. doi:10.1002/stem.2111

Soo, K., O'Rourke, M. P., Khoo, P. L., Steiner, K. A., Wong, N., Behringer, R. R., & Tam, P. P. (2002). Twist function is required for the morphogenesis of the cephalic neural tube and the differentiation of the cranial neural crest cells in the mouse embryo. *Dev Biol, 247*(2), 251-270.

Sparrow, D. B., Jen, W. C., Kotecha, S., Towers, N., Kintner, C., & Mohun, T. J. (1998). Thylacine 1 is expressed segmentally within the paraxial mesoderm of the Xenopus embryo and interacts with the Notch pathway. *Development, 125*(11), 2041-2051.

Spemann H., M. H. (1924). über Induktion von Embryonalanlagen durch Implantation artfremder Organisatoren. *Archiv f mikr Anat u Entwicklungsmechanik, 100*(3-4), 599-638.

Steinbach, O. C., Ulshofer, A., Authaler, A., & Rupp, R. A. (1998). Temporal restriction of MyoD induction and autocatalysis during Xenopus mesoderm formation. *Dev Biol, 202*(2), 280-292. doi:10.1006/dbio.1998.8993

Tajbakhsh, S. (2009). Skeletal muscle stem cells in developmental versus regenerative myogenesis. *Journal of Internal Medicine, 266*(4), 372-389. doi:10.1111/j.1365-2796.2009.02158.x

Takahashi, Y., Hiraoka, S., Kitajima, S., Inoue, T., Kanno, J., & Saga, Y. (2005). Differential contributions of Mesp1 and Mesp2 to the epithelialization and rostro-caudal patterning of somites. *Development, 132*(4), 787-796. doi:10.1242/dev.01597

Takahashi, Y., Koizumi, K., Takagi, A., Kitajima, S., Inoue, T., Koseki, H., & Saga, Y. (2000). Mesp2 initiates somite segmentation through the Notch signalling pathway. *Nat Genet, 25*(4), 390-396. doi:10.1038/78062

Takahashi, Y., Yasuhiko, Y., Kitajima, S., Kanno, J., & Saga, Y. (2007). Appropriate suppression of Notch signaling by Mesp factors is essential for stripe pattern formation leading to segment boundary formation. *Dev Biol, 304*(2), 593-603. doi:10.1016/j.ydbio.2007.01.007

Tazumi, S., Yabe, S., Yokoyama, J., Aihara, Y., & Uchiyama, H. (2008). PMesogenin1 and 2 function directly downstream of Xtbx6 in Xenopus somitogenesis and myogenesis. *Dev Dyn, 237*(12), 3749-3761. doi:10.1002/dvdy.21791

Tetelin, S., & Jones, E. A. (2010). Xenopus Wnt11b is identified as a potential pronephric inducer. *Dev Dyn, 239*(1), 148-159. doi:10.1002/dvdy.22012

Thiery, J. P., & Sleeman, J. P. (2006). Complex networks orchestrate epithelial-mesenchymal transitions. *Nat Rev Mol Cell Biol, 7*(2), 131-142. doi:10.1038/nrm1835

Tsilimigras, D. I., Oikonomou, E. K., Moris, D., Schizas, D., Economopoulos, K. P., & Mylonas, K. S. (2017). Stem Cell Therapy for Congenital Heart Disease: A Systematic Review. *Circulation, 136*(24), 2373-2385. doi:10.1161/circulationaha.117.029607

Tucker, B., Hepperle, C., Kortschak, D., Rainbird, B., Wells, S., Oates, A. C., & Lardelli, M. (2007). Zebrafish Angiotensin II Receptor-like 1a (agtrl1a) is expressed in migrating hypoblast, vasculature, and in multiple embryonic epithelia. *Gene Expr Patterns, 7*(3), 258-265. doi:10.1016/j.modgep.2006.09.006

Tzahor, E. (2009). Heart and craniofacial muscle development: a new developmental theme of distinct myogenic fields. *Dev Biol, 327*(2), 273-279. doi:10.1016/j.ydbio.2008.12.035

Ueno, S., Weidinger, G., Osugi, T., Kohn, A. D., Golob, J. L., Pabon, L., . . . Murry, C. E. (2007). Biphasic role for Wnt/beta-catenin signaling in cardiac specification in zebrafish and

embryonic stem cells. *Proc Natl Acad Sci U S A, 104*(23), 9685-9690. doi:10.1073/pnas.0702859104

van den Ameele, J., Tiberi, L., Bondue, A., Paulissen, C., Herpoel, A., Iacovino, M., . . . Vanderhaeghen, P. (2012). Eomesodermin induces Mesp1 expression and cardiac differentiation from embryonic stem cells in the absence of Activin. *EMBO Rep, 13*(4), 355-362. doi:10.1038/embor.2012.23

van der Linde, D., Konings, E. E., Slager, M. A., Witsenburg, M., Helbing, W. A., Takkenberg, J. J., & Roos-Hesselink, J. W. (2011). Birth prevalence of congenital heart disease worldwide: a systematic review and meta-analysis. *J Am Coll Cardiol, 58*(21), 2241-2247. doi:10.1016/j.jacc.2011.08.025

Walmsley, M., Cleaver, D., & Patient, R. (2008). Fibroblast growth factor controls the timing of Scl, Lmo2, and Runx1 expression during embryonic blood development. *Blood, 111*(3), 1157-1166. doi:10.1182/blood-2007-03-081323

Wang, J., Li, S., Chen, Y., & Ding, X. (2007). Wnt/beta-catenin signaling controls Mespo expression to regulate segmentation during Xenopus somitogenesis. *Dev Biol, 304*(2), 836-847. doi:10.1016/j.ydbio.2006.12.034

Weintraub, H., Davis, R., Tapscott, S., Thayer, M., Krause, M., Benezra, R., . . . et al. (1991). The myoD gene family: nodal point during specification of the muscle cell lineage. *Science, 251*(4995), 761-766.

Wen, J. W., & Winklbauer, R. (2017). Ingression-type cell migration drives vegetal endoderm internalisation in the Xenopus gastrula. *Elife, 6*. doi:10.7554/eLife.27190

WHO. (2018). WHO-MCEE estimates for child causes of death 2000–2016.

Yang, J., Tan, C., Darken, R. S., Wilson, P. A., & Klein, P. S. (2002). Beta-catenin/Tcf-regulated transcription prior to the midblastula transition. *Development, 129*(24), 5743-5752.

Yoon, J. K., & Wold, B. (2000). The bHLH regulator pMesogenin1 is required for maturation and segmentation of paraxial mesoderm. *Genes Dev, 14*(24), 3204-3214.

Zeng, X. X., Wilm, T. P., Sepich, D. S., & Solnica-Krezel, L. (2007). Apelin and its receptor control heart field formation during zebrafish gastrulation. *Dev Cell, 12*(3), 391-402. doi:10.1016/j.devcel.2007.01.011

7. Acknowledgement

Ein ganz besonderer Dank geht an Professor Ralph Rupp, der mich für die Arbeit an einem besonderen Organismus begeisterte, mich in die Weite der Embryologie und Molekularbiologie einwies und sein umfangreiches Wissen mit mir teilte.

Weiterhin möchte ich den Laborassistentinnen Edith und Barbara danken, die mir jederzeit mit Rat und Tat bei der Arbeit an der Bench zur Seite standen, sowie Post Doc Gabi und die PhD-Studenten Alessandro und Daniil, mit denen ich mich nicht nur fachlich austauschen konnte, sondern auch darüber hinaus dafür sorgten, dass die Zeit im Labor angenehm gestaltet wurde und nicht zuletzt den anderen Föfole-StudentInnen Steffi, die mir sehr in der Einarbeitung in das mespa-Projekt half und Adrian und Julian, die ein ähnliches Durchhaltevermögen neben dem Studium zeigten.

Nicht ungenannt sollen alle weiteren Mitglieder und KollegInnen der Arbeitsgruppen der Molekularbiologie des BMC bleiben. Es war eine schöne, lehrreiche, aber auch harte Zeit.

Was wäre diese Arbeit nur ohne die linguistische und grammatikalische Hilfe von Neal Conway gewesen? Vielen Dank dafür.

Zu guter Letzt und allen voran Danke an meine Familie und Freunde, die mich stets unterstützten und mir die Energie gaben diese Arbeit abzuschließen.